AN ABSTRACT OF THE THESIS OF

Rebecca J. Bliesner for the degree of Doctor of Philosophy in Chemistry presented on July 19, 2001. Title: Synthesis and Structural Determination of Alkali and Alkaline Earth Metal Containing Bismuth Vanadates.

Abstract Approved: _____

Arthur W. Sleight

Exploratory synthesis plays an important role in the quest to discover new materials. There are very few structurally characterized alkali metal containing bismuth vanadates. Hybridization of the 6s and 6p orbitals of Bi^{3+} and the resulting lone electron pair yields some very interesting stereochemistry and steric related properties. Some of those properties include ferroelectricity, ferroelasticity, electronic and ionic conduction, superconductivity, nonlinear optical capabilities and selective catalysis.

Systematic exploration of the Na-Bi-V ternary system produced a new phase of $NaBi_3V_2O_{10}$. This material crystallizes in the $P\bar{1}$ space group and the reported oxygen ion conductivity is apparently due to the presence of interstitial oxygen rather than oxygen vacancies.

Stabilization of the tetragonal scheelite phase of $BiVO_4$ has been achieved by the substitution of a M^{2+} for Bi^{3+}. This has not been accomplished previously by a M^{2+} cation substitution. The compound $Ca_{0.29}Bi_{0.71}VO_{3.855}$ crystallizes in the $P\bar{4}$ space group.

An investigation of the K-Bi-V ternary system resulted in the discovery of a new potassium vanadate. $K_{10}Bi_4V_4O_{21}$ crystallizes in the $P\bar{6}$ space group with *a* equal to 10.205(2)Å and *c* equal to 7.669(2)Å.

Other new compounds prepared, for which structures have not been determined are α-$Na_3BiV_2O_8$, β-$Na_3BiV_2O_8$, $K_8Bi_5V_5O_{24}$, Rb_2BiVO_5, a rubidium compound with a 3:3:2 stoichiometric ratio of Rb:Bi:V, a rubidium compound with 2:1:1, a sodium compound with 2:1:1 and a lithium compound with a 1:1:1 stoichiometric ratio of Li:Bi:V.

Synthesis and Structural Determination of Alkali and Alkaline Earth Metal Containing Bismuth Vanadates

by
Rebecca J. Bliesner

A THESIS

submitted to

Oregon State University

in partial fulfillment of
the requirements for the
degree of

Doctor of Philosophy

Presented July 19, 2001
Commencement June 2002

Doctor of Philosophy thesis of Rebecca J. Bliesner presented on July 19, 2001.

APPROVED:

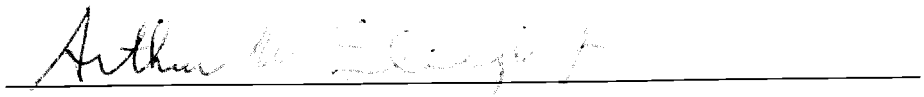

Major Professor, representing Chemistry

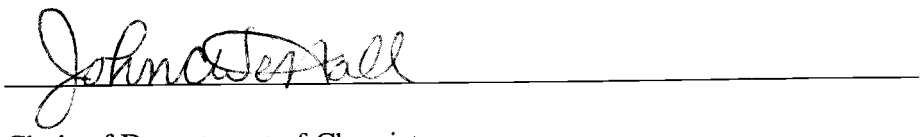

Chair of Department of Chemistry

Dean of the Graduate School

I understand that my thesis will become part of the permanent collection of Oregon State University libraries. My signature below authorizes release of my thesis to any reader upon request.

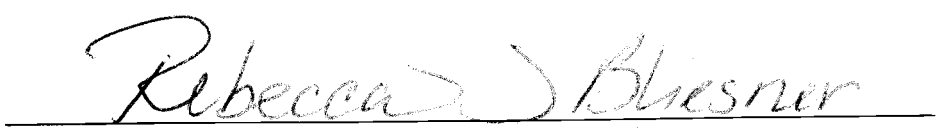

Rebecca J. Bliesner, Author

ACKNOWLEDGMENT

I would like to extend a huge thank you to my major professor, A.W. Sleight. From the moment I walked into his office he has fully supported and believed in my abilities. I would also like to thank the other members of the Sleight group, both past and present for their scientific insight, encouragement and the occasional beer: Dr. Tammy Amos, Dr. Ivana Radosavljevic, Dr. Niangao Duan, Dr. Uma , Dr. Raj, Dr. Alex Yokochi, Tao Juzhou, Jun Li, Xuimei Xun, Sasha Oblezov, and Vanaja Achuthan.

CONTRIBUTION OF AUTHORS

This work would not have been possible without the help of several collaborators. Dr. Alex Yokochi and Dr. Uma were involved in the single crystal X-ray diffraction data collection and provided insight and advice for the structural solutions presented in this thesis.

TABLE OF CONTENTS

Page

TABLE OF CONTENTS (CONTINUED)

Page

LIST OF FIGURES

LIST OF FIGURES (CONTINUED)

LIST OF TABLES

LIST OF TABLES (CONTINUED)

SYNTHESIS AND STRUCTURAL DETERMINATION OF ALKALI AND ALKALINE EARTH METAL CONTAINING BISMUTH VANADATES

Chapter 1

Introduction

1.1. Exploratory Synthesis

Exploratory synthesis in solid-state chemistry, in its pure form is the search for new materials with no preconceived notions about composition, structure or properties. It provides a means to push the boundaries established by the present knowledge base, to escape the intellectual confines of synthetic systematic thinking and to discover the unexpected.

It is essential to pursue the question "what if". Before Einstein's theory of relativity, some physicists believed the laws of Newton described all there was to know regarding the field of physics. It is intellectually arrogant to assume that we have nothing more to discover. Our present knowledge base cannot predict the new, exciting materials with spectacular new properties that are awaiting discovery.

High temperature superconductors and materials exhibiting negative thermal expansion are two examples of properties that were not predicted, but instead stumbled upon through exploratory synthesis. The rational approach of developing new materials by design is an essential part of solid-state materials

research. As exploratory synthesis broadens our knowledge base, expands the structural catalog and improves our understanding of complex systems, our methodology for designing new materials blossoms.

New materials may require special synthesis techniques. Complex structures, both in three-dimensional framework and element composition need to be attempted. Many spectacular new materials are waiting to be uncovered and their properties will have a profound impact on science and technology.

When new discoveries are made, they will be exploited to the fullest through systematic and applied studies. The goal is to make useful, inexpensive, nontoxic and easy to manufacture materials. This research project explores oxides containing bismuth, vanadium and alkali metals.

1.2. Intrigue of Bismuth Compounds

1.2.1. Lone Pair Electron Steric Effect

Bi^{3+} has an electronic configuration of $[Xe]4f^{14}5d^{10}6s^2$. The $6s^2$ electrons are commonly referred to as the lone pair electrons. Hybridization of the 6s and 6p orbitals, and the resulting lone electron pair yields some very interesting stereochemistry and steric related properties.

Bismuth environments commonly have seven-fold coordination with some long and some short bonds due to the stereoactive lone pair of electrons. These arrangements are found in solid-state materials and organometallics (1).

One common environment is the distorted monocapped trigonal prism or distorted monocapped octahedron (Figure 1.1). In this coordination strong bonds occur opposite to weak bonds and four intermediate bonds are found in the equatorial plane (2).

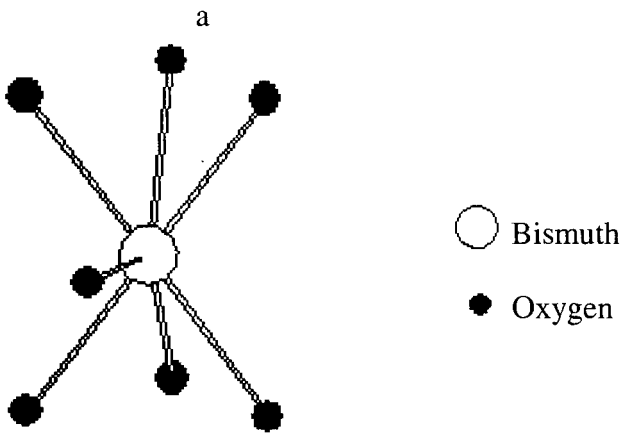

Figure 1.1. Distorted Monocapped Trigonal Prism Coordination for Bismuth

Two common bismuth-oxygen chains are known. The environment for the formation of $(BiO_2)^-$ (3) chains is depicted in Figure 1.2. A graphic representation of the very common $(Bi_2O_2)^{2+}$ sheets of the Aurivilluis phases (4) can be found in Figure 1.3.

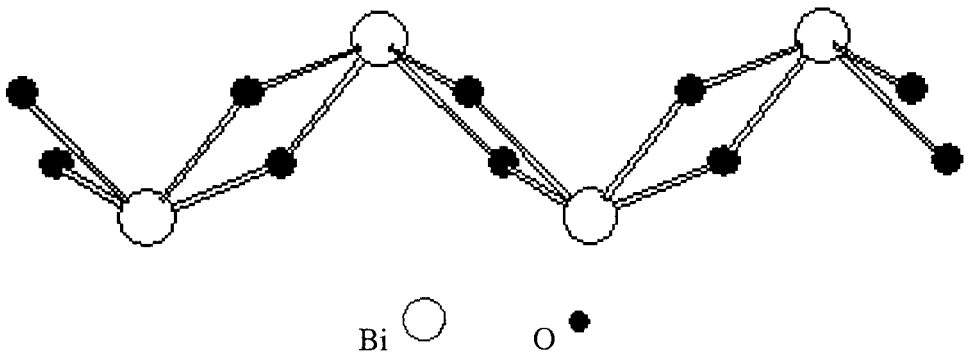

Figure 1.2. $(BiO_2)^-$ Chain Configuration for Bismuth

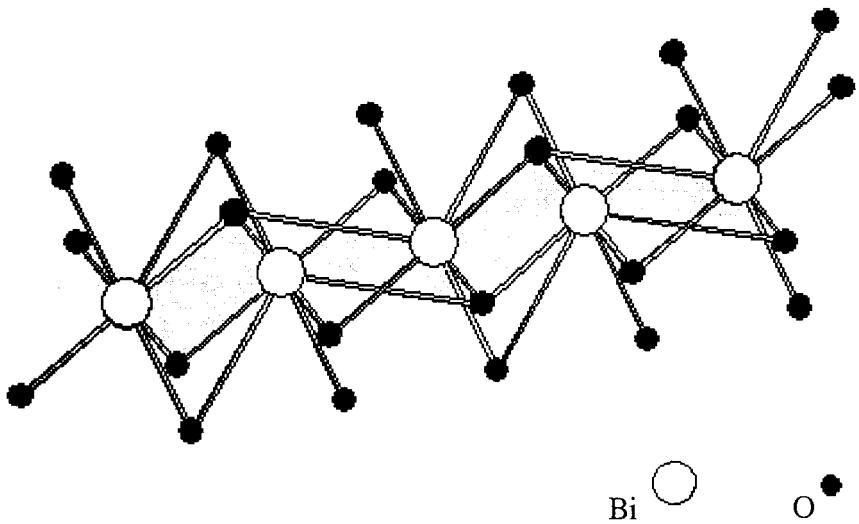

Figure 1.3. $(Bi_2O_2)^{2+}$ Chain Configuration for Bismuth

Bi^{3+} compounds normally contain two, three or four short bonds that are never opposite one another. In $BiCu_2AsO_6$ (5) an unusual five short bonds to bismuth is observed. This highly unusual arrangement is depicted in figure 1.4.

Hybridization of the 6s and 6p orbitals is required for lone pair stereochemistry. As covalency of the bonds increases, the lone pair influence on

coordination tends to disappear (6). Non-distorted polyhedron are a result of this increase in covalency.

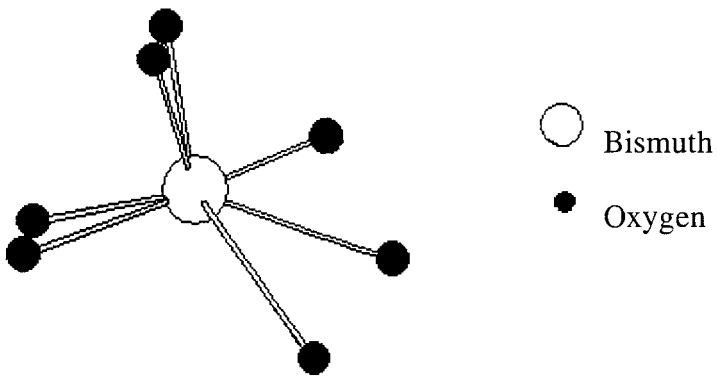

Figure 1.4. Unusual Five Short and Two Long Coordination for Bismuth

1.2.2. Ferroelectric and Ferroelastic Properties

Ferroelectric materials contain oriented or aligned dipoles within the structure. Multiple domains with distinct directions for dipole alignments are common. Applying an electric field to these materials can change the net polarization due to a shift in dipole direction orientation (7). Materials exhibiting this behavior must be in a space group that lacks an inversion center (8) and must contain a cation capable of undergoing significant displacement. Many Aurivilluis phases, $Bi_2A_{n-1}B_nO_{3n+3}$, are ferroelectrics (9).

Ferroelastic materials contain a net spontaneous strain that is altered by applying a mechanical stress (10,11). $BiVO_4$ undergoes a ferroelastic transition at 255°C that is associated with the monoclinic to tetragonal scheelite transformation

(12). It has been proposed that ferroelastic ability is intimately connected to displacement ability of Bi^{3+} cations due to the lone pair electron steric effect.

1.2.3. Conductivity

Many bismuth oxides are good oxygen ion conductors. This was first reported for δ-Bi_2O_3 (13). The high oxygen ion conductivity has been explained by lone pair electron stereochemistry. The highly polarizable bismuth cation network can accommodate oxygen disordering within the structure and thus promote oxygen ion mobility (14).

Additional examples of oxygen ion conductors within the bismuth oxides include the entire $BiMeVO_x$ family (15), variants of $Bi_{23}M_4O_{44.5}$ where M can be phosphorus or vanadium (16) and $NaBi_3V_2O_{10}$, addressed in Chapter 2. Oxide ion conductors have numerous applications in solid-state electrochemical devices, from oxygen sensors to fuel cell electrodes (17).

Electrical conductivity based on electron charge carriers is also known for bismuth oxides. For example, semiconductor behavior has been observed for $(CdBi)(V_{0.5}Sb_{1.5})O_7$, $(CdBi)(Rh_{0.5}Sb_{1.5})O_7$, $(CdBi)(VW)O_7$ and $(CdBi)(RhW)O_7$ (18).

Two compounds, $RbBiNb_2O_7$ and $CsBiNb_2O_7$ were found to be poor electronic and oxide ion conductors, but very good proton conductors (19). Treating both $RbBiNb_2O_7$ and $CsBiNb_2O_7$ with aqueous nitric acid promoted an

exchange of alkali metal ions for protons upon dehydration. The resulting dehydration product $HBiNb_2O_7$ is a very good proton conductor.

Perhaps the most interesting type of conductivity among bismuth containing compounds is superconductivity. Two major categories of bismuth superconductors are currently known. One set involves only Bi^{3+} cations, such as $Bi_2Cr_2Ca_2Cu_3O_{10}$ (20). In this and related superconductors, the bismuth stereochemistry plays not active role in the expression of superconductivity.

The second category of bismuth compounds exhibiting superconductivity are a mixed bismuth valent variety. In these systems superconductivity is associtated with the presence of both Bi^{3+} and Bi^{5+} (21). Phases within the $Ba(Pb,Bi)O_3$ (22) and $(Ba,K)BiO_3$ (23) families are especially known for their superconductivity. Some compounds in the $(Ba,K)BiO_3$ system have reached T_c's of 34 K (24).

1.2.4. Optical Properties

Bi^{3+} is an attractive activator for luminescent materials (25-34). Its use has been widely studied and luminescence has been found to depend on the bismuth environment. UV emission is achieved from Bi^{3+} doped $LaGaO_3$ and Bi^{3+} doped La_2SO_2 while red emission occurs for Bi^{3+} doped $BaSO_4$ and the compound $Bi_4Ge_3O_{12}$. $Bi_4Ge_3O_{12}$ is well established in luminescent applications. Bismuth oxyhalides have been investigated as light-sensitive layers for silver-free film development (35).

Some bismuth compounds exhibit nonlinear optics capabilities. These materials can produce a phase change or frequency conversion to laser light. Bi_2WO_6 was found to be a reasonably second harmonic generator (36) and $BiCa_9V_7O_{28}$ has proven to be a second harmonic generator with three times the intensity of KH_2PO_4 (37), one of the more common doubling crystals used today. Applications in the area of nonlinear optics include fiber optic communications, optical couplers, optical modulators and optical switches.

The monoclinic phase of $BiVO_4$ has been examined for its acoustooptical parameters (38) and its bright yellow-orange color makes it useful as a pigment (39).

1.2.5. Catalytic Properties

Many bismuth molybdates are used as oxidation catalysts for organic compounds such as butene, propene, carbon monoxide and methanol (40-42). Despite the disagreements regarding multiple features of these bismuth molybdates, the necessity for an efficient oxygen diffusion mechanism has surfaced. Bi^{3+} cation lone pair electron stereochemistry allows for polyhedron displacements, which enhances oxygen mobility within the structure.

1.3. Brief History of Bismuth Compounds in the Sleight Group

New bismuth containing compounds in the Sleight group have been obtained through exploratory synthesis and through designed synthesis. Table 1.1 lists the characterized compounds, their synthesis approach and the year of publication.

All high temperature superconducting oxides within the copper oxide superconducting family contain CuO_2 sheets. These sheets must be sufficiently oxidized or reduced for the compound to exhibit superconductivity. T_c, the temperature where superconductivity is first observed, has been found to be correlated to the degree of oxidation or reduction of the CuO_2 sheets and the number of CuO_2 sheets. In 1990, Huang and Sleight obtained and characterized the new compound $Nd_{1.7}Bi_{0.1}Sr_{0.9}Ca_{0.3}Cu_2O_6$ (43). Despite containing CuO_2 sheets, this compound was determined to be nonsuperconducting.

Another property driven quest involved the oxyhalides. Oxyhalides tend to have interesting optical properties. BiOBr can luminesce with excitation from X-rays, UV light or cathode rays if doped with an appropriate rare earth activator (44-49). BiOCl has been investigated as the light-sensitive layer in photographic imaging (35).

Two new bismuth containing oxychlorides were characterized, $BiSr_3O_3Cl_3$ and $BiCa_3O_3Cl_3$ (50). Both are unique among bismuth oxyhalides in that the three-dimensional network contains oxygen and chlorine sites in one layer.

Table 1.1. Bismuth Containing Compounds Discovered by the Sleight Group

Compound	Synthesis Method	Year of Publication
$Nd_{1.7}Bi_{0.1}Sr_{0.9}Ca_{0.3}Cu_2O_6$	Designed	1990
$BiSr_3O_3Cl_3$, $BiCa_3O_3Cl_3$	Designed	1991
$BiSr_2V_3O_{11}$	Exploratory	1992
$BiMg_2VO_6$	Exploratory	1992
$KBiO_3$	Designed	1992
$BiMg_2PO_6$, $BiMg_2AsO_6$	Designed	1993
$Na_2Bi^{3+}{}_4Bi^{5+}AuO_{11}$	Exploratory	1993
$BiCa_4V_3O_{13}$	Exploratory	1993
$BiBa_2V_3O_{11}$	Exploratory	1994
$BiBa_2V_2PO_{11}$	Designed	1994
$La_{0.26}Bi_{0.74}OOH$	Exploratory	1994
$HBi_3(CrO_4)_2O_3$	Exploratory	1994
Bi_2O_4	Exploratory	1995
$Bi_{12.7}Co_{0.3}O_{19.35}$	Designed	1995
$LiBiO_3$	Designed	1996
$MgBi_2O_6$, $ZnBi_2O_6$	Exploratory	1997
$BiCa_2VO_6$	Exploratory	1998
$Bi_{1.74}Ti_2O_{6.62}$	Exploratory	1998
$RBi_2O_4NO_3$ R = Rare Earth Elements	Exploratory	1998
$BiCu_2VO_6$	Designed	1998
$AgBiO_3$	Exploratory	1998
$Hf_{1-x}Bi_xO_{2-x/2}$, $Zr_{1-x}Bi_xO_{2-x/2}$	Designed	1998
$Sr_xNa_{1-2x}BiO_3 \cdot nH_2O$	Exploratory	1999
$Ba_xNa_{1-2x}BiO_3 \cdot nH_2O$	Exploratory	1999
$BiCu_2AsO_6$	Designed	1999
$BiCdVO_5$, $BiCdVO_6$	Exploratory	2000
$BiCa_2AsO_6$	Designed	2000
$Bi_2CaV_2O_9$	Exploratory	2000
$Bi_3Ca_9V_{11}O_{41}$	Exploratory	2000
$Ca_{1.29}Bi_{0.14}VO_4$	Designed	2000
$ACa_9(VO_4)_7$ A = Bi or Rare Earth Element	Exploratory,Designed	2001
$NaBiO_3$, $AgBiO_3$	Designed	2001

Huang and Sleight synthesized two new compounds, $BiSr_2V_3O_{11}$ and $BiBaV_3O_{11}$, containing two distinct vanadium groups, the orthovanadate group (VO_4) and the pyrovanadate group (V_2O_7) (51). Phosphorus substitution for one vanadium in the barium system provided the compound $BiBa_2V_2PO_{11}$ (6). The phosphorus was found to have no preference for the ortho or pyro environments. Another difference between the barium system and the strontium system was the disappearance of the stereoactive lone pair electrons on Bi^{3+}. This disappearance accounts to the fact that the barium system can have Bi replaced by In or any rare earth cation whereas in the strontium system this replacement is not possible.

Exploratory synthesis within the Bi-V-Me, Me being any cation, ternary system yielded the compound $BiMg_2VO_6$ (52). The structure exhibits a very unusual five-fold MgO_5 coordination. This magnesium coordination had been previously reported in both magnesium arsenates (53) and magnesium phosphates (54). Characterization of $BiMg_2VO_6$ led to the systematic design of the isostructural compounds $BiMgPO_6$ and $BiMg_2VO_6$.

Bi^{3+}, in a solid-state material, is simple to obtain. Bi^{5+} is more difficult due to instability. Bismuth mixed valent superconductors drove a design-oriented search for new materials within the alkali metal-bismuth oxide system. A collection of Bi^{5+} compounds were developed using electrodeposition and hydrothermal techniques.

The first crystals of $KBiO_3$ were grown and characterized (55), $LiBiO_3$, the only missing member of the $AM^{5+}O_3$ family (A= Li, Na, K and M = Nb, Ta, Sb,

Bi) was obtained (56). $MgBi_2O_6$ and $ZnBi_2O_6$, both Bi^{5+} compounds, were the first bismuth oxides ever to be reported with the trirutile-type structure (57).

Multiple valence bismuth materials were discovered. $Na_2Bi_4^{3+}Bi^{5+}AuO_{11}$ (58) was unusual because gold oxides are rare due to gold's inert chemical behavior. This compound was the first mixed valent bismuth material to contain completely distinct crystallographic sites for the Bi^{3+} and Bi^{5+} cations.

A mixed valent bismuth oxide $Bi^{3+}Bi^{5+}O_4$ was classified and found to also contain distinct Bi^{3+} and Bi^{5+} crystallographic sites. This compound was stumbled on during syntheses of $La_{0.26}Bi_{0.74}OOH$ (59) and $HBi_3(CrO_4)_2O_3$. Lanthanum bismuth oxyhydroxides are the first example of complete substitution of OH on the halide site for a PbFCl-type structure.

Sillenite-type materials, $Bi_{12}MO_{20}$, are of interest for their optical and piezoelectric properties. Mary , Mackay, Nguyen and Sleight obtained the first single crystals of any cobalt sillenite phase with the growth of $Bi_{12.7}Co_{0.3}O_{19.35}$ (60). The structural characterization of this material provided insight into the γ-Bi_2O_3 proposed sillenite phase $Bi_{12.3}O_{19.5}$ (61).

In 1998 a new family of rare earth bismuth oxynitrates was obtained from low temperature hydrothermal synthesis (62). Eight members of the $RBi_2O_4NO_3$, R = Y, Sm, Eu, Gd, TB, Dy, Er, Yb, were isolate and characterized.

While looking for interesting ferroelectric and nonlinear optics properties within the BiA_2MO_6 (A = divalent cation, M= pentavalent cation) system, $BiCu_2AsO_6$ (63) and $BiCuVO_6$ (64) were discovered. $BiCu_2AsO_6$ contains

unusually short bismuth to oxygen bond distances. $BiCu_2VO_6$ is different from other BiA_2MO_6 members because its VO_4 tetrahedron do not lie on any symmetry element. The tetrahedra do not point in directions along any of the unit cell axes.

Radosovljevic, Evans and Sleight synthesized and characterized the first ever pyrochlore-type bismuth titanate (65). $Bi_{1.74}Ti_2O_{6.62}$ deviates from the ideal $A_2^{3+}M_2^{4+}O_7$ formula but still maintains the pyrochlore-type structure. In this material, the bismuth displaces off the three-fold site to create a better environment for the lone pair electrons.

Sometimes the motivation for exploring a specific binary or ternary system can simply be the lack of published structures within that system. Solid solutions of $Hf_{1-x}Bi_xO_{2-x/2}$ and $Zr_{1-x}Bi_xO_{2-x/2}$ were explored by Sorokina and Sleight with the goal of finding new materials (66). For the hafnium solid solution x ranges from 0.40 to 0.75 with the single phase $Bi_2Hf_2O_7$ resulting from calcinations at 700°C for any value of x. The zirconium system formed solid solutions with x varying form 0.50 to 0.75. No single-phase product resulted from this sample exploration. $Bi_2Hf_2O_7$ was characterized and found to generate a second harmonic signal, much like the isostructural $Bi_2Sn_2O_7$ (67).

Bismuth and calcium complex oxides have been of interest in the Sleight group since the discovery of $BiCa_9V_7O_{28}$ (68). $BiCa_9V_7O_{28}$ has a second harmonic signal three times that of KH_2PO_4 (69) and large crystals can be grown (70) making this material a possible NLO device.

Other calcium containing bismuth oxides have been characterized. Huang and Sleight isolated $BiCa_4V_3O_{13}$ (8) in 1993. In 1998 Radosovljevic, Evans and Sleight obtained $BiCa_2VO_6$ (71). $BiCa_2AsO_6$ and $Bi_2CaV_2O_9$ (72) were characterized in 2000. $BiCa_4V_3O_{13}$, $BiCa_9V_7O_{28}$ and $Bi_2CaV_2O_9$ all contained disordered Bi/Ca sites and $BiCaVO_6$ and $BiCaAsO_6$ both generated second harmonic signals.

Kumada, Kinomura and Sleight explored the solid solutions $Sr_xNa_{1-2x}BiO_3 \cdot nH_2O$ and $Ba_xNa_{1-2x}BiO_3 \cdot nH_2O$ (73). Both systems involve mixed valent bismuth due to the replacement of Na^+ by Sr^{2+} or Ba^{2+}. The strontium system could maintain an x concentration of 0.48. The barium system was capable of forming single-phase products throughout the x = 0.11 to x = 0.36 range. The product formed was dependent on reaction time. Another unexpected phenomena with these structures was in their comparative unit cell dimensions. The strontium compound crystallized in a larger unit cell than any of the barium materials. The larger cation size of barium is not great enough to counteract the higher Bi^{3+} concentration found in the strontium system.

Two new bismuth cadmium vanadates were discovered in 2000, $BiCdVO_5$ and $BiCd_2VO_6$ (72). Also discovered in 2000 was the $Bi_3Ca_9V_{11}O_{41}$ (74) compound. This material was originally identified as a contaminant phase in attempts to grow $BiCa_9V_7O_{28}$. $Bi_3Ca_9V_{11}O_{41}$ contains three distinct vanadium environments. The orthovanadate, VO_4, and pyrovandate, V_2O_7, are quite common. The third environment involves a pair of edge sharing VO_5 square

pyramids each sharing a corner with a VO_4 tetrahedron, creating the unique V_4O_{14} polyhedron arrangement. This arrangement has never previously been reported.

Revisiting known structure and locating new phases is quite common. Ilmenite-type structures were obtained as new phases of $AgBiO_3$ (75) and $NaBiO_3$ (76). A second phase of $BiMgVO_6$ has also been determined and structurally characterized (72).

1.4. Systems Investigated

The motivation for the research project described in this thesis is exploratory synthesis of alkali metal containing bismuth vanadates. Very few alkali metal containing bismuth vanadates are reported in the literature. Three alkali doped $Bi_4V_2O_{11}$ phases are known, $Li_{0.2}Bi_4V_{1.8}O_{10.6}$ (77), $Bi_{4.10}V_{1.80}K_{0.10}O_{10.70}$ and $Bi_4V_{1.90}K_{0.10}O_{10.80}$ (78). Two phases for $NaBi_3V_2O_{10}$ have been reported (79,80). The three remaining materials reported in the literature all contain potassium; $NaK_2Bi_2(VO_4)_3$, $K_3Bi_2(VO_4)_3$ (81) and $K_{0.2}Bi_{1.45}V_8O_{16}$ (82). There are currently no reported rubidium bismuth vanadates.

The systems investigated in this project and the phases obtained are summarized in Table 1.2. Ternary phase diagrams for each of the alkali metals are depicted in Figures 1.5 – 1.8. Compounds residing on the edges of the diagrams are not included for clarity of the figure.

Table 1.2. Investigated Systems[a]

Alkali Metal Ratio	Bismuth Ratio	Vanadium Ratio	Predominate Phase
Li, 1	1	1	$BiVO_4$, **unknown phase**
Li, 3	3	2	$Bi_8V_2O_{17}$
Li, 1	1	2	$BiVO_4$
Na, 1	1	2	$BiVO_4$
Na, 1	2	1	Multiphase powder XRD pattern
Na, 1	3	2	**$NaBi_3V_2O_{10}$**
Na, 2	1	2	**$NaBi_3V_2O_{10}$**
Na, 2	2	1	**$NaBi_3V_2O_{10}$**
Na, 1	4	3	$BiVO_4$
Na, 2	1	1	**$NaBi_3V_2O_{10}$, $Na_3BiV_2O_8$, unknown phase**
Na, 3	1	2	**$Na_3BiV_2O_8$**
Na, 1	2	2	**unknown phase**
Na, 1	1	1	Multiphase powder XRD pattern
K, 2	1	1	**$K_{10}Bi_4V_4O_{21}$**
K, 8	5	5	**$K_8Bi_5V_5O_{24}$**
Rb, 3	3	2	$Bi_{12.38}V_{0.62}O_{21.02}$, **unknown phase**
Rb, 1	1	1	Bi_2O_3
Rb, 2	1	1	**unknown phase**

[a]Outcome compounds in bold represent potential new species

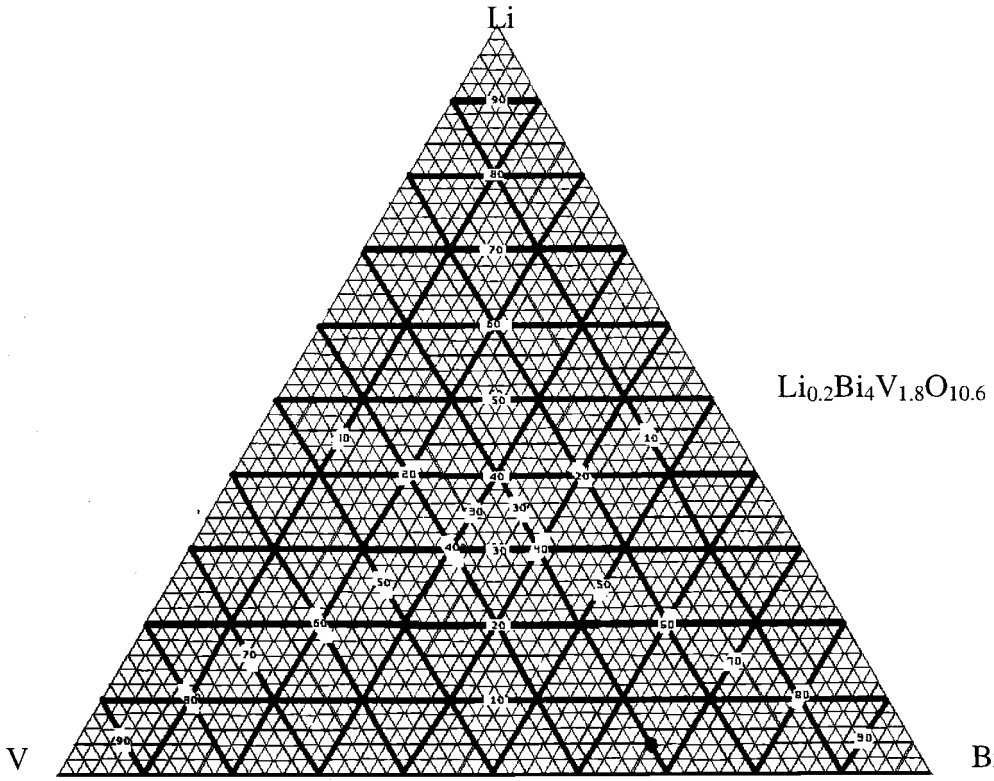

Figure 1.5. Ternary Phase Diagram For Lithium Containing Bismuth Vanadates

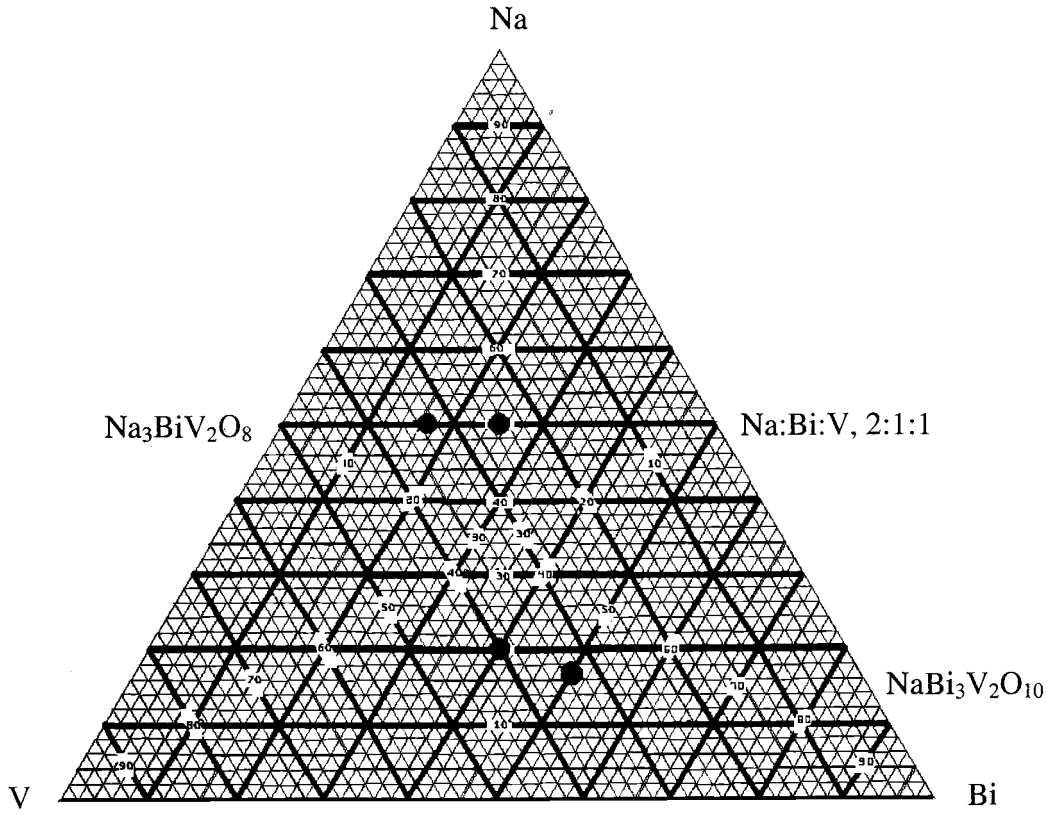

Figure 1.6. Ternary Phase Diagram For Sodium Containing Bismuth Vanadates

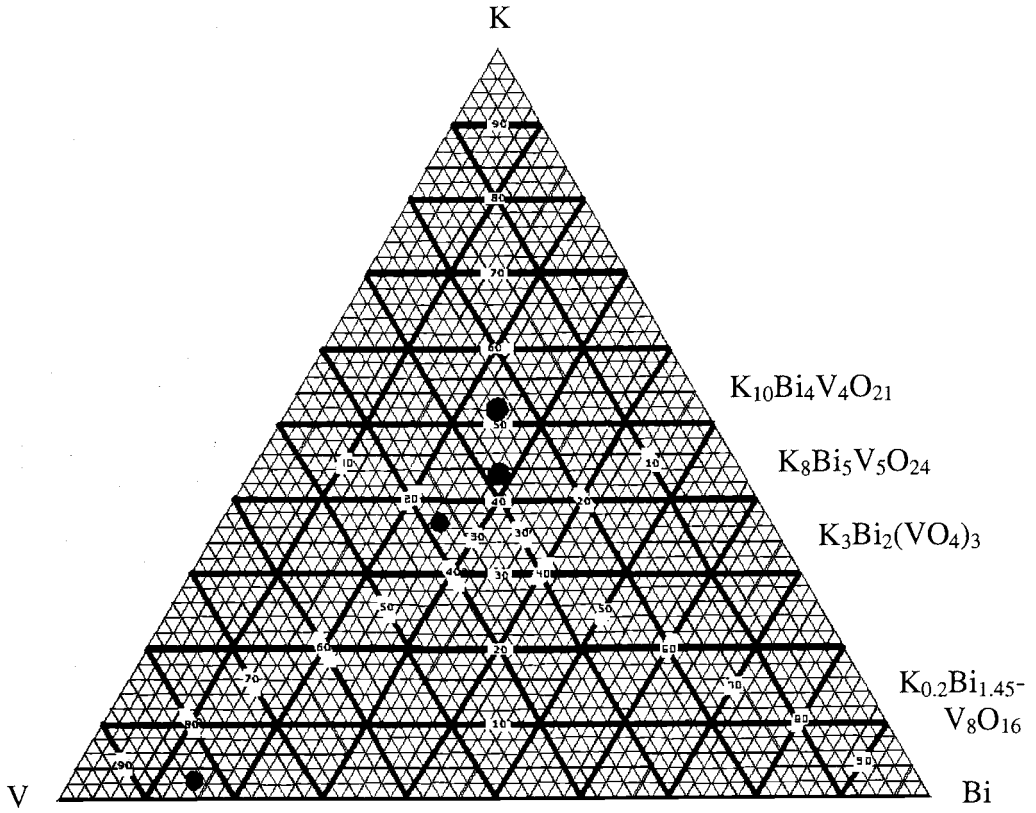

Figure 1.7. Ternary Phase Diagram For Potassium Containing Bismuth Vanadates

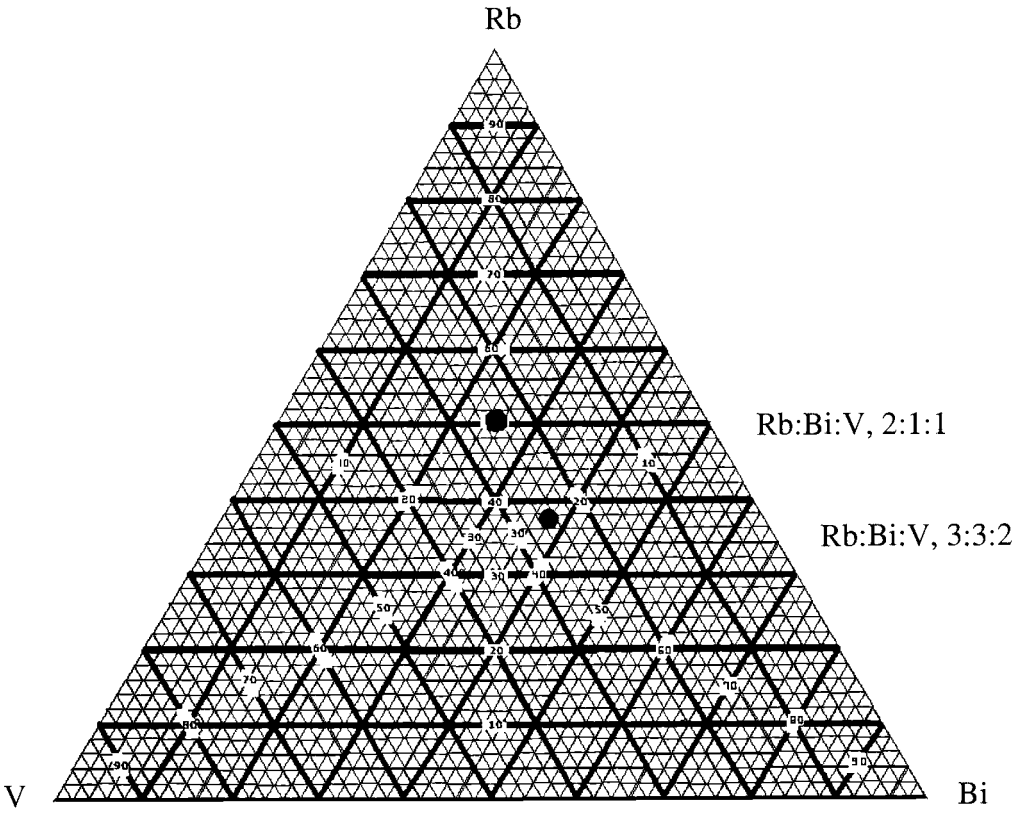

Figure 1.8. Ternary Phase Diagram For Rubidium Containing Bismuth Vanadates

Exploratory synthesis within the Na_2CO_3-Bi_2O_3-V_2O_5 system with initial reactant stoichiometry of 3:2:3 of Na:Bi:V resulted in the discovery of a new phase of $NaBi_3V_2O_{10}$. Single crystal x-ray diffraction and powder neutron diffraction data for this material are the topic of Chapter 2.

Attempts to prepare a K_2CO_3-Bi_2O_3-V_2O_5 phase with K:Bi:V molar ratios of 8:5:5 were unsuccessful due to a contaminant. The later determined $CaCO_3$ contaminant provided enough of a presence for the formation of a new calcium stabilized scheelite structure of $BiVO_4$. Structural characterization of this new material is discussed in Chapter 3.

Chapter 4 follows the synthesis and structural determination of a new potassium bismuth vanadate. Single crystals of this new compound were grown from an intimate 2:1:1 mixture of K:Bi:V from the K_2CO_3-Bi_2O_3-V_2O_5 trinary system.

Continuing work within the alkali metal containing bismuth vanadates as well as recommendations for future work and concluding remarks are examined in Chapter 5.

1.5. References

1. V. Garcia-Montalvo, R. Cea-Olivares, D.J. Williams and G. Espinosa-Perez, *Inorg. Chem.*, 35, 3948 (1996)

2. J.D. Brown, *J. Solid State Chem.*, 11, 214 (1974)

3. R. Enjalbert, R. Sorokina, S. Castro and J. Galy, *Acta chemica Scandinavica*, 49, 813 (1995)

4. B. Aurivillius, *Ark. Kemi., 1*, 54, 469 (1949)

5. I. Radosavljevic, J.S.O. Evans and A.W. Sleight, *J. Alloys and Compds.*, 284, 99, (1999)

6. J. Huang, Q. Gu and A.W.Sleight, *J. Solid State Chem.*, 110, 226 (1994)

7. A.R. West, Basic Solid State Chemistry, 2nd Edition, John Wiley & Sons, 1996.

8. J. Huang and A.W. Sleight, *J. Solid State Chem.*, 104, 52 (1993)

9. E.C. Subbarao, *J. Chem. Phys.*, 34/2, 695 (1961)

10. K. Aizu, *J. Phys. Soc. Japan*, 27/2, 287 (1969)

11. K. Aizu, *J. Phys. Soc. Japan*, 28/3, 706 (1970)

12. J.D. Bierlein and A.W. Sleight, *Solid State Commun.*, 16, 69 (1975)

13. T. Takahashi and H. Iwahara, *Mat. Res. Bull.*, 13, 1447 (1978)

14. G. Mairesse, Fast Ion Transport in Solids, Edited by B. Scrosati, Kluver Amsterdam, The Netherlands (1993)

15. F. Abraham, M.F. Debreuille-Gresse, G. Mairesse and G. Nowogrocki, *Solid State Ionics*, 28/30, 529 (1988)

16. A. Watanabe, *Solid State Ionics*, 96, 75 (2997)

17. M.E. Arroyo y de Dompablo, F. Garcia-Alvarado and E. Moran, *Solid State Ionics*, 91, 273 (1996)

18. M.A. Subramanian and A.W. Sleight, *Mat. Res. Bull.*, 21, 727 (1986)

19. M.A. Subramanian, J. Gopalakrishnan and A.W. Sleight, *Mat. Res. Bull.*, 23, 837 (1988)

20. A.W. Sleight, *Science*, 242, 1519 (1988)

21. A.W. Sleight, J.L. Gillson and P.E. Bierstedt, *Solid State Commun.*, 17, 27 (1975)

22. L.F. Mattheiss, E.M. Gyorgy and D.W. Johnson, *Phys. Rev. B*, 37, 3745 (1988)

23. R.J. Cava, B. Batlogg, J.J. Krajewski, R. Farrow, L.W. Rupp, A.E. White, K. Short, W.F. Peck and T. Komentani, *Nature (London)*, 332, 814 (1988)

24. N.L. Jones, J.B. Parise, R.B. Flippen and A.W. Sleight, *J. Solid State Chem.*, 78, 319 (1989)

25. B. Jacquier, G. Boulon, G. Sallavuard and F. Gaume, *J. Solid State Chem.*, 4, 374 (1972)

26. A. Wolfert and G. Blasse, *Mat. Res. Bull.*, 19, 67 (1984)

27. F. Kellendonk and G. Blasse, *Phys. Status Solidi B*, 108, 541 (1981)

28. C.W.M. Timmermans and G. Blasse, *Phys. Status Solidi B*, 106, 647 (1981)

29. C.W.M. Timmermans and G. Blasse, *J. Lunim.*, 24/25, 75 (1981)

30. C.W.M. Timmermans, O. Boen Ho and G. Blasse, *Solid State Commun.*, 42, 505 (1982)

31. C.W.M. Timmermans, S.O. Cholakh, R.L. Van Der Woude and G. Blasse, *Phys. Status Solidi B*, 115, 267 (1983)

32. C.W.M. Timmermans, S.O. Cholakh and G. Blasse, *J. Solid State Chem.*, 46, 222 (1983)

33. A.C. Van Der Steen, *Phys. Status Solidi B*, 100, 603 (1980)

34. F. Pelle, B. Jacquier, J.P. Denis and B. Blanzat, *J. Lunim.*, 17, 61 (1978)

35. S.K. Poznyak, V.V. Sviridov and A.I. Kulak, *Elektrokhimiya*, 20/7, 996 (1984)

36. R.J. Wolfe, R.E. Newnham and M.I. Kay, *Solid State Comm.*, 7, 1797 (1969)

37. J.S.O. Evans, J. Huang and A.W. Sleight, *J. Solid State Chem.*, 157, 255 (2001)

38. S.V. Akimov, I.E. Mnushkina and E.F. Dudnik, *Sov. Phys. Tech. Phys.*, 27, 4 (1983)

39. Balducci et al., U.S. Patent, No. 4,230,500

40. T. Tsunoda, T. Hayakawa, T. Kameyama and K. Takehira, *J. Chem. Soc. Farad. Trans.*, 91, 1117 (1995)

41. D. H. Galvan, S. Fuentes, M. Alvalosborja, L. Cotaaraiza, E.A. Early, M.B. Maple and J. Cruzreyles, *J. Phys. Condens. Matter*, 5, A217 (1993)

42. R.K. Grasseli and J.F. Burrington, *Adv. Catal.*, 30, 133 (1981)

43. J. Huang and A.W. Sleight, *Physica C*, 169, 169 (1990)

44. G. Blasse and A. Bril, *J. Chem. Phys.*, 47, 1920 (1967)

45. J. Holsa, M. Leskela, and L. Niinisto, *J. Solid State Chem*, 37, 267 (1981)

46. P. De Maayer and R. Bollen, *J. Electrochem. Soc.*, 130, 437 (1983)

47. L.Y. Mo, F. Guillen, C. Fouassier and Pl Hagenmuller, *J. Electrochem. Soc.*, 132, 717 (1985)

48. H. Haeuseler and M. Jung, *Mat. Res. Bull.*, 21, 1291 (1986)

49. G. Blasse, J. Sytsma and L.H. Brixner, *Chem. Phys. Lett.*, 155, 64 (1989)

50. J. Huang and A.W. Sleight, *J. Solid State Chem.*, 96, 154 (1992)

51. J. Huang and A.W. Sleight, *J. Solid State.Chem.*, 97, 228 (1992)

52. J. Huang and A.W. Sleight, *J. Solid State Chem.*, 100, 170 (1992)

53. Y.S. Ng, G.A. Rodley and W.T. Robinson, *Mat. Res. Bull.*, 15, 303 (1976)

54. A. Benmoussa, M.M. Borel, A. Leclaire and B. Raveau, *J. Solid State Chem.*, 84, 299 (1990)

55. S. Kodialam, V.C. Korthius, R.-D. Hoffmann and A.W. Sleight, *Mat. Res. Bull.*, 27, 1379 (1992)

56. N. Kumada, N. Takahashi, N. Kinomura and A.W. Sleight, *J. Solid State Chem.*, 126, 121 (1996)

57. N. Kumada, N. Takahashi, N. Kinomura and A.W. Sleight, *Mat. Res. Bull.*, 32/8, 1003 (1997)

58. J. Pannetier, D. Tranqui and A.W. Sleight, *Mat. Res. Bull.*, 28, 989 (1993)

59. N. Kumada, N. Kinomura, S. Kodialam and A.W. Sleight, *Mat. Res. Bull.*, 29/5, 497 (1994)

60. T.A. Mary, R. Mackay, P. Nguyen and A.W. Sleight, *Eur. J. Solid State Inorg. Chem.*, 33, 285 (1996)

61. S.F. Radaev, L.A. Muradyan and V.I. Simonov, *Acta Cryst.*, B47, 1 (1991)

62. N. Kumada, N. Takahashi, N. Kinomura and A.W. Sleight, *J. Solid State Chem.*, 139, 321 (1998)

63. I. Radosavljevic, J.S.O. Evans and A.W. Sleight, *J. Alloys and Compds.*, 284, 99 (1999)

64. I. Radosavljevic, J.S.O. Evans and A.W. Sleight, *J. Solid State Chem.*, 141, 149 (1998)

65. I. Radosavljevic, J.S.O. Evans and A.W. Sleight, *J. Solid State Chem.*, 136, 63 (1998)

66. S.L. Sorokina and A.W. Sleight, *Mat. Res. Bull.*, 33/7, 1077 (1998)

67. R.D. Shannon, J.D. Bierlein, J.L. Gillson, G.A. Jones and A.W. Sleight, *J. Phys. Chem. Solids*, 41, 117 (1980)

68. A.W. Sleight and J. Huang, U.S.A. Patent No. 5202,891 (1993)

69. J.S.O. Evans, J. Huang and A.W. Sleight, *J. Solid State Chem.*, 157, 255 (2001)

70. H.K. Kim, M.S. Kim, S.M. Park and A.W. Sleight, *J. Crystal Growth*, 219, 61 (2000)

71. I. Radosavljevic, J.S.O. Evans and A.W. Sleight, *J. Solid State Chem.*, 136, 63 (1998)

72. I. Radosavljevic, J.A.K. Howard and A.W. Sleight, *Int. J. Inorg. Mat.*, submitted

73. N. Kumada, N. Kinomura and A.W. Sleight, *Solid State Ionics*, 122, 183 (1999)

74. I. Radosavljevic, J.A.K. Howard, A.W. Sleight and J.S.O. Evans, *J. Mater. Chem.*, 10, 2091 (2000)

75. N. Kumada, N. Takahashi, N. Kinomura and A.W. Sleight, *Royal Soc. Chem.*, 239, 212 (1999)

76. N. Kumada, N. Kinomura and A.W. Sleight, *Mat. Res. Bull.*, 35, 2397 (2000)

77. Grant in Aid: Scotland

78. C.K. Lee, A.M. Coats and A.R. West, *Powder Diffr.*, 12/4, 245 (1997)

79. D. Sinclaire, E. Marinou and J.M.S. Skakle, *J. Materials Chem.*, 9, 2617 (1999)

80. D.G. Porob and T.N. Guru Row, *Chem. Mater.*, 12, 3658 (2000)

81. M.F. Debreuille-Gresse and F. Abraham, *J. Solid State Chem.*, 71, 466 (1987)

82. O. Mentre, A.C. Dhaussy and F. Abraham, *J. Materials Chem.*, 9, 1023 (1999)

Chapter 2

Structure of α-$NaBi_3V_2O_{10}$ and Implications for Ionic Conductivity

2.1. Introduction

In 1998, Sinclair and co-workers reported the preparation of a new oxide ion conductor $NaBi_3V_2O_{10}$ (1). The crystal structure of β-$NaBi_3V_2O_{10}$, solved by neutron diffraction, was found to be isostructural to $Pb_2Bi_2V_2O_{10}$ with a P1 triclinic space group (2). A second phase, α-$NaBi_3V_2O_{10}$, with a $P\bar{1}$ triclinic space group was reported by Porob and Guru Row in 2000 (3). The second phase structure was determined based on powder X-ray diffraction data. All previous studies maintain that single crystal growth was not possible and that oxide ion conductivity is most likely due to oxygen deficiency in the structure.

2.2. Experimental

Single crystals were first obtained from a 3:3:2 stoichiometric mixture of Na:V:Bi from $NaNO_3$ (Spectrum), V_2O_5 (Johnson Matthey) and Bi_2O_3 (Alpha Aesar). The reagents were ground for twenty minutes in an agate mortar and heated in a Lindberg furnace, at 800°C for 15 hours. The sample was cooled at a rate of 5°C/min. All crystals were yellow but two different shapes were apparent

under a microscope. Some crystals were shaped like very fat needles while others had a more equal three-dimensional appearance.

A similar powder X-ray diffraction pattern and two-phase crystals were obtained from a 2:2:1 stoichiometric ratio of Na:V:Bi from $NaNO_3$ (Spectrum), V_2O_5 (Johnson Matthey) and Bi_2O_3 (Alfa Aesar). Wavelength dispersive electron microprobe analysis with a beam current of 48.5 nA, an accelerating voltage of 15 kV and a 5 μm beam diameter, of both samples indicated the presence of two phases $NaBi_3V_2O_{10}$ and $Na_3BiV_2O_8$ (4).

Multiple syntheses using 1:2:3 stoichiometric ratios for Na:V:Bi were attempted. All attempts resulted in a two-phase product. An increase in the $NaBi_3V_2O_{10}$ to $Na_3BiV_2O_8$ ratio was enhanced using Na_2CO_3 (Aldrich) in the place of $NaNO_3$ (Spectrum). Syntheses between 700°C and 775°C produced a highly complex multi-phase product containing $NaBi_3V_2O_{10}$, $Na_3BiV_2O_8$ and the contaminants previously addresed in the literature (1,2,3). Slow cooling enhanced crystallite size, but made differentiation of the two products more difficult.

Single phase, polycrystalline $NaBi_3V_2O_{10}$ was prepared from a 1:2:3 stoichiometric ratio of Na:V:Bi from Na_2CO_3 (Aldrich), V_2O_5 (Johnson Matthey) and Bi_2O_3 (Alpha Aesar). These reagents were ground for twenty minutes with an agate mortar and pestle, and heated in air at 625°C for 24 hours. The material was then reground and heated for another 15 hours at 625°C.

Heating temperature and time of calcination had a significant impact on the single-phase nature of the product. Temperatures below 600°C and above 675°C

produced multiphase products. The multiphase powders were a pale green-maize color and many contained small amounts of bismuth metal. Some samples calcinated above 675°C contained both brown and dark purple particulates. Samples that did not contain brown or purple components could be reground, reheated to 625°C for 24 hours and reground and reheated at 625°C for another 15 hours to achieve single phase $NaBi_3V_2O_{10}$.

To achieve single phase $NaBi_3V_2O_{10}$ with one heating, it was necessary to calcinate at 625°C for 8 days. Using a two-step heat-and-grind process was more efficient and more reliable. Shortened calcination times, less than 24 hours followed by 15 hours, reduced the single-phase nature of the polycrystalline product. Single phase, polycrystalline $NaBi_3V_2O_{10}$ was pale yellow.

Powder X-ray diffraction was used to monitor the content of the obtained products. Patterns were recorded from a Siemens D5000 powder diffractometer with a Kevex detector, CuKα radiation ($\lambda = 1.5418$ Å) and vertical Soller slits.

Single crystal X-ray diffraction data were collected at room temperature on a Rigaku AFC6R diffractometer with monochromatic MoKα radiation ($\lambda = 0.71069$ Å). No decay was noted during data collection. The observed intensities were corrected for Lorentz polarization and absorption. Data reduction was carried out using a local program, capable of creating a data file containing the crystal dependent direction cosines of the diffracted and reverse incident beam, for purposes of correction of absorption anisotropy problems. Correction for the effects of absorption anisotropy was carried out using the program SORTAV (5), as

programmed in the software collection WINGX V1.64.02 (6). Structure solution was carried out using Patterson Map interpretation as programmed in SHELXS-90 and refined using full-matrix least-squares refinement on F^2 using the program SHELXL-97 (7). Details of the single crystal data collection are given in Table 2.1.

Powder neutron diffraction data were collected on BT-1 at the NIST Center for Neutron Research using a wavelength of 1.5402 Å. Structural refinements were carried out using the GSAS software package (8). Both LeBail and Reitveld refinements were completed using the single crystal structural solution as the initial model. The peaks were fit using T.H.C. psuedo-Voigt profiles (9). Details of the neutron data collection are given in Table 2.2.

Table 2.1. Crystallographic Data for $NaBi_3V_2O_{10}$ Single Crystal X-ray Diffraction

radiation source	Rigaku AFC6R
radiation	Mo Kα
λ (Å)	0.71069, graphite monochrometer
θ range (deg)	3.12 – 35.07
hkl regions	-8 – 8, 0 – 11, -11 – 10
crystal size (mm)	0.25, 0.20, 0.15
color	pale yellow
formula	$Na_{0.96}Bi_{3.04}V_2O_{10.04}$
fw	919.79
density (g/cm^3)	6.408
absorption correction	Psi-scans & symmetry equivalents
absorption coefficient (mm^{-1})	57.92
refinement method	full-matrix least squares on F^2
extinction coefficient	0.004(1)
space group	$P\bar{1}$
a (Å)	5.538(5)
b (Å)	7.058(4)
c (Å)	7.120(7)
α (deg)	107.66(6)
β (deg)	112.21(8)
γ (deg)	95.65(7)
V ($Å^3$)	238.2(3)
z	1
no. of measured reflections	2246
no. of independent reflections	2092 (R_{int}= 6.36)
no. of reflections $I > 2\sigma(I)$	1286
no. of refined parameters	75
R_1 (%)	6.31
wR_2 (%)	14.91
goodness of fit	1.077

Table 2.2. Crystallographic Data for $NaBi_3V_2O_{10}$ Neutron Powder Study

radiation source	BT-1 at NIST
radiation	neutron
λ (Å)	1.5402
data collection range (2θ, deg)	3.000 – 168.000
step scan increment (2θ, deg)	0.05
step scan time (s)	300
color	yellow
formula	$Na_{0.96}Bi_{3.04}V_2O_{10.04}$
fw	919.79
density (g/cm^3)	6.465
space group	$P\bar{1}$
profile function	pseudo-voigt (T.H.C.)
a (Å)	5.5363(1)
b (Å)	7.0628(2)
c (Å)	7.1418(2)
α (deg)	107.882(2)
β (deg)	112.046(2)
γ (deg)	95.549(2)
V ($Å^3$)	239.123(6)
z	1
no. of data points	2599
no. of contributing reflections	932
no. of structural parameters	64
no. of profile parameters	10
χ^2	2.415
R_{wp}(%)	5.49
R_p(%)	4.30

2.3. Structural Analysis

α-$NaBi_3V_2O_{10}$ crystallizes in space group $P\bar{1}$ (No. 2) with one molecular unit per unit cell. Lattice parameters for both single crystal and neutron powder analyses can be found in Table 2.3.

Table 2.3. Comparison of Lattice Parameters for $NaBi_3V_2O_{10}$

Parameter	Single Crystal X-Ray	Powder Neutron
a (Å)	5.538(5)	5.5363(1)
b (Å)	7.058(4)	7.0628 (2)
c (Å)	7.120(7)	7.1418(2)
Alpha (°)	107.66(6)	107.882(2)
Beta (°)	112.21(8)	112.046(2)
Gamma (°)	95.65(7)	95.549(2)

The bismuth positions were determined using a Patterson, heavy-atom, approach. Subsequent least-squares refinements and fourier map analyses were used to determine vanadium and oxygen positions. Two problems arose with the first attempts at structure determination. First, no apparent sodium site was identified. Second, the remaining residuals from the electron density maps were on the order of magnitude ¾ of that of an oxygen.

Additional electron microprobe analysis of crystals, from the same batch as the one for which X-ray data were collected on, indicated that sodium was present. Occupancy refinement of the Bi 2 position, anisotropic displacement parameters for the Bi 2 position and the similar size of Na^{1+} and Bi^{3+} ions (10) all pointed toward the possibility of a shared site. This was confirmed by a large lowering of the R value as well as improvement in the anisotropic displacement parameters. (At the time this structure was being solved, the paper by Porob and Guru Row had not yet been published.) Shared sites are not uncommon for Na^{1+} and Bi^{3+} cations, such as in the scheelite $Na_{0.5}Bi_{0.5}MoO_4$ (11) and the defect pyrochlore $NaBi_2Ta_5O_{16}$ (12).

Axial photographs using the Rigaku AFC6R system were obtained to provide insight into the large residuals. At first the crystal appeared to have a supercell. Another axial photograph, taken over a longer period of time, showed that the observed reflections of weaker intensity could not be explained as superstructure reflections. Instead, these reflections of weaker intensity appeared to be due to a satellite crystal. Close analysis of the strongest deviating reflections did indeed suggest the presence of a satellite crystal. Nineteen reflections were removed from the data refinement, and an overall improvement in the structure solution was obtained.

All atomic site occupancies were refined and found to be 1.0 with the Bi 2 / Na 1 site refining to a 52:48 ratio of bismuth to sodium. Atomic positions and occupancy data for the single crystal structural solution and displacement parameters can be found in Table 2.4 and 2.5.

Table 2.4. Single Crystal Atom Parameters for $NaBi_3V_2O_{10}$

Atom	x	y	z	Occupancy
Bi 1	0.0838(1)	0.7574(1)	0.5283(1)	1.000
Bi 2	0.3134(2)	0.3822(2)	0.2103(2)	0.523(6)
Na 1	0.3134(2)	0.3822(2)	0.2103(2)	0.476(6)
V	0.3446(6)	0.8440(4)	0.1446(4)	1.000
O 1	0.159(3)	0.690(2)	0.217(2)	1.000
O 2	0.147(3)	0.803(2)	0.875(2)	1.000
O 3	0.252(3)	0.500(2)	0.527(2)	1.000
O 4	0.566(3)	0.895(2)	0.693(2)	1.000
O 5	0.380(3)	0.235(2)	0.833(3)	1.000

Table 2.5. Single Crystal Displacement Parameters[a] for $NaBi_3V_2O_{10}$

Atom	Ueq	U11	U22	U33	U12	U13	U23
Bi 1	13(1)	14(1)	13(1)	13(1)	4(1)	6(1)	5(1)
Bi 2	14(1)	12(1)	16(1)	13(1)	2(1)	5(1)	4(1)
Na 1	14(1)	12(1)	16(1)	13(1)	2(1)	5(1)	4(1)
V	13(1)	10(1)	18(1)	7(1)	-2(1)	2(1)	2(1)
O 1	15(2)	18(5)	19(5)	13(4)	0(4)	13(4)	5(4)
O 2	20(3)	18(6)	35(6)	8(4)	2(5)	5(4)	11(4)
O 3	20(3)	7(5)	27(7)	29(7)	4(5)	8(5)	16(5)
O 4	22(3)	13(6)	25(7)	23(6)	-2(5)	5(5)	8(5)
O 5	27(3)	21(7)	30(8)	34(8)	15(6)	11(7)	15(6)

[a]All values represent displacement parameters multiplied by 1000

Due to the transparency of vanadium to neutron radiation the vanadium parameters determined in the single crystal system were fixed for the neutron refinement. Background, zero, lattice parameters, atomic positions, atomic occupancies and atomic displacement parameters were all refined. The Bi/Na site was found to have a 52:48, bismuth to sodium, occupancy. All other sites were found to be fully occupied. Atom positions and occupancies for the neutron solution and displacement parameters can be found in Table 2.6 and 2.7. The observed and calculated diffraction patterns are shown in Figure 2.1.

Table 2.6. Powder Neutron Atom Parameters for $NaBi_3V_2O_{10}$

Atom	X	y	z	Occupancy
Bi 1	0.0816(6)	0.7598(4)	0.5288(5)	1.0000
Bi 2	0.3091(8)	0.3794(7)	0.2004(8)	0.521(1)
Na 1	0.3091(8)	0.3794(7)	0.2004(8)	0.479(1)
V[a]	0.3446	0.8440	0.1446	1.000
O 1	0.1562(9)	0.6926(6)	0.2170(7)	1.000
O 2	0.1460(9)	0.8043(7)	0.8800(7)	1.000
O 3	0.2552(9)	0.4988(6)	0.5333(7)	1.000
O 4	0.5660(9)	0.8970(6)	0.6949(7)	1.000
O 5	0.377(1)	0.2362(8)	0.8333(9)	1.000

[a]Fixed at values obtained from single crystal analysis

Table 2.7. Powder Neutron Displacement Parameters[a] for $NaBi_3V_2O_{10}$

Atom	Ueq	U11	U22	U33	U12	U13	U23
Bi 1	18	26(2)	14(2)	14(2)	4(1)	8(1)	7(1)
Bi 2	30	20(3)	29(2)	37(3)	7(2)	18(2)	12(2)
Na 1	30	20(3)	29(2)	37(3)	7(2)	18(2)	12(2)
V[b]	13	10	18	7	-2	2	2
O 1	23	32(3)	24(3)	14(3)	0(2)	18(2)	2(2)
O 2	26	22(3)	32(3)	11(2)	-6(2)	-4(2)	12(2)
O 3	29	13(2)	21(3)	45(3)	0(2)	11(2)	15(2)
O 4	24	27(3)	13(2)	24(3)	-2(2)	7(2)	2(2)
O 5	39	27(3)	43(3)	38(3)	13(2)	12(3)	16(3)

[a]All values represent displacement parameters multiplied by 1000
[b]Fixed at values obtained from single crystal analysis

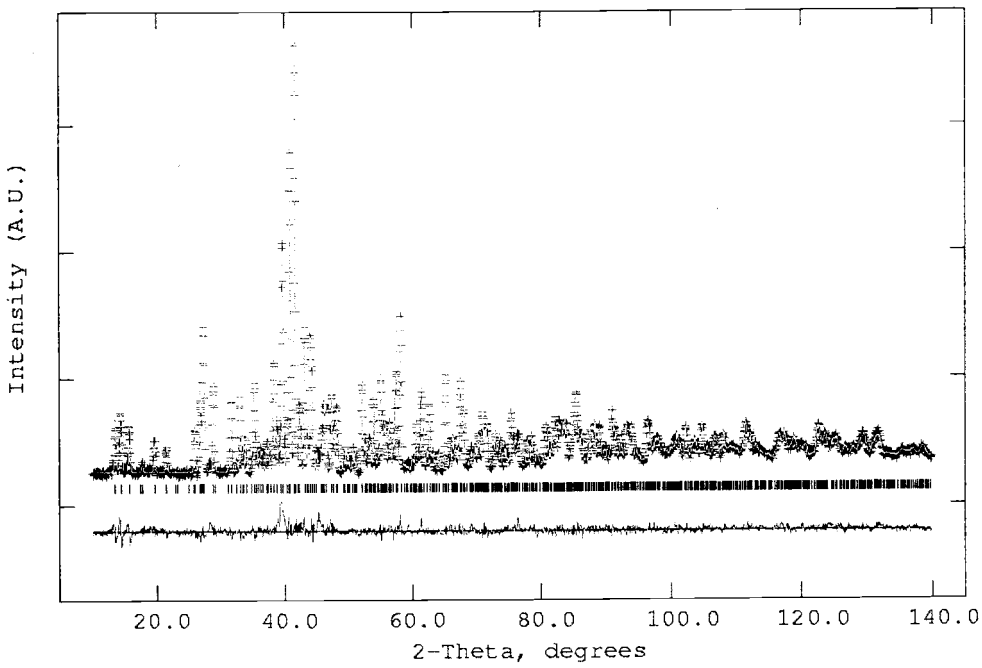

Figure 2.1. Observed, Calculated and Difference Profiles for $NaBi_3V_2O_{10}$

The three dimensional framework of $NaBi_3V_2O_{10}$ can be described as groupings of edge sharing Bi/NaO_6 and BiO_6 octahedron perpetuating up and down the a axis, connected by corner sharing VO_4 tetrahedron along the b and c axis directions. Figure 2.2 depicts the $NaBi_3V_2O_{10}$ structure with only the VO_4 tetrahedron included. Figure 2.3 includes all polyhedron.

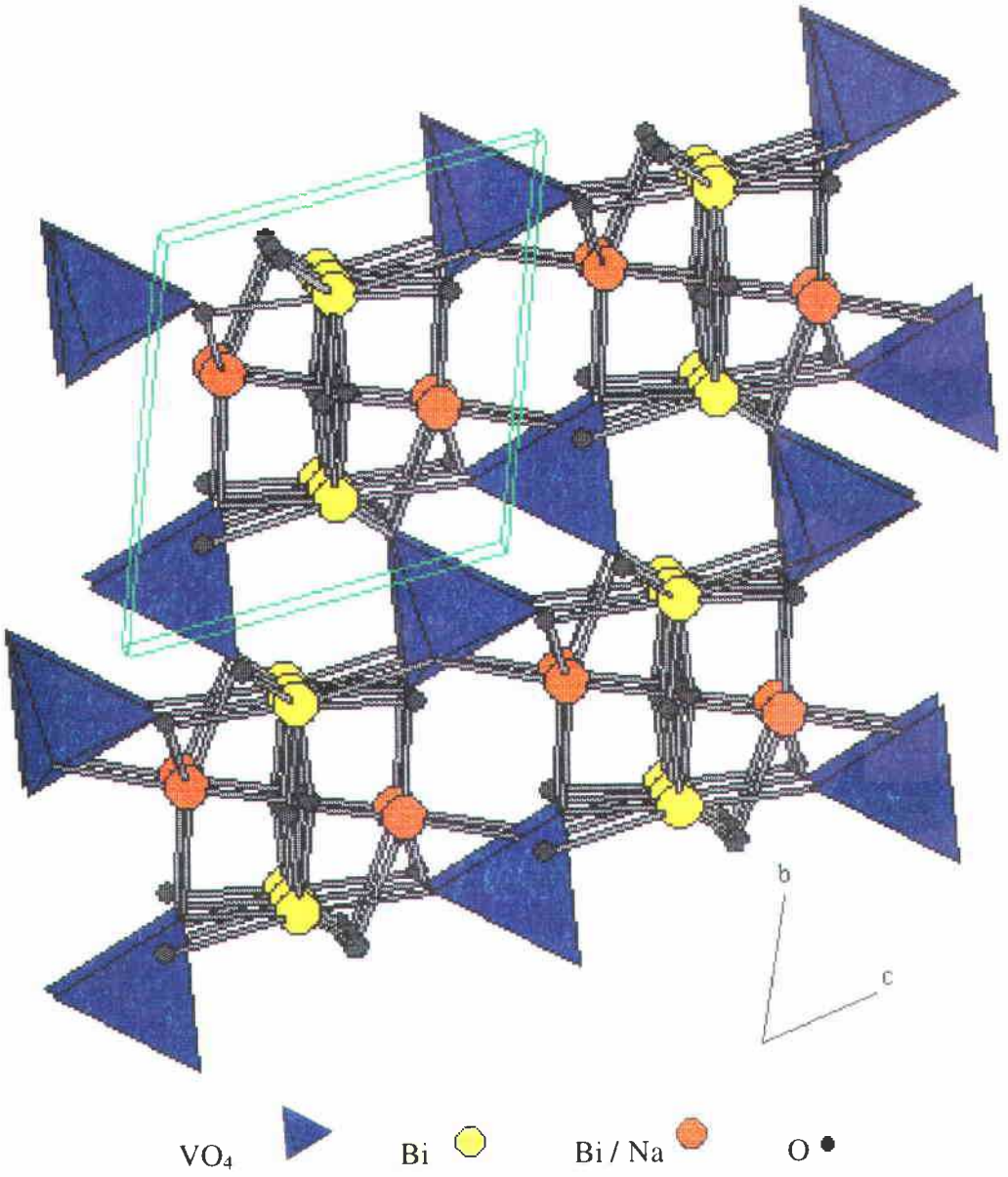

Figure 2.2. Crystal Structure of $NaBi_3V_2O_{10}$ with VO_4 Tetrahedron

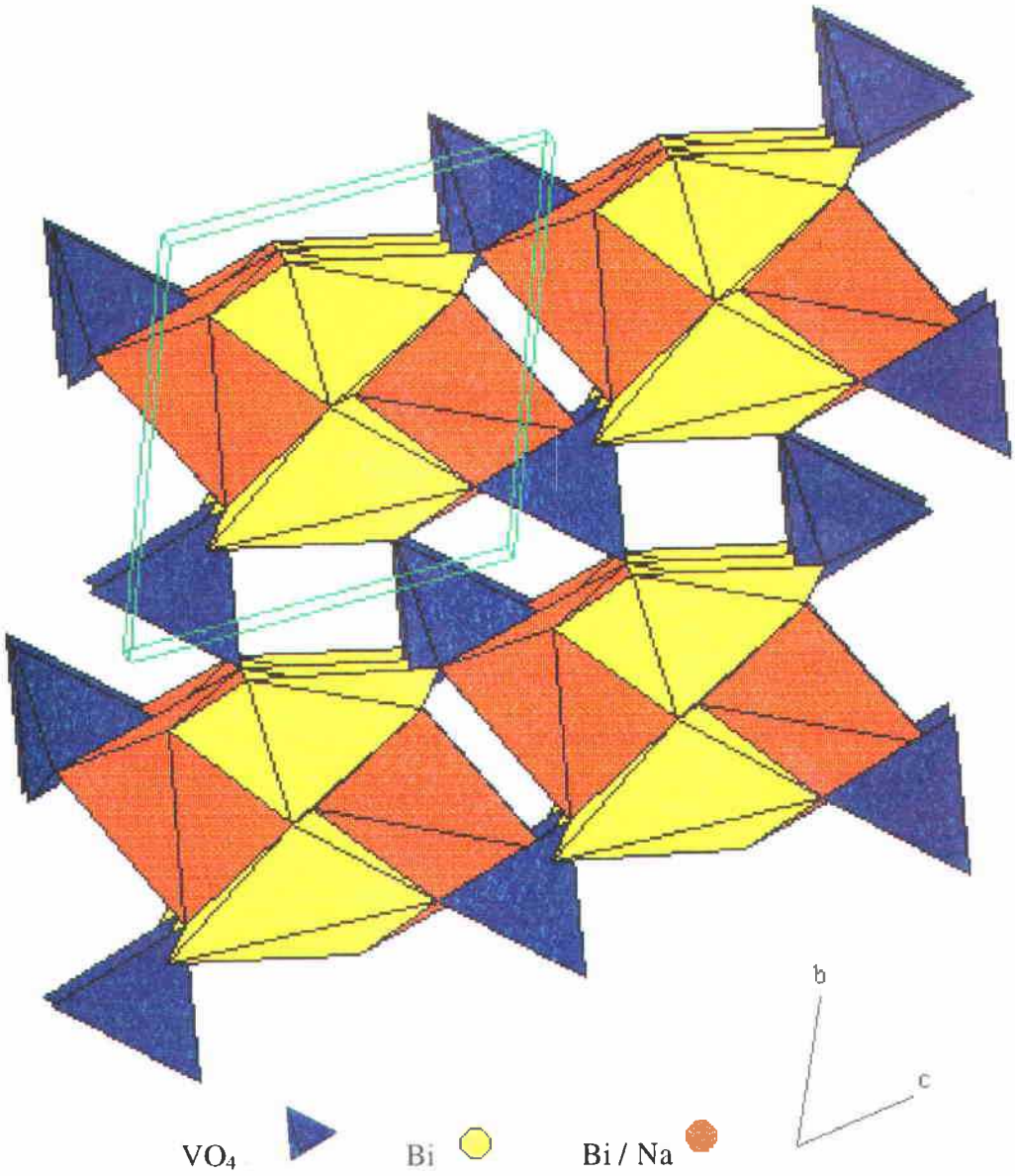

Figure 2.3. Crystal Structure of $NaBi_3V_2O_{10}$ with all Polyhedron

Two BiO_6, bismuth site one, octahedron share an O 3 to O 3 edge to form a Bi_2O_{10} dimeric unit. Each dimeric unit is connected to additional dimeric units in the a, b and c axis directions by corner sharing VO_4 tetrahedron. Figure 2.4 depicts the Bi_2O_{10} dimeric unit. This is not the standard bismuth-oxygen unit, but has been observed in $BiNiOPO_4$ (13) and $BiCoPO_4$ (14).

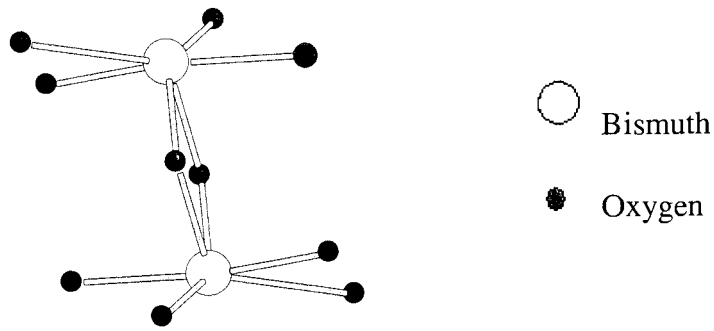

Figure 2.4. Bi_2O_{10} Dimeric Unit

2.4. Comparison of the α-$NaBi_3V_2O_{10}$ Structure with that in the Literature

A comparison of the structure obtained with that previously reported (3) was impeded by the fact that the previous report used a nonstandard triclinic crystal setting. Lepage, a program within the WINGX suite (6) was used to obtain the lattice transformation matrix and the atom parameter transformation matrix (Figure 2.5). The transformation was calculated by hand and verified by comparing the X-ray powder patterns, using PowderCell (15), of the system before and after the conversion.

$$T_{lattice} = \begin{matrix} 0 & 0 & -1 \\ 0 & 1 & 0 \\ 1 & 0 & 1 \end{matrix} \qquad T_{atoms} = \begin{matrix} 1 & 0 & 1 \\ 0 & 1 & 0 \\ -1 & 0 & 0 \end{matrix}$$

Figure 2.5. Transformation Matrixes Used for Conversion of Reported Structure

For a direct comparison of the newly transformed system with the structure we determined, it was necessary to translate the published system so both structures were defined by the same origin. The transformed and translated atomic positions and the method of translation can be found in Table 2.8.

Table 2.8. Transformed and Translated Published Atomic Positions

Atom	x	y	z	method	New Label
Bi 1	0.0816	0.7586	0.5264	0, + ½, + ½	Bi 1
Bi 2	0.3168	0.3792	0.2070	Inv, Inv + ½, Inv + ½	Bi 2
Na 1	0.3168	0.3792	0.2070	Inv, Inv + ½, Inv + ½	Na 1
V	0.3458	0.8474	0.1444	0, + ½, + ½	V
O 1	0.2372	0.4850	0.5458	+ 1, + ½, + ½	O 3
O 2	0.5891	0.9004	0.7175	+ 1, + ½, + ½	O 4
O 3	0.4014	0.2451	0.8238	1 – #, 1 – (# + ½), 2 – (# + ½)	O 5
O 4	0.1779	0.6698	0.2334	Inv, Inv + ½, Inv + ½	O 1
O 5	0.1504	0.7881	0.8645	0, + ½, + ½	O 2

The published positions were relabeled for direct comparison with our structure. Table 2.9 shows the atomic parameters for the published system, the single crystal solved system and the neutron refinement structure solution.

Table 2.9. Comparison of Atomic Positions for $NaBi_3V_2O_{10}$

Atom	Data Type	x	y	z
Bi 1	Published	0.082(1)	0.759(1)	0.526(5)
	Single Crystal	0.0838(1)	0.7574(1)	0.5283(1)
	Neutron	0.0816(6)	0.7598(4)	0.5288(5)
Bi 2 / Na	Published	0.3168(5)	0.379(2)	0.2070(2)
	Single Crystal	0.3134(2)	0.3822(2)	0.2103(2)
	Neutron	0.3091(8)	0.3794(7)	0.2004(8)
V	Published	0.346(1)	0.847(3)	0.1444(3)
	Single Crystal	0.3446(6)	0.8440(4)	0.1446(4)
	Neutron	0.3446(6)	0.8440(4)	0.1446(4)
O 1	Published O4	0.178(3)	0.7(2)	0.233(3)
	Single Crystal	0.159(3)	0.690(2)	0.217(2)
	Neutron	0.1562(9)	0.6926(6)	0.2170(7)
O 2	Published O5	0.150(2)	0.79(1)	0.86(2)
	Single Crystal	0.147(3)	0.803(2)	0.875(2)
	Neutron	0.1460(9)	0.8043(7)	0.8800(7)
O 3	Published O1	0.24(2)	0.48(2)	0.546(4)
	Single Crystal	0.252(3)	0.500(2)	0.527(2)
	Neutron	0.2552(9)	0.4988(6)	0.5333(7)
O 4	Published O2	0.59(1)	0.900(9)	0.718(5)
	Single Crystal	0.566(3)	0.895(2)	0.693(2)
	Neutron	0.5660(9)	0.8970(6)	0.6949(7)
O 5	Published O3	0.401(3)	0.245(4)	0.82(6)
	Single Crystal	0.380(3)	0.235(2)	0.833(3)
	Neutron	0.377(1)	0.2362(8)	0.8333(9)

ATOMS (16) was used to determine the difference in atomic positions, in Angstroms, for both the single crystal system and the reported system compared to the neutron data solution (Table 2.10). All three refinements give very similar positional parameters for the cations, and there is also good agreement between oxygen parameters obtained from single crystal X-ray diffraction data and neutron diffraction data. However, there is poor agreement between our results and the reported results for the oxygen positions. This difference is as great as 0.24 Å.

This of course results in very different bond lengths and calculated valences (17). A comparison of these bond distances and valence values is shown in Table 2.11.

Table 2.10. Difference Comparison of Atomic Positions for $NaBi_3V_2O_{10}$

Atom	Single Crystal vs. Neutron Difference in Position (Å)	Published vs. Neutron Difference in Position (Å)
Bi 1	0.0005	0.0003
Bi 2 / Na	0.0610	0.0507
V	0.0000	0.0249
O 1	0.0252	0.2420
O 2	0.0366	0.1441
O 3	0.0454	0.1934
O 4	0.0003	0.1560
O 5	0.0003	0.1842

The reported structure gives a very distorted VO_4 tetrahedron with V-O distances varying from 1.56 to 1.88 Å, whereas we find a much more regular VO_4 tetrahedron with V-O distances varying from 1.65 to 1.74 Å. Valences calculated for our refined structure are generally closer to expected values with the exception of the site occupied by both bismuth and sodium. Good agreement is not expected in this situation because local relaxation is expected to give somewhat different bond lengths depending on whether sodium or bismuth actually occupies the site.

Table 2.11. Bond Distances and Valence for Neutron Solution[a]

Atoms	Bond Length (Å)	Bond Valence	Bond Valence Totals
Bi 1 – O 1	2.331(6) *2.25(2)*	0.527 *0.642*	
Bi 1 – O 2	2.311(5) *2.23(3)*	0.556 *0.694*	
Bi 1 – O 3	2.163(6) *2.11(3)*	0.830 *0.935*	
Bi 1 – O 3	2.287(5) *2.20(4)*	0.592 *0.743*	
Bi 1 – O 4	2.438(6) *2.54(3)*	0.396 *0.298*	
Bi 1 – O 5	2.876(6) *2.88(4)*	0.121 *0.119*	Total Bi(1) = 3.022 *3.431*
Bi 2 / Na – O 1	2.429(7) *2.23(3)*	0.404 / 0.184 *0.691 / 0.315*	
Bi 2 / Na – O 2	2.487(7) *2.51(3)*	0.346 / 0.157 *0.317 / 0.144*	
Bi 2 / Na – O 3	2.408(8) *2.50(2)*	0.427 / 0.194 *0.326 / 0.148*	
Bi 2 / Na – O 3	2.308(6) *2.31(4)*	0.562/ 0.256 *0.558 / 0.254*	Total Bi only = 2.414
Bi 2 / Na – O 4	2.370(6) *2.25(3)*	0.474 / 0.216 *0.652 / 0.297*	Total Na only = 1.099
Bi 2 / Na – O 5	2.689(7) *2.82(3)*	0.200 / 0.091 *0.139 / 0.063*	Mean Sum[b] = 1.783 *1.952*
V – O 1	1.738(4) *1.87(3)*	1.186 *0.821*	
V – O 2	1.711(4) *1.76(3)*	1.296 *1.120*	
V – O 4	1.738(4) *1.66(3)*	1.195 *1.444*	
V – O 5	1.655(5) *1.56(4)*	1.472 *1.903*	Total V = 5.149 *5.288*

[a]Values in italics are from reference 3

[b]Mean Bond Valence Sum calculated as weighted average of 0.52 occupancy of Bi

The most important discrepancy between our results and those reported is with the occupation parameters for the oxygen atoms. We find that all five oxygen sites are fully occupied. The reported structure claims that one site (O 1 in Table 2.9. or O 3 in their paper) is only 90% occupied. Porob and Guru Row suggest that the high oxygen ion conductivity is related to this partial occupancy (3). All three refinements, and electron microprobe data, of α-$NaBi_3V_2O_{10}$ agree that the Bi:Na ratio on the Bi/Na site is not 1.0. Instead this site is bismuth rich by a small but significant amount. The reported structure gives this Bi:Na ratio as 56:44. Electron microprobe data identifies a ratio of 53:47 and both X-ray and neutron data find 52:48. This agreement between both occupancy refinements is good evidence that there are no vacancies on the Bi / Na site.

The oxygen conductivity in α-$NaBi_3V_2O_{10}$ is likely due to a small concentration of oxygen interstitials given by the formula $Na_{0.96}Bi_{3.04}V_2O_{10.04}$. Assuming that all the interstitial oxygen occupies one general position site, this would mean searching for a site only 2% occupied. There is no possibility that such a small amount of interstitial oxygen could be found with current x-ray and neutron data.

2.5. References

1. Derek C. Sinclair, Craig J. Watson, R. Alan Howie, Janet M.S. Skakle, Alison M. Coats, Caroline A. Kirk, Eric E. Lachowski and James Marr, *J. Mater. Chem.*, 8/2, 281 (1998)

2. Derek C. Sinclair, Eugenia Marinou and Janet M.S. Skakle, *J. Mater. Chem.*, 9, 2617 (1999)

3. Digamber G. Porob and T.N. Guru Row, *Chem. Mater.*, 12, 3658 (2000)

4. Oregon State University Microprobe Lab

5. R.H. Blessing, *Acta Crystallogr.*, Sect. A, 51, 33, (1995)

6. L.J. Farrugia, *J. Appl. Crystallogr.*, 32, 837 (1999)

7. G.M. Sheldrick, SHELX97-Programs for Crystal Structure Analysis, University of Goettingen, Germany (Release 97-2)

8. A.C. Larson, R.B. von Dreele, *Los Alamos Lab. Rep.*, LA-UR-86-748 (1987)

9. P. Thompson, D.E. Cox and J.B. Hastings, *J. Appl. Cryst.*, 20, 79 (1987)

10. R.D. Shannon, *Acta Cryst.*, A32, 751 (1976)

11. R.G. Teller, *Acta Cryst.*, C48, 2101 (1992)

12. O.A.S. Ahmed, A. Tairi, A. Chagraoui, S. Khairoun, J.-C. Champarnaud-Mesjard and B. Frit, *Ann. Chim. Sci. Mat.*, 25, 201 (2000)

13. F. Abraham and M. Ketatni, *Eur. J. Solid State Inorg. Chem.*, 32, 429, (1995)

14. Said Nadir, J.S. Swinnea and H. Steinfink, *J. Solid State Chem.*, 148,295 (1999)

15. W. Kraus and G. Nolze, PowderCell for Windows Version 2.3, Federal Institute for Materials Research and Testing, Berlin, Germany (1999)

16. E. Dowty, ATOMS Version 4.1 (1998)

17. I.D. Brown, Bond Valence Calculator, Institute for Materials Research, McMaster University, Hamilton, Ontario, Canada, L8S 4M1

Chapter 3

Structure of a Calcium Substituted Scheelite $BiVO_4$ Phase

3.1. Introduction

Scheelite, ABO_4, structures are commonly known for their mixed ionic and electric conductivity (1,2) and their ability to function as oxidative catalysts (3,4). $BiVO_4$ is a compound of this group that has been heavily explored. $BiVO_4$ is found in the scheelite, I $4_1/a$ (No. 88) space group at temperatures above 255°C and in the monoclinic I 2/b (No. 15) space group below 255°C (5). $BiVO_4$ occurs naturally as the mineral pucherite and can be prepared in the laboratory only in the tetragonal zircon or more stable monoclinic structure (5). The transition from the tetragonal space group to the monoclinic space group is reversible (6).

In 1994, a German research team discovered that the monoclinic structural phase of $BiVO_4$ could be doped up to 7% with calcium. They noted very little change in the lattice parameters but did no further investigation into the crystal structure (7).

The high temperature tetragonal phase of $BiVO_4$ has been stabilized at standard temperature by the substitution of Mo^{6+} for V^{5+} (8). For the first time M^{2+} substitution for Bi^{3+} in the tetragonal phase of $BiVO_4$ has been achieved. The monoclinic to tetragonal structural transition has been shown to be possible by the substitution of calcium for bismuth to form a new compound with the formula

$Ca_{0.29}Bi_{0.71}VO_{3.855}$. This calcium doped scheelite phase has recently been determined to be an oxide ion conductor comparable to that of yttria stabilized zironia (9).

3.2. Experimental

Single crystals were obtained, by serendipity, from an 8:5:5 stoichiometric mixture of K:V:Bi from K_2CO_3 (Mallinckrodt), NH_4VO_3 (Alpha Aesar) and Bi_2O_3 (Cerac). (The K_2CO_3 reagent, by use of powder X-ray diffraction, was later found to contain a $CaCO_3$ contaminant.) The reagents were ground for fifteen minutes in an agate mortar and heated in a Lindberg furnace for four cycles with ten-minute grinds between each cycle. The calcinations cycles can be found in Table 3.1. The final calcinations cycle was quenched from 534°C to room temperature.

Table 3.1. Calcination Cycles for Single Crystal Growth

Cycle	Plateau Temperature (°C)	Holding Time (Hours)	Cooling Rate (°C/min)
Cycle 1	500	22	5
Cycle 2	700	18	5
Cycle 3	700	18	5
Cycle 4	900	72	0.03

Very small, pale yellow and pale green, crystallites were obtained. Powder X-ray diffraction indicated a multiphase product and the resulting pattern did not

give any matches with the Siemens D5000 database. Patterns were recorded from a Siemens D5000 powder diffractometer with a Kevex detector, CuKα radiation (λ = 1.5418 Å) and vertical Soller slits.

A 0.10 by 0.10 by 0.08 mm, pale yellow, crystal was mounted onto a glass fiber with epoxy. Single crystal X-ray diffraction data were collected at room temperature on a Rigaku AFC6R diffractometer with monochromatic MoKα radiation (λ = 0.71069 Å). No decay was noted during data collection. The initial data processing and an absorption correction, by Psi-scans, to the full data set were applied using the programs from the TEXSAN crystallographic software package (10). Structure solution was carried out using Patterson Map interpretation as programmed in SHELXS-97 (11) and refined using full-matrix least-squares refinement on F^2 using the program SHELXL-97 incorporated in the WINGX suite (12). Details of the single crystal data collection are given in Table 3.2.

Qualitative wavelength dispersive electron microprobe analysis with a beam current of 49.65 nA, an accelerating voltage of 15.16 kV and a 5 μm beam diameter was performed on the crystallite used to obtain single crystal X-ray data and also on multiple crystallites from the sample (13). The majority of crystallites contained potassium while a minority contained calcium. The crystallite used to collect single crystal X-ray diffraction data contained calcium and no significant amount of potassium.

3.3 Structural Analysis

$Ca_{0.29}Bi_{0.71}VO_{3.855}$ crystallizes in the tetragonal space group $P\bar{4}$ (No. 81) with four molecular units per unit cell. Lattice parameters can be found in Table 3.2.

Table 3.2. Crystallographic Data for $Ca_{0.29}Bi_{0.71}VO_{3.855}$

radiation source	Rigaku AFC6R
radiation	Mo Kα
λ (Å)	0.71069, graphite monochrometer
θ range (deg)	1.74 – 27.49
hkl regions	-1 – 6, -1 – 6, -1 – 15
crystal size (mm)	0.10, 0.10, 0.08
color	pale yellow
formula	$Ca_{0.29}Bi_{0.71}VO_{3.855}$
fw	272.62
density (g/cm^3)	5.132
absorption correction	Psi-scans & symmetry equivalents
absorption coefficient (mm^{-1})	30.918
refinement method	full-matrix least squares on F^2
extinction coefficient	0.032(7)
space group	$P\bar{4}$
a (Å)	5.121(5)
c (Å)	11.701(5)
V ($Å^3$)	306.9(4)
z	4
no. of measured reflections	708
no. of independent reflections	590 (R_{int}= 11.56)
no. of reflections $I > 2\sigma(I)$	275
no. of refined parameters	58
R_1 (%)	7.20
wR_2 (%)	13.65
goodness of fit	1.506

The space group was determined from merging statistics of the Laue symmetries, systematic absences and systematic structure solution attempts using SIR92 (14). A partial list of reflections violating the body-centered condition are displayed in Table 3.3.

Table 3.3. Reflections Violating Body-Centered Condition

h	k	l	F^2	Sigma
-1	0	0	242.74	10.43
-1	0	2	313.29	14.43
-1	0	4	183.54	8.51
-1	1	-1	111.70	6.99
-1	2	0	233.92	10.99
-1	2	2	115.88	7.53
0	-1	0	533.64	24.18
0	-1	2	675.22	30.78
0	-1	4	256.90	12.26
0	1	0	550.18	24.55
0	1	2	829.80	35.36
0	1	4	159.49	7.93
1	0	0	239.03	10.46
1	0	2	365.69	17.04
1	0	4	223.09	10.38
1	2	0	238.53	7.47
1	2	2	148.60	8.16
2	1	0	182.40	6.34
2	-1	2	123.33	8.20
2	1	0	186.74	5.30

The bismuth positions were determined using a Patterson, heavy-atom, approach. Subsequent least-squares refinements and Fourier map analyses were used to determine the vanadium and oxygen positions. Potassium positions could not be located.

Electron microprobe data revealed the presence of calcium and the absence of potassium in the single crystal used to collect X-ray diffraction data. Specific calcium sites were not apparent in the structure solution. The ionic radii of Bi^{3+} and Ca^{2+} being very similar (1.17 *vs* 1.12 Å for 8 fold coordination)(15) and reported disorder of both Bi^{3+} and Ca^{2+} on the same site in $BiCa_9V_7O_{28}$ (16) and $BiCa_4V_3O_{12}$ (17) suggested a shared site might be possible for the new compound $Ca_{0.29}Bi_{0.71}VO_{3.855}$. The bismuth/calcium disorder was modeled by placing both atom types on each site and refining occupancies. The necessary constraints were introduced on positional and displacement parameters for these sites. Two of the three bismuth sites were found to contain significant amounts of calcium.

All remaining atomic site occupancies and anisotropic displacement parameters were refined. All atom sites were found to be fully occupied, excluding O 1, which was refined to have an occupancy of 0.92 from the original 1.00. Atomic positions, occupancy data and displacement parameters can be found in Table 3.4 and 3.5.

Table 3.4. Atom Parameters for $Ca_{0.29}Bi_{0.71}VO_{3.855}$

Atom	x	y	z	Occupancy
Bi 1	1.0000	1.0000	0.0000	0.732(3)
Ca 1	1.0000	1.0000	0.0000	0.268(3)
Bi 2	0.5000	0.5000	0.5000	1.00000
Bi 3	1.0000	0.5000	0.2501(5)	0.576(8)
Ca 2	1.0000	0.5000	0.2501(5)	0.424(8)
V 1	0.5000	0.5000	0.0000	1.00000
V 2	0.0000	0.0000	0.5000	1.00000
V 3	0.5000	0.0000	0.249(1)	1.00000
O 1	0.132(5)	0.237(5)	-0.578(2)	0.92(4)
O 2	0.360(5)	-0.248(4)	0.328(2)	1.00000
O 3	0.252(5)	0.142(6)	0.167(2)	1.00000
O 4	0.738(9)	1.379(6)	0.069(2)	1.00000

Table 3.5. Displacement Parameters[a] for $Ca_{0.29}Bi_{0.71}VO_{3.855}$

Atom	Ueq	U11	U22	U33	U12	U13	U23
Bi 1	23(1)	21(2)	21(2)	26(2)	0	0	0
Ca 1	23(1)	21(2)	21(2)	26(2)	0	0	0
Bi 2	35(1)	32(2)	32(2)	40(2)	0	0	0
Bi 3	16(1)	15(2)	14(2)	19(2)	-6(204)	0	0
Ca 2	16(1)	15(2)	14(2)	19(2)	-6(204)	0	0
V 1	10(3)	15(4)	15(4)	5(5)	0	0	0
V 2	48(8)	60(12)	60(12)	22(10)	0	0	0
V 3	9(2)	16(5)	9(5)	1(3)	-2(5)	0	0
O 1	15(5)	16(13)	28(15)	0(9)	-11(13)	-1(9)	8(9)
O 2	14(6)	22(15)	4(11)	15(12)	-6(12)	-4(11)	9(9)
O 3	27(7)	20(14)	45(17)	17(13)	26(13)	-17(9)	-7(13)
O 4	9 (14)	24(40)	47(18)	8(13)	-9(21)	8(18)	-28(12)

[a]All values represent displacement parameters multiplied by 1000

All bismuth and bismuth/calcium sites have an 8-fold coordination with oxygen while the vanadium sites have 4 coordinate VO_4 tetrahedron. Figure 3.1 depicts the $Ca_{0.29}Bi_{0.71}VO_{3.855}$ structure with only the VO_4 tetrahedron included.

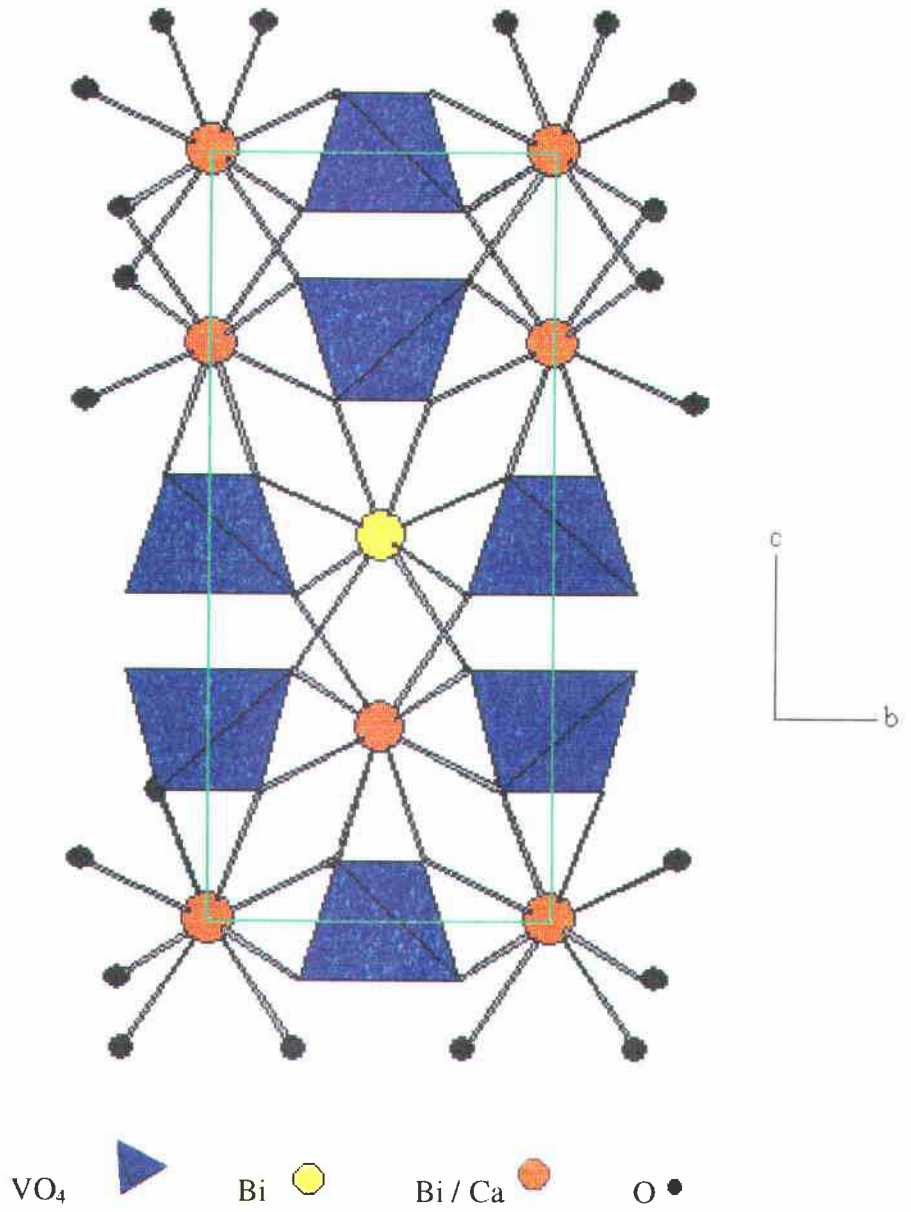

Figure 3.1. Crystal Structure of $Ca_{0.29}Bi_{0.71}VO_{3.855}$ with VO_4 Tetrahedron

The three dimensional framework of $Ca_{0.29}Bi_{0.71}VO_{3.855}$ can be described as interpenetrating rings of edge sharing BiO_8, or Bi/CaO_8, polyhedron with VO_4 tetrahedron bridging the centers of each ring. Figure 3.2 depicts this three-dimensional polyhedron network.

3.4. Discussion

The monoclinic to tetragonal structural transition of $BiVO_4$ was shown to be possible, for the first time, by the substitution of Ca^{2+} for Bi^{3+}. Table 3.6 shows the lattice parameters for tetragonal, scheelite, $BiVO_4$ and the new species $Ca_{0.29}Bi_{0.71}VO_{3.855}$. The calcium substituted compound data was at room temperature while the unsubstituted compound data were obtained at 293°C. Very little changes to the lattice parameters occur due to the calcium substitution. The calcium doped monoclinic $BiVO_4$ phase also maintained the original lattice parameters (7). Figure 3.3 depicts the tetragonal crystal structure of $BiVO_4$.

Table 3.6. Lattice Parameter Comparison of $BiVO_4$[a] and $Ca_{0.29}Bi_{0.71}VO_{3.855}$

Compound	Space Group	a (Å)	c (Å)	V (Å^3)
$BiVO_4$	$I\,4_1/a$	5.1470(4)	11.721(1)	310.5(3)
$Ca_{0.29}Bi_{0.71}VO_{3.855}$	$P\,\bar{4}$	5.121(5)	11.701(5)	306.9(4)

[a]$BiVO_4$ values obtain from reference 5

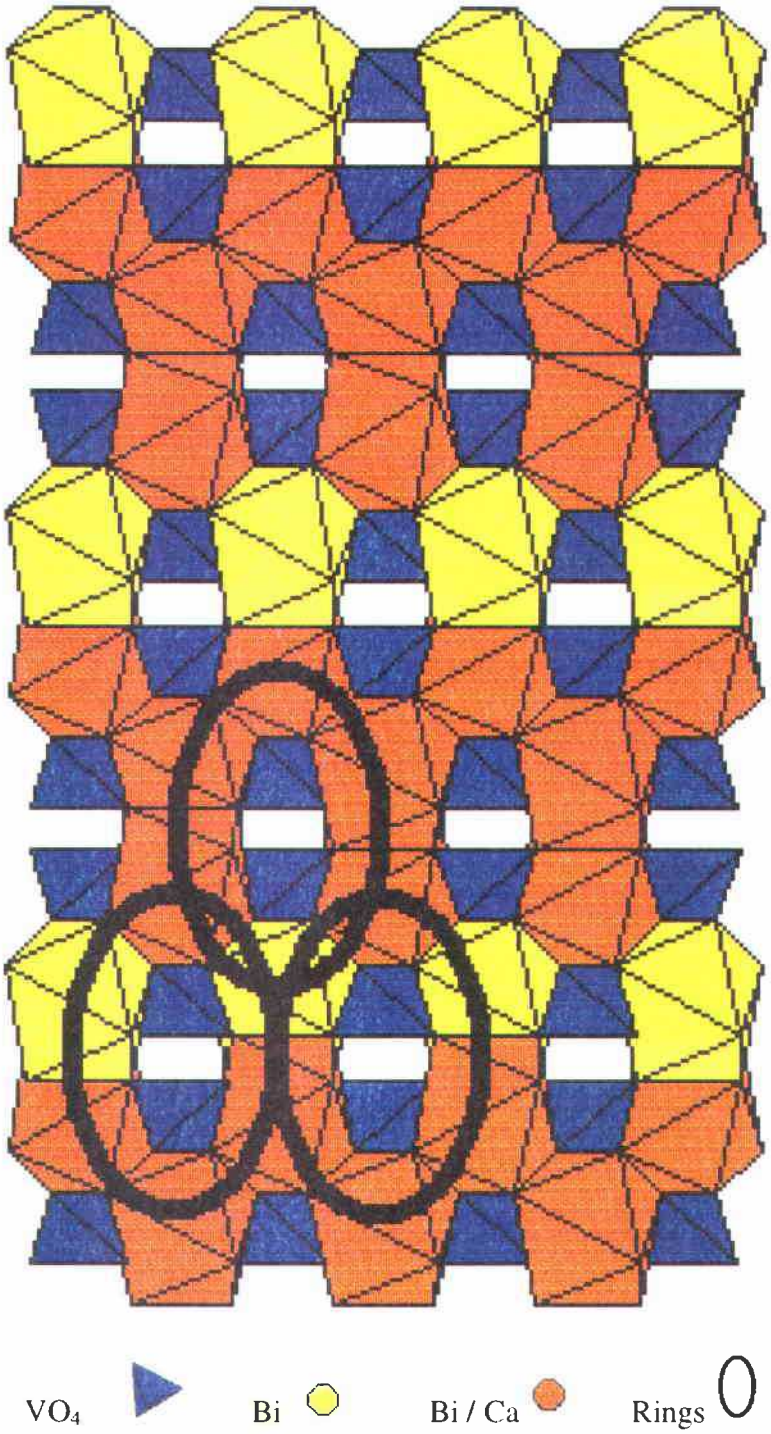

Figure 3.2. Three Dimensional Polyhedron Ring Network of $Ca_{0.29}Bi_{0.71}VO_{3.855}$

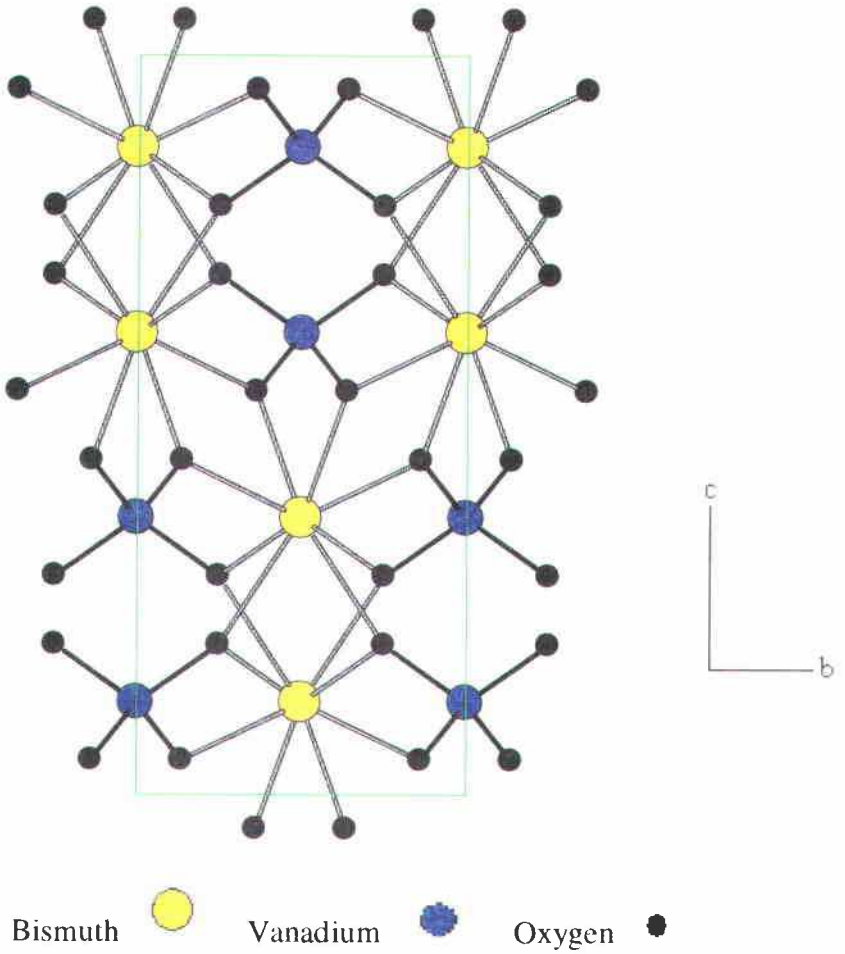

Figure 3.3. Tetragonal Scheelite Crystal Structure of $BiVO_4$

The substitution of Ca^{2+} for Bi^{3+} results in a reduction of net cation charge. Color indicates no oxidation of Bi^{3+} or reduction of V^{5+}. Thus, to maintain charge balance with Bi^{3+}, Ca^{2+}, V^{5+} and O^{2-} it is necessary for the structure of $Ca_{0.29}Bi_{0.71}VO_{3.855}$ to have oxygen vacancies. This vacancy is largely accounted for in the occupancy refinement of O 1, which would give $(Ca,Bi)VO_{3.92}$. The displacement parameters of V 2 and Bi 2, which are connected to the partially

occupied O 1 site, are expected to be higher than those of the other sites. This is indeed true in our structure solution. The $Ca_{0.29}Bi_{0.71}VO_{3.855}$ structure with the O 1 site is clearly depicted in Figure 3.4.

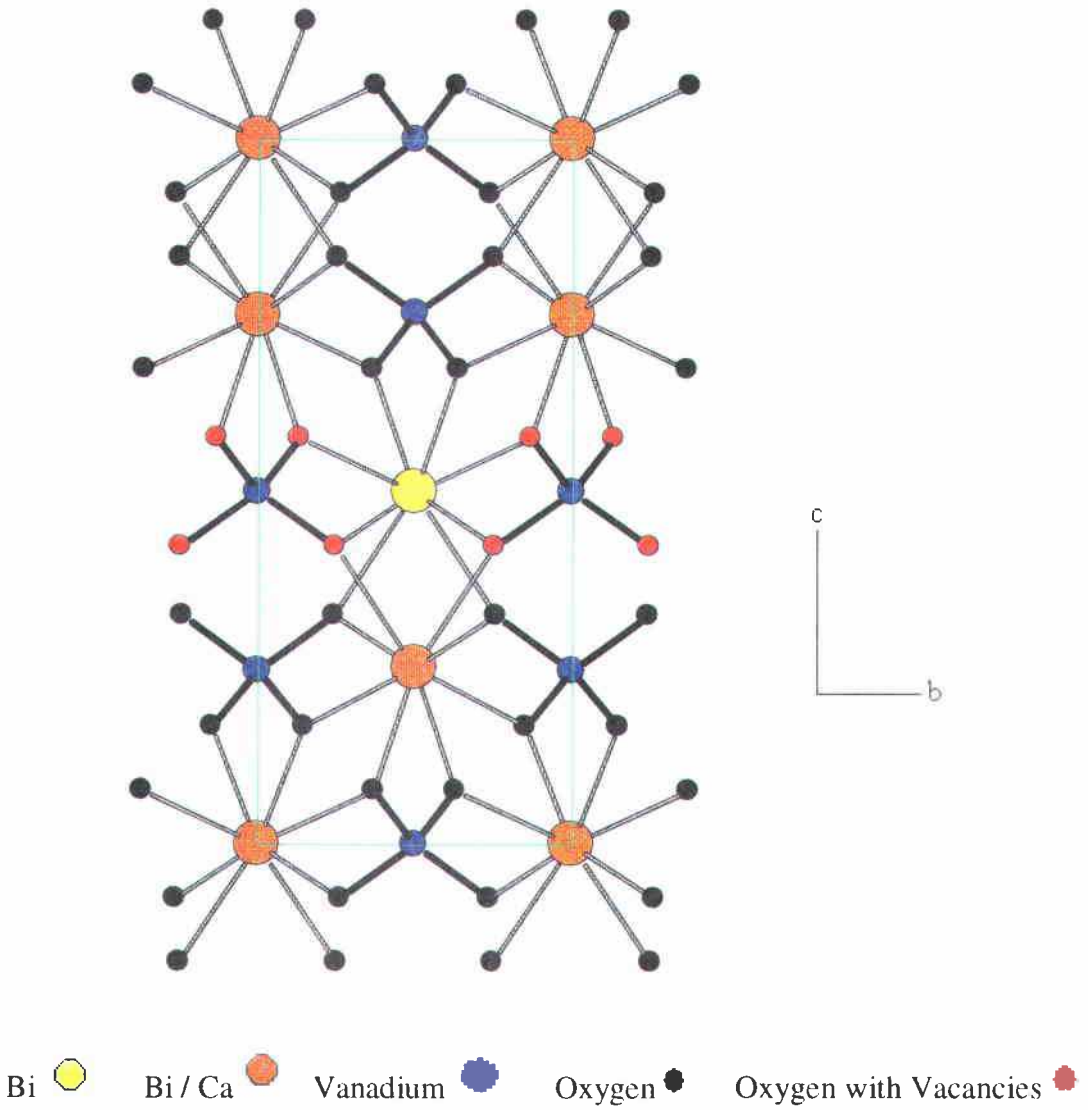

Figure 3.4. $Ca_{0.29}Bi_{0.71}VO_{3.855}$ Structure with Oxygen Vacancies Depicted

The substitution of calcium for bismuth reduces the symmetry of the crystal structure. We believe a reasonable explanation for this decrease in symmetry is due to the partial ordering of the Bi/Ca sites and the disorder of the oxygen positions. Bond length and bond valence (18) values can be found in Table 3.7. The discrepancies between the bond valence sums and the expected values, are illustrative of the limits of current bond valence programs for representing local relaxation for mixed atom sites, and are suggestive of the oxygen disorder we believe to be present.

Electron diffraction was performed on the powder samples. No appearance of a superstructure was found. This result is in agreement with the search for a superstructure performed by X-ray diffraction techniques on the single crystal.

Further studies are necessary to confirm the precise structure of $Ca_{0.29}Bi_{0.71}VO_{3.855}$. A structurally analogous cadmium substituted tetragonal $BiVO_4$ system is currently under investigation. Once a precise structural determination is achieved models to explain the high oxide ion conductivity (8) can be explored.

Table 3.7. Bond Distances and Bond Valence for $Ca_{0.29}Bi_{0.71}VO_{3.855}$

Atoms	#	Bond Length (Å)	Bond Valence	Bond Valence Totals
Bi 1 / Ca 1 – O 3	4	2.45(2)	0.382 / 0.271	Sum All Bi = 2.900
Bi 1 / Ca 1 – O 4	4	2.49(4)	0.343 / 0.243	Sum All Ca = 2.057
				Mean Sum = 2.674
Bi 2 – O 1	4	2.48(2)	0.352	
Bi 2 – O 2	4	2.49(2)	0.343	Sum = 2.781
Bi 3 / Ca 2 – O 1	2	2.52(2)	0.325 / 0.230	
Bi 3 / Ca 2 – O 2	2	2.43(2)	0.403 / 0.286	Sum All Bi = 2.874
Bi 3 / Ca 2 – O 3	2	2.44(2)	0.393 / 0.278	Sum All Ca = 2.039
Bi 3 / Ca 2 – O 4	2	2.52(4)	0.316 / 0.224	Mean Sum = 2.520
V 1 – O 4	4	1.59(4)	1.778	Sum = 7.113
V 2 – O 1	4	1.66(2)	1.472	Sum = 5.887
V 3 – O 2	2	1.73(2)	1.218	
V 3 – O 3	2	1.75(2)	1.154	Sum = 4.744
O 1 – V 2	1	1.66(2)	1.472	Sum All Bi = 2.149
O 1 – Bi 2	1	2.48(2)	0.352	Sum All Ca = 2.054
O 1 – Bi 3 / Ca 2	1	2.52(2)	0.325 / 0.230	Mean Sum = 2.109
O 2 – V 3	1	1.73(2)	1.218	Sum All Bi = 1.964
O 2 – Bi 2	1	2.49(2)	0.343	Sum All Ca = 1.847
O 2 – Bi 3 / Ca 2	1	2.43(2)	0.403 / 0.286	Mean Sum = 1.914
O 3 – V 3	1	1.75(2)	1.154	Sum All Bi = 1.929
O 3 – Bi 1 / Ca 1	1	2.45(2)	0.382 / 0.271	Sum All Ca = 1.703
O 3 – Bi 3 / Ca 2	1	2.44(2)	0.393 / 0.278	Mean Sum = 1.850
O 4 – V 1	1	1.59(4)	1.778	Sum All Bi = 2.437
O 4 – Bi 1 / Ca 1	1	2.49(4)	0.343 / 0.243	Sum All Ca = 2.245
O 4 – Bi 3 / Ca 2	1	2.52(4)	0.316 / 0.224	Mean Sum = 2.371

[b]Mean Bond Valence Sum calculated as weighted average of Calcium and Bismuth site occupation

3.5. References

1. T. Lu and B.C.H. Steele, *Solid State Ionics*, 21, 339 (1986)

2. I.C. Vinke, J.Diepgrond, B.A. Boukamp, K.J. de Vries and A.J. Burggraaf, *Solid State Ionics*, 57, 83 (1992)

3. A.W. Sleight and W.J. Linn, *Ann. New York Acad. Sci.*, 272, 23 (1976)

4. A.W. Sleight, K. Aykan and D.B. Rogers, *J. Solid State Chem.*, 13, 231 (1975)

5. A.W. Sleight, H.-y. Chen and A. Ferretti, *Mat. Res. Bull.*, 14, 1571, (1979)

6. R.S. Roth and J.L. Waring, *Amer. Miner.*, 48, 1348 (1963)

7. L. Hoffart, U. Heider, L. Jorissen, R.A. Huggins and W. Witschel, *Solid State Ionics*, 72, 195 (1994)

8. A.W. Sleight, K. Aykan and D.B. Rogers, *J. Solid State Chem.*, 13, 231 (1975)

9. S. Uma, R.J. Bliesner and A.W. Sleight, "Gross Oxygen Deficiency and Oxide Ion Conductivity in the Scheelite Structure", presented June 13-17, 2001 NORM American Chemical Society Meeting

10. TEXSAN, Single Crystal Structure Analysis Software, Version 5.0, Molecular Structure Corporation, The Woodlands, TX, 1989

11. G.M. Sheldrick, SHELX97-Programs for Crystal Structure Analysis, University of Goettingen, Germany (Release 97-2)

12. WinGX Ver 1.63.01, L.J. Farrugia, *J. Appl. Cryst.*, 32, 837 (1999)

13. Electron Microprobe Lab at Oregon State University

14. A. Altomare, G. Cascarano, C. Giacov and A. Gualardi, *J. Appl. Cryst.*, 26, 343 (1993)

15. R.D. Shannon, *Acta Cryst.*, A32, 751 (1976)

16. J.S.O. Evans, J. Huang and A.W. Sleight, J. Solid State Chem., 157, 255 (2001)

17. J. Huang and A.W. Sleight, *J. Solid State Chem.*, 104, 52 (1993)

18. I.D. Brown, Bond Valence Calculator, Institute for Materials Research, McMaster University, Hamilton, Ontario, Canada, L8S 4M1

Chapter 4

Disorder in a New Potassium Bismuth Vanadate: $K_{10}Bi_4V_4O_{21}$

4.1. Introduction

There are two structurally characterized potassium bismuth vanadates on record. The first was obtained in 1987 by Debreuille-Gresse and Abraham, $K_3Bi_2(VO_4)_3$ (1). In 1999 Mentre, Dhaussy and Abraham characterized $K_{0.2}Bi_{1.45}V_8O_{16}$ (2). Other potassium containing bismuth vanadates-including $Na_2Bi_2(VO_4)_3$ (1), variants within the hollandite-type family (2) and potassium doped $Bi_4V_2O_{11}$ (3) solid solutions-have been cited, but no crystallographic structural solution has been reported. Single crystals of a new potassium bismuth vanadate, $K_{10}Bi_4V_4O_{21}$, have been grown and a $P\bar{6}$ crystal structure has been proposed.

4.2. Experimental

Single crystals were first obtained from a 2:1:1 stoichiometric mixture of K:Bi:V from KNO_3 (Mallinckrodt), Bi_2O_3 (Cerac) and NH_4VO_3 (Alfa Aesar). All reagents were dried overnight at 200°C. The reagents were ground for twenty minutes in an agate mortar and calcinated, in three cycles, with intermediate fifteen minute grinds. Alumina crucibles and covers were used for calcinations in a Lindberg furnace. An additional sample with identical stoichiometric ratios was

prepared simultaneously. This second sample contained V_2O_5 (Johnson Matthey) in the place of NH_4VO_3.

Both preparations yielded pale yellow crystallites in the crucibles and iridescent green crystallites along the upper crucible walls. The distinguishing difference between the two sample preparations was that the NH_4VO_3 sample contained slightly darker yellow crystallites. Powder X-ray diffraction indicated the multiphase nature of the NH_4VO_3 prepared sample.

Multiple syntheses using 2:1:1 stoichiometric ratios of K:Bi:V were attempted. Table 4.1 describes the optimal single-phase synthesis approach. A multistep calcination process was essential to obtain a single-phase material. The best single crystals arose from the polycrystalline samples prepared in this manner.

Table 4.1. Calcination Cycles for Single Crystal Growth

Cycle	Plateau Temperature (°C)	Holding Time (Hours)	Cooling Rate (°C/min)
Cycle 1	400	18	5
Cycle 2	550	18	5
Cycle 3	650	18	5
Cycle 4	850	36	0.1

An initial calcination temperature greater than 550°C generated the monoclinic form of $BiVO_4$. A calcination time longer than 48 hours, for the final cycle, yielded a mixture of the desired pale yellow product and a darker maize-yellow polycrystalline product.

All synthesis attempts in sealed silica tubes proved unsuccessful. The tubes exploded during the cooling cycle. An alumina lid or covering for the crucibles was needed to prevent sample evaporation during the heating process.

Wavelength dispersive electron microprobe analysis with a beam current of 50.0 nA, an accelerating voltage of 15 kV and a beam diameter of 5 μm, was used to establish an approximate molar ratio of 2:1:1 for potassium, bismuth and vanadium (4).

Powder X-ray diffraction was used to monitor the content of the obtained products. Patterns were recorded from a Siemens D5000 powder diffractometer with a Kevex detector, CuKα radiation (λ = 1.5418 Å) and vertical Soller slits.

Single crystal X-ray diffraction data were collected for two crystallites. Each crystal was from a different synthesis but both samples generated identical powder X-ray diffraction patterns. These data were collected at room temperature on a Rigaku AFC6R diffractometer with monochromatic MoKα radiation (λ = 0.71069 Å). A decay in intensity was apparent. The decay was corrected for using a first order polynomial. The final intensities of the reference peaks were at 84% their original value.

The observed intensities were corrected for Lorentz polarization and absorption. Data reduction was carried out using a local program, capable of creating a data file containing the crystal dependent direction cosines of the diffracted and reverse incident beam, for purposes of correction of absorption anisotropy problems. Once a suitable structural model was obtained, absorption

corrections were applied using the program DIFABS (5) as programmed in the software collection WINGX V1.64.02 (6). Structure solution was carried out using Patterson Map interpretation and refined using full-matrix least-squares refinement on F^2 using the program SHELXL-97 (7).

A complete data set was not obtained for the first crystal collected on, crystal A. The data collection stopped midway through the experiment because the reference peaks could not be found. Initially it was assumed that the crystallite deteriorated so much over time that the diffraction intensities simply disappeared. A thorough analysis of the data, including a plot of intensity verses time for the reference peaks, provided a more optimistic answer. As depicted in Figure 4.1 the reference peaks do indeed deteriorate over time, but there was a sudden plummet in the intensity of all three reference peaks. This can be best explained by the crystallite dislodging from its centered position atop the glass fiber. Nail polish is not an efficient adhesive for mounting these crystals.

The lattice parameters obtained from the single crystal X-ray diffraction data of crystal A were used in conjunction with the program CELREF (8) to index the powder X-ray diffraction for the single phase samples. The X-ray diffraction pattern for the title compound is depicted in Figure 4.2. Table 4.2 provides a partial indexing list for the compound $K_{10}Bi_4V_4O_{21}$.

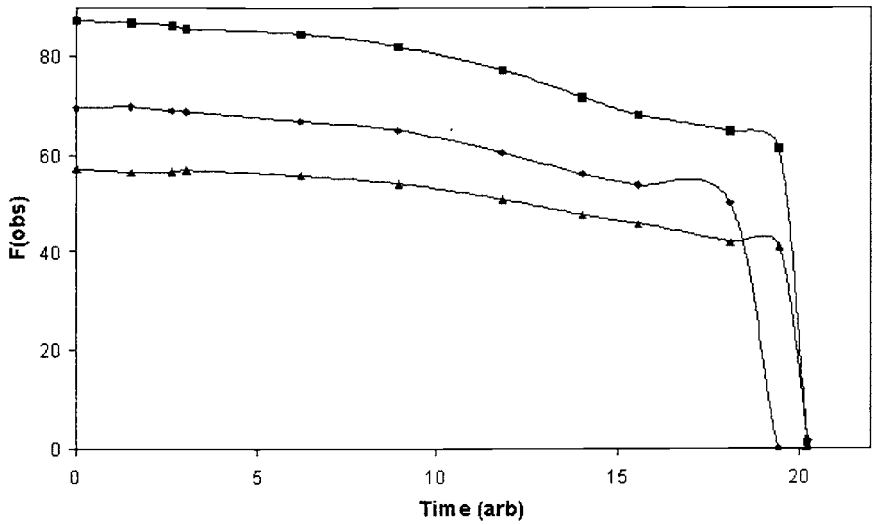

Figure 4.1. Dramatic Drop in Reference Peak Intensities for Crystal A

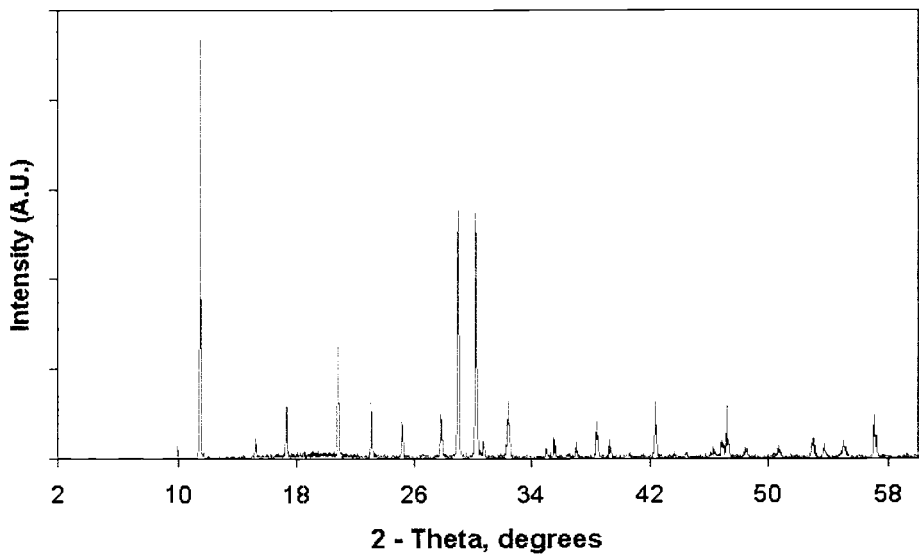

Figure 4.2. Powder X-ray Diffraction Pattern for $K_{10}Bi_4V_4O_{21}$

Table 4.2. Pattern Indexing for $K_{10}Bi_4V_4O_{21}$

h	k	l	2 - Theta
1	0	0	10.000
0	0	1	11.529
1	0	1	15.285
1	1	0	17.366
1	1	1	20.894
0	0	2	23.178
1	0	2	25.298
1	2	0	26.665
1	1	2	29.108
0	3	0	30.235
2	0	2	30.850
3	0	1	32.533
0	0	3	35.075
1	2	2	35.616
2	2	1	37.108
3	0	2	38.506
1	1	3	39.392
0	2	3	40.616
2	2	2	42.526
3	1	2	43.799
1	2	3	44.598
3	0	3	47.027
4	1	0	47.083
1	0	4	48.550
2	2	3	50.500
5	0	1	53.131
3	3	0	53.859
1	2	4	55.194
3	0	4	57.288

A complete single crystal X-ray diffraction data set was recorded for crystal B. Details of this data collection, including lattice parameters, are given in Table 4.3.

Table 4.3. Crystallographic Data for $K_{10}Bi_4V_4O_{21}$

radiation source	Rigaku AFC6R
radiation	Mo Kα
λ (Å)	0.71069, graphite monochrometer
θ range (deg)	2.30 – 29.96
hkl regions	-14 – 12, -1 – 14, -1 – 6
crystal size (mm)	0.05, 0.03, 0.03
color	pale yellow
formula	$K_{10}Bi_4V_4O_{21}$
fw	883.34
density (g/cm^3)	4.241
absorption correction	DIFABS
absorption coefficient (mm^{-1})	28.219
refinement method	full-matrix least squares on F^2
extinction coefficient	0.004(2)
space group	P $\bar{6}$
a (Å)	10.205(2)
c (Å)	7.669(2)
α (deg)	90
γ (deg)	120
V ($Å^3$)	691.7(3)
z	2
no. of measured reflections	2309
no. of independent reflections	1168
no. of reflections $I > 2\sigma(I)$	1010
no. of refined parameters	57
R_1 (%)	8.76
wR_2 (%)	10.17
goodness of fit	1.564

4.3. Structural Analysis

$K_{10}Bi_4V_4O_{21}$ crystallizes in the hexagonal space group P $\bar{6}$ (No. 174) with Two molecular units per unit cell. Initial selection of a space group was not trivial. E-statistics strongly suggested a noncentrosymmetric space group (9). The R_{int} values for merging under all Laue symmetries were similar

for $\bar{3}$ (hex), $\bar{3}$ m1(hex), $\bar{3}$ 1m(hex), 6/m and 6/mmm. The smallest R_{int} was for the $\bar{3}$ (hex) Laue group so this became the starting point.

No systematic absences were observed, which narrowed the space group selections to P 3 (No. 143) and P $\bar{3}$ (No. 147). SIR92 (10) was used to select P 3 base on R_1 values. A wagon wheel composed of bismuth and potassium emerged. There were atoms remaining to be assigned, but the residuals did not make any sense. The structure appeared to have additional symmetry and PLATON (11) was used to establish that a hexagonal space group may prove to be a better model.

Attempts to solve the structure in P $\bar{6}$ m2 and P 6/mmm were hindered by high R_1 values, undetermined atom placement and residual ghosts. The wagon wheel once again appeared in these two space groups, as well as any space group the structure solution was attempted in.

Debreuille-Gresse and Abraham were unable to locate oxygen positions in the $K_3Bi_2(VO_4)_3$ structure, until additional absorption corrections were carried out (1). After applying an absorption correction through DIFABS(5), using the stable atom positions, additional oxygen positions were detectable. The high displacement parameters and residual ghosts still indicated a space group problem.

SIR92 (10) was used to determine the structural solutions for a number of different space groups. Table 4.4 depicts the SIR92 results.

Table 4.4. SIR92 Structural Solution Statistics

Space Group	R_1 (%)	Space Group	R_1 (%)
P 3	11.54	P 622	24.23
$P\bar{3}$	21.85	P 6mm	15.55
P 6	24.28	$P\bar{6}2m$	13.35
$P\bar{6}$	10.08	$P\bar{6}m2$	12.61
P 6/m	31.35	P 6/mmm	15.32

The $P\bar{6}$ space group was selected for four reasons. First, all cation positions were determined by SIR92 and the resulting R_1 statistic was pleasing. Secondly, applying the DIFABS correction, using the stable model that arises independent of space group, decreases both R_1 and wR_2 by 24% and the R_{int} drops to 8.85%. The third reason is that all atoms can be assigned to residual peaks and charge balance is obtained. Lastly, the ghost peaks disappear for the majority of atomic positions.

The bismuth positions were determined using a Patterson, heavy atom, approach. Subsequent least-squares refinements and Fourier map analyses were used to determine the potassium, vanadium and oxygen positions. Two bismuth, three potassium, three vanadium and six oxygen sites were located. Site occupancies were refined, while maintaining the necessary constraints, and found to be fully occupied. The V 2, V 3 positions represent a split vanadium site. Each has an occupancy of 0.5, providing a total occupancy of 1.00. Atomic positions, isotropic displacement parameters for V 2, V 3, O 1, O 2, O 3, O 4, O 5 and anisotropic displacement parameters for Bi 1, Bi 2, K 1, K 2, K 3 and V 1 were

refined. Atomic positions and occupancy data can be found in Table 4.5. Table 4.6 displays the appropriate isotropic and/or anisotropic displacement parameters. The structure of $K_{10}Bi_4V_4O_{21}$ is depicted in Figures 4.3 and 4.4.

Table 4.5. Atomic Parameters[a] for $K_{10}Bi_4V_4O_{21}$

Atom	x	y	z	Occupancy
Bi 1	0.0000	0.0000	0.0000	1.0000
Bi 2	-0.3403(2)	-0.3398(2)	0.0000	1.0000
K 1	0.3159(8)	0.3108(7)	0.237(2)	1.0000
K 2	0.343(2)	0.993(2)	0.5000	1.0000
K 3	0.962(4)	-0.02(2)	0.5000	1.0000
V 1	0.6667	0.3333	0.281(2)	1.0000
V 2	0.3333	0.6667	0.149(5)	0.5000
V 3	0.3333	0.6667	0.26(1)	0.5000
O 1	-0.166(4)	-0.164(4)	0.174(5)	1.0000
O 2	-0.504(7)	-0.327(7)	0.213(7)	1.0000
O 3	-0.333(7)	-0.503(7)	0.211(7)	1.0000
O 4	0.3333	0.6667	0.5000	1.0000
O 5	-0.698(8)	-0.290(8)	0.0000	1.0000
O 6	0.725(9)	0.384(8)	0.5000	1.0000

[a]V 2 and V 3 represent a split vanadium site

Table 4.6. Displacement Parameters[a] for $K_{10}Bi_4V_4O_{21}$

Atom	Ueq	U11	U22	U33	U12	U13	U23
Bi 1	28(1)	30(1)	30(1)	24(2)	15(1)	0	0
Bi 2	45(1)	36(1)	39(1)	48(2)	10(1)	0	0
K 1	35(2)	34(3)	26(2)	50(6)	21(2)	6(3)	-15(3)
K 2	70(4)	65(7)	102(11)	62(12)	56(8)	0	0
K 3	20(9)	12(14)	50(40)	4(14)	20(30)	0	0
V 1	20(3)	27(2)	27(2)	6(10)	13(1)	0	0
V 2	23(3)	-	-	-	-	-	-
V 3	150(20)	-	-	-	-	-	-
O 1	67(6)	-	-	-	-	-	-
O 2	112(13)	-	-	-	-	-	-
O 3	116(14)	-	-	-	-	-	-
O 4	8(9)	-	-	-	-	-	-
O 5	26(15)	-	-	-	-	-	-
O 6	18(12)	-	-	-	-	-	-

[a]All values represent displacement parameters multiplied by 1000

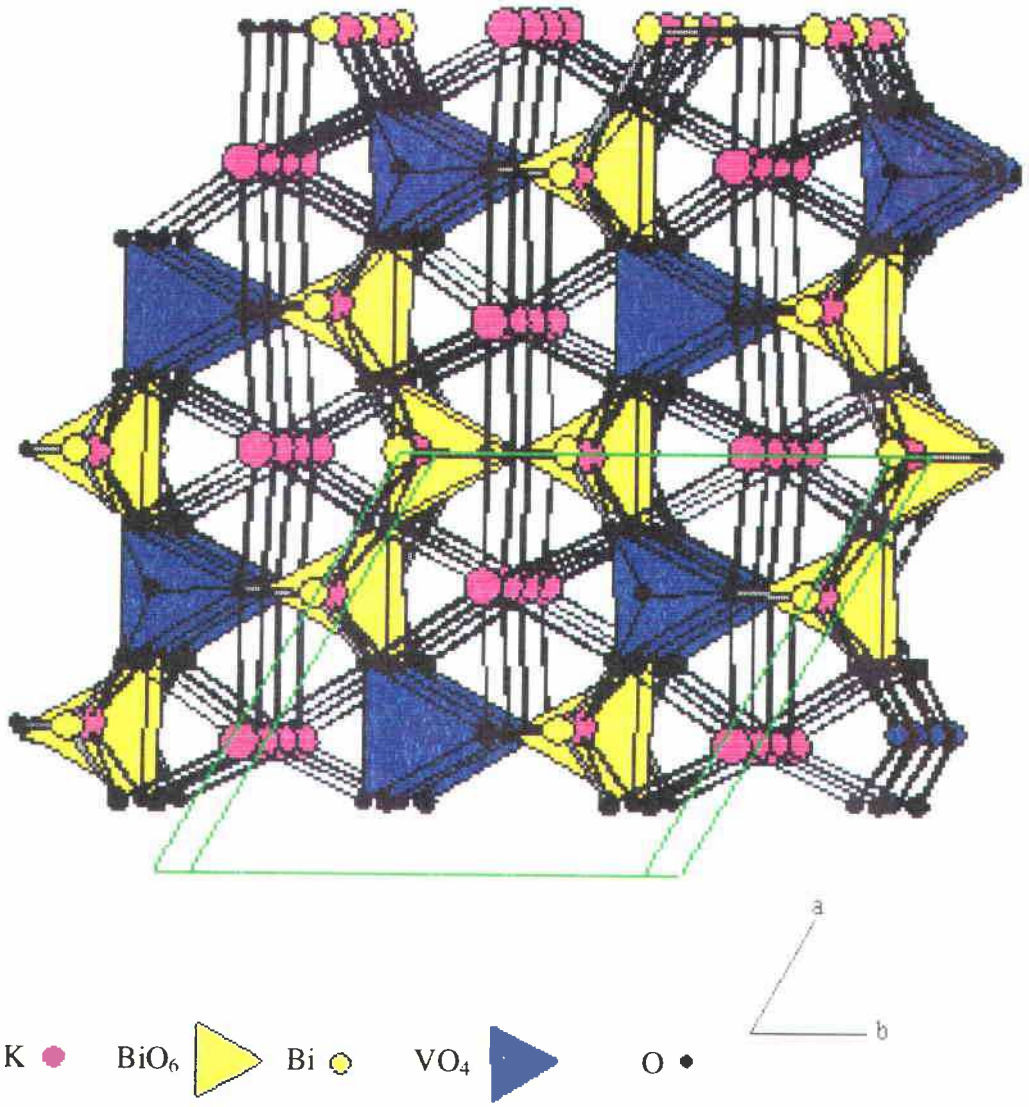

Figure 4.3. Crystal Structure of $K_{10}Bi_4V_4O_{21}$ in Wagon Wheel Orientation

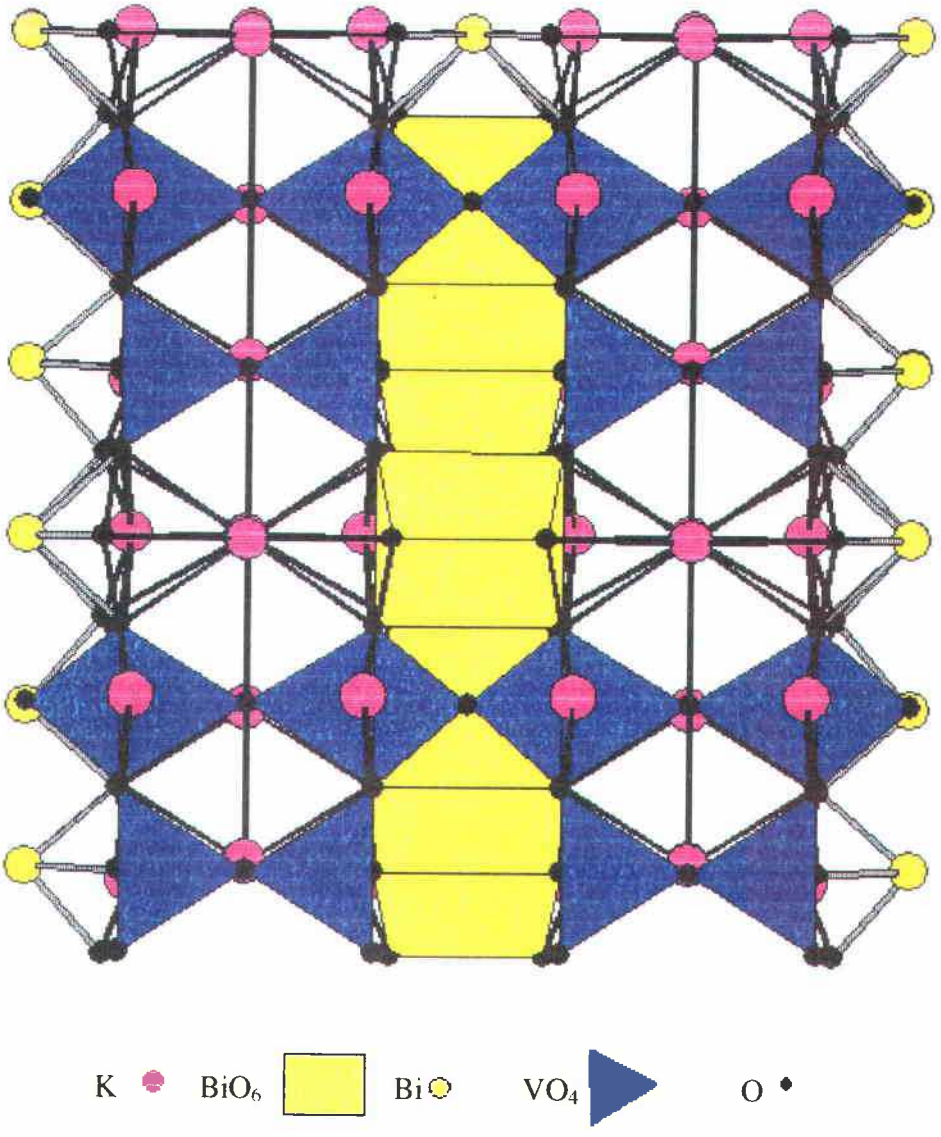

Figure 4.4. Crystal Structure of $K_{10}Bi_4V_4O_{21}$ Looking Down the B Axis

The three dimensional framework of $K_{10}Bi_4V_4O_{21}$ can be described from the bismuth environment. Both bismuth sites are involved in forming a Bi_4O_{18} grouping of polyhedron. A central BiO_6 trigonal prism formed by Bi 1 is connected to three additional, edge sharing BiO_6 trigonal prisms formed by the Bi 2 position (Figure 4.5). These four edge sharing trigonal prisms are connected together in the a and b directions by corner sharing VO_4 tetrahedron. This generates the wagon wheel structural character. The central BiO_6 trigonal prism is connected to another BiO_6 central trigonal prism in the c direction by a face sharing KO_6 trigonal prism generated by K 3.

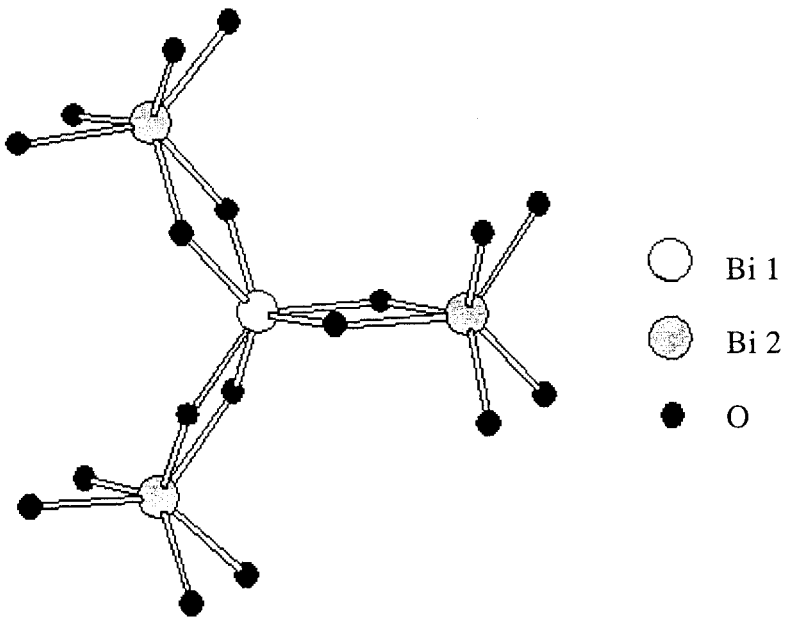

Figure 4.5. Bi_4O_{18} polyhedron arrangement of Bismuth Positions Bi 1 and Bi 2

K 1 forms the hub of the wagon wheel. It has six-fold coordination that falls slightly off the 2b plane. Three intersecting, linear K-O-K sheets are formed from the K 1 bonding pattern. These sheets are shown in Figure 4.6.

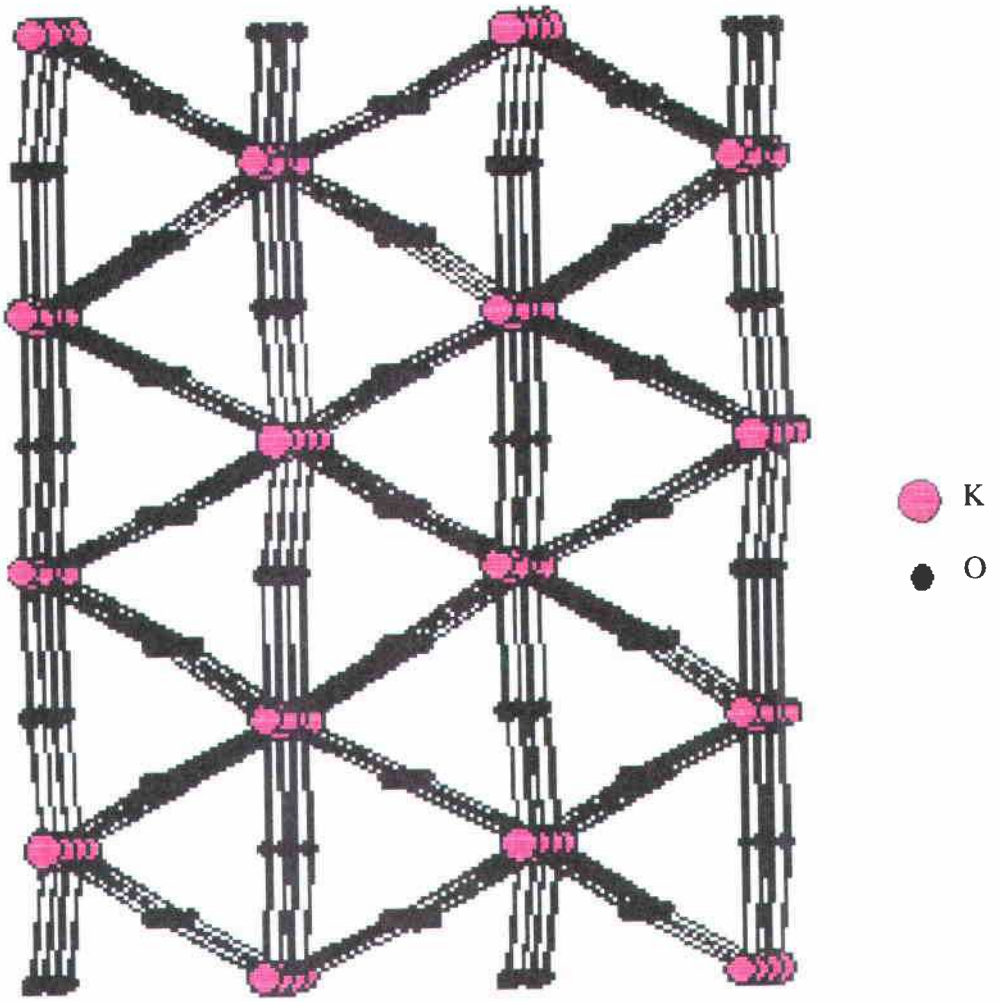

Figure 4.6. Three Linear K-O-K sheets Generated by K 1 Bonding Environment

K 2 and K 3 together form honeycomb-like wrinkled sheets (Figure 4.7). K 3 has a six fold, trigonal prism coordination while K 2 maintains an eight-fold coordination sphere.

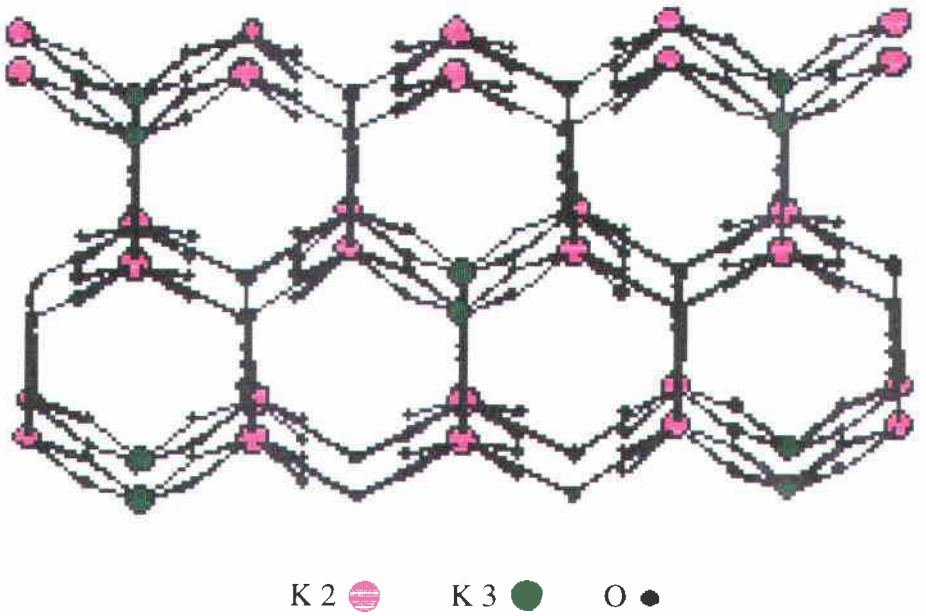

Figure 4.7. Honeycomb Arrangement of K 2 and K 3 Bonding Environments

4.4. Disorder

$K_{10}Bi_4V_4O_{21}$ appears to have many symmetry elements. Much of the apparent symmetry in this system is a façade and to accommodate the actual disorder present, the space group $P\bar{6}$ must be used.

Three atoms on $\bar{6}$ special positions are actually slightly off the special position. K 3 had an isotropic displacement parameter of 0.183. Relaxation from the 0, 0, 0.5 position to the refined 0.962, -0.02, 0.5 reduced the displacement

parameter, improved the overall R and removed the ghost peak from the residual map.

O 5 and O 6 are also relaxed from the special positions 0.3333, 0.66667, 0 and 0.66667, 0.3333, 0.5 to –0.698, -0.290, 0 and 0.725, 0.384, 0.5 respectively. This relaxation and refinement reduced their problematic displacement parameters, improved the overall R and removed the two ghost peaks in the residual map. The relaxation of the O 6 position enables the K 2 to O 6 bonds to form, thus connecting the wrinkled sheets previously mentioned. The relaxation of O 5 elongates the bond distance between O 5 and V 2. Figure 4.8 depicts the newly allowed bond formation between K 2 and the relaxed O 6.

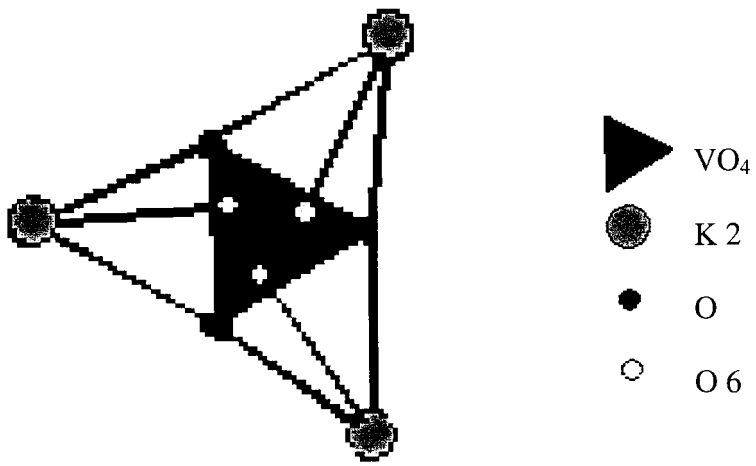

Figure 4.8. Relaxation of O 6 Enables Bonding Between O 6 and K 2

To improve refinement stability, all three atoms were relaxed from the special positions. Other than Figure 4.8, all structure depictions of the titled compound structure have the special positions constrained for easy viewing.

Anisotropic refinement for the entire model suggests the splitting of the O 2 and O 3 sites. Both oxygen sites form three of the bonds associated with the VO4 tetrahedron. O 2 is associated with V 2 and V 3 while O 3 is intimately involved with V 1. The displacement parameters of O 2 and O 3 are unreasonably high. Splitting the oxygen positions and refining the structure was problematic due to the high correlation between these two oxygen and the displacement parameters of a large number of other atoms. To verify the splitting of the two sites, the occupancies were refined. Both sites refined to approximately 0.5 and their resulting displacement parameters are reasonable. These sites are most logically split. Simply reducing the occupancy in the sites would cause severe anion deficiency within the structure. The O 2 and O 3 sites are most likely split into –0.5215, -0.3274, 0.2559 and –0.5122, -0.3220, 0.1930 for O 2 and –0.3371, -0.5222, 0.2441 and –0.3334, -0.5025, 0.1807 for O 3. These oxygens are depicted in their nonsplit positions in Figure 4.9.

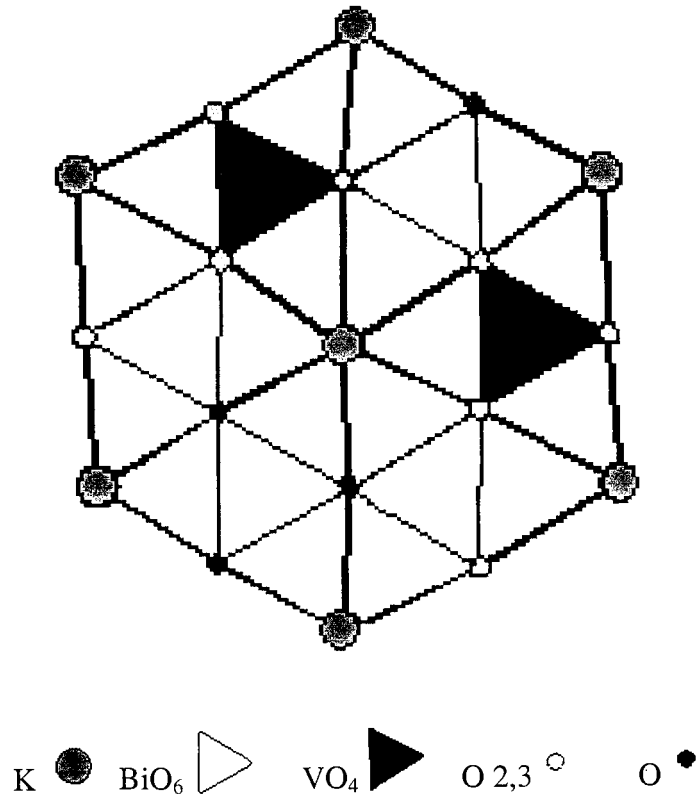

Figure 4.9. O 2 and O 3 Locations Within the $K_{10}Bi_4V_4O_{21}$ Framework

The largest source of disorder within the $K_{10}Bi_4V_4O_{21}$ system resides with the vanadium positions. Both vanadium positions V 1 and V 2, are anisotropically diffuse. Figures 4.10 and 4.11 represent the resulting Fourier map when all vanadium positions are omitted from the refinement.

It is reasonable to say that the structure contains two vanadium positions that are split, into two additional vanadium sites. Removing all vanadium positions completely from the refinement generates four residual peaks. Two with larger intensity at 0.6667, 0.3333, 0. 27 and 0.3333, 0.6667, 0.27 and two with smaller

intensity at 0.6667, 0.3333, 0.16 and 0.3333, 0.6667, 0.16. The smaller pair of intensity peaks are greater than that of any other residual and therefore cannot be ignored.

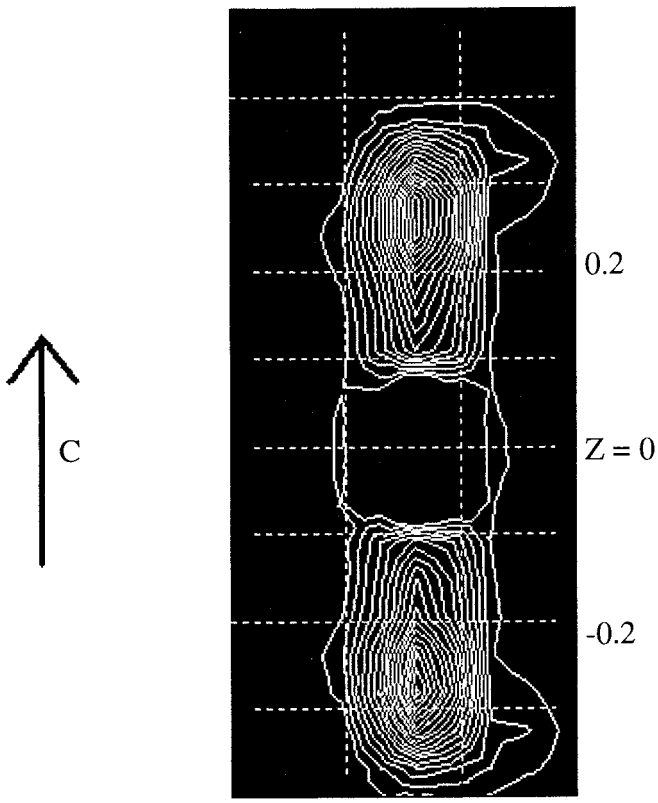

Figure 4.10. Fourier Map Generated for the Site V 1

The V 2 and V 3 positions represent one pair of the split vanadiums. The V 3 site is included to illustrate potential positioning. Including V 3 in the refinement prevents a stable anisotropic refinement of V 2 and V 3 and the displacement parameter for V 3 is unreasonable. The V 4 position was not included due to further complications endured by the refinement upon inclusion.

Vanadium site splitting is not that uncommon. Site splitting for vanadium and its associated oxygens was observed for $Bi_4V_{1.5}Sb_{0.5}O_{10.7}$ (11). A similar splitting in α-$Bi_4V_2O_{11}$ occurred for vanadium positions and associated oxygens (12).

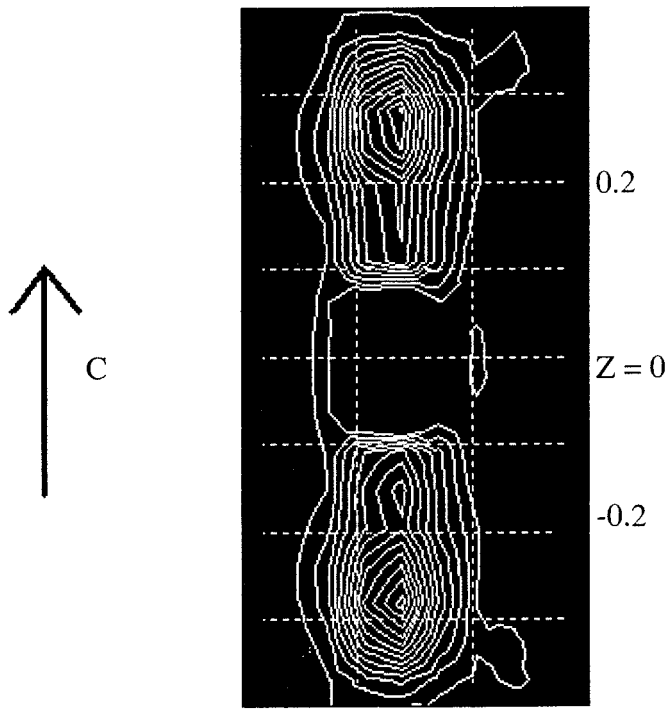

Figure 4.11. Fourier Map Generated for the Site V 2, V 3

Bond distances and valence for the cations in $K_{10}Bi_4V_4O_{21}$ are shown in Table 4.7. Note that in all relaxed cases, the valence values improve. The only significant valence problem arises from the V 2, O 5 bond distance. Additional relaxation or movement for the either the V 2 or O 5 is needed when V 2 is occupied.

The six oxygen coordination at equal bond distances for Bi 1 is completely unreasonable for Bi^{3+} and strongly indicates that this bismuth site is Bi^{5+}. This is also indicated by the bond valence. If this is indeed the case, additional oxygen must be present to accommodate charge balance. The compound color argues against the presence of Bi^{5+}. But the high K/Bi ratio may have effectively stabilized some Bi^{5+}. $KBiO_3$ is the most stable Bi^{5+} compound (13).

Table 4.8 depicts the bond distances and valence (14) with respect to the oxygen's. The valence of O 1 is quite good and is relatively unchanged by the relaxation of K 3. Splitting of the O 2 position yields a good valence total for the case of V 3 involvement in one setting and a good valence for V 2 involvement in the other position. Clearly the splitting of the O 2 site occurs to satisfy the bonding demands for the vanadium, whether it is in site V 2 or site V 3.

In the case of O 3, one side of the split position provides very reasonable valence sums for V 1. In the refined model, V 1 has not been split into its two components, instead it represents one half of the split. It is reasonable to assume that the alternate site for V 1 would have optimum bonding conditions when associated to O 3a.

Table 4.7. Cation Bond Distances[a,b] and Valence for $K_{10}Bi_4V_4O_{21}$

Atoms	#	Bond Length (Å)	Bond Valence	Bond Valence Totals
Bi 1 – O 1	6	2.15(3)	0.860	Sum $_{Bi\,1}$ = 5.157
Bi 2 – O 1	2	2.23(4)	0.692	
Bi 2 – O 2	2	2.39(6)	0.449	
Bi 2 – O 3	2	2.35(6)	0.501	Sum $_{Bi\,2}$ = 3.285
K 1 – O 1	1	2.81(4)	0.160	
K 1 – O 1	1	2.82(4)	0.156	
K 1 – O 2	1	2.95(6)	0.110	
K 1 – O 2	1	3.21(6)	0.054	
K 1 – O 3	1	2.92(6)	0.119	
K 1 – O 3	1	3.11(6)	0.071	Sum $_{K\,1}$ = 0.670
K 2 – O 1	2	3.11(4)	0.071	
K 2 – O 2	2	2.76(6)	0.183	
K 2 – O 3	2	2.81(6)	0.160	
K 2 – O 3	1	3.28(2)	0.045	
K 2 – O 3	1	3.39(5)	0.033	Sum $_{K\,2}$ = 0.907
K 2 – O 6	*1*	*3.07(7)*	*0.079*	
K 2 – O 6	*1*	*3.23(6)*	*0.051*	*Sum $_{K\,2\,relax}$ = 1.004*
K 3 – O 1	6	3.01	0.093	Sum $_{K\,3}$ = 0.559
K 3 – O 1	*2*	*2.87(7)*	*0.136*	
K 3 – O 1	*2*	*3.0(1)*	*0.088*	
K 3 – O 1	*2*	*3.19(5)*	*0.057*	*Sum $_{K\,3\,relax}$ = 0.563*
V 1 – O 3	3	1.75(6)	1.154	
V 1 – O 6	1	1.77(2)	1.093	Sum $_{V\,1}$ = 4.555
V 2 – O 2	3	1.70(6)	1.321	
V 2 – O 5	1	1.32(5)	3.689	Sum $_{V\,2}$ = 7.652
V 3 – O 2	3	1.66(6)	1.472	
V 3 – O 4	1	1.86(8)	0.857	Sum $_{V\,3}$ = 5.273

[a]Italics represents resulting bonds from relaxation of a special position, O 6 or K 3
[b]Bond distances without SD values were obtained from ATOMS (15)

Table 4.8. Oxygen Bond Distances[a,b,c] and Valence for $K_{10}Bi_4V_4O_{21}$

Atoms	#	Bond Length (Å)	Bond Valence	Bond Valence Totals
O 1 – Bi 1	1	2.15(3)	0.860	
O 1 – Bi 2	1	2.23(4)	0.692	
O 1 – K 1	1	2.81(4)	0.160	
O 1 – K 1	1	2.82(4)	0.156	
O 1 – K 2	1	3.11(4)	0.071	Sum $_{O\,1no\,K\,3}$ = 1.939
O 1 – K 3_i	1	2.87(7)	0.136	Sum $_{O\,1i}$ = 2.075
O 1 – K 3_{ii}	1	3.0(1)	0.088	Sum $_{O\,1ii}$ = 2.027
O 1 – K 3_{iii}	1	3.19(4)	0.057	Sum $_{O\,1iii}$ = 1.996
O 2a – Bi 2	1	2.74	0.174	
O 2a – V 2	1	1.67	1.433	
O 2a – V 3	1	1.45	2.596	
O 2a – K 1	1	2.98	0.101	
O 2a – K 1	1	3.21	0.054	Sum $_{O\,2a\,V\,2}$ = 2.029
O 2a – K 2	1	2.62	0.267	Sum $_{O\,2a\,V\,3}$ = 3.192
O 2b – Bi 2	1	2.37	0.474	
O 2b – V 2	1	1.56	1.929	
O 2b – V 3	1	1.60	1.731	
O 2b – K 1	1	2.93	0.116	
O 2b – K 1	1	3.26	0.047	Sum $_{O\,2b\,V\,2}$ = 2.202
O 2b – K 2	1	2.95	0.110	Sum $_{O\,2b\,V\,3}$ = 2.004
O 3a – Bi 2	1	2.65	0.223	
O 3a – V 1	1	1.52	2.149	
O 3a – K 1	1	2.96	0.107	
O 3a – K 1	1	3.07	0.079	
O 3a – K 2	1	2.73	0.199	Sum $_{O\,3a}$ = 2.756
O 3b – Bi 2	1	2.19	0.771	
O 3b – V 1	1	1.84	0.905	
O 3b – K 1	1	2.94	0.113	
O 3b – K 1	1	3.13	0.067	
O 3b – K 2	1	2.99	0.098	Sum $_{O\,3b}$ = 1.955
O 4 – V 3	2	1.86(8)	0.857	
O 4 – K 2	3	3.28(2)	0.045	Sum $_{O\,4}$ = 1.804
O 5 – V 2	2	1.32(5)	3.689	Sum $_{O\,5}$ = 3.689
O 6 – V 1	2	1.77(3)	1.093	
O 6 – K 2	1	3.07(7)	0.079	
O 6 – K 2	1	3.23(6)	0.051	Sum $_{O\,6}$ = 2.316

[a]K 3, O 5, and O 6 have been relaxed from special positions
[b]O 2 and O 3 are shown in their split positions labeled a and b
[c]Bond distances without SD values were obtained from ATOMS(15)

The disorder within the structure of $K_{10}Bi_4V_4O_{21}$ inhibits refinement statistics. The proposed model justifies the special position relaxations and demonstrates the necessary oxygen splitting needed to accommodate the diffuse vanadium positions. The O 5, V 2 bond distance is too close. The only coordination for O 5 is to the V 2 site, when it is occupied. It is therefore anticipated that the O 5 to V 2 bond distance be shorter than normally expected. The Bi – O distance of 1.32 Å is too close to be explained purely on coordination number. The possibility of Bi^{5+} must be investigated further. Despite the hexagonal lattice found for both powder and single crystal X-ray diffraction, the true space group for this material may be of lower symmetry. Neutron data would prove very helpful in clarifying the structural uncertainties, especially the O 5 paradox, of $K_{10}Bi_4V_4O_{21}$. The vanadium transparency to neutrons would remove their disorder completely from the structure solution.

4.5. References

1. M.F. Debreuille-Gresse and F. Abraham, *J. Solid State Chem.*, 71, 466 (1987)
2. O. Mentre, A.C. Dhaussy and F. Abraham, *J. Mater. Chem.*, 9, 1023 (1999)
3. C.K. Lee, A.M. Coats and A.R. West, *Powder Diffraction*, 12/4, 245 (1997)
4. Oregon State University Microprobe Lab
5. N. Walker and D. Stuart, *Acta Cryst.* A39, 158 (1983)
6. L.J. Farrugia, *J. Appl. Crystallogr.*, 32, 837 (1999)

7. G.M. Sheldrick, SHELX97-Programs for Crystal Structure Analysis, University of Goettingen, Germany (Release 97-2)

8. J. Laugier and B. Bochu, www.inpg.fr/LMGP

9. R.E. Marsh, *Acta Cryst.*, B51, 897 (1995)

10. A. Altomare, G. Cuscarano, C. Giacovazzo and A. Gualardi, *J. Appl. Cryst.*, 26, 343 (1993)

11. O. Joubert, A. Jouanneaux, M. Ganne and M. Tournoux, *Mat. Res. Bull.*, 27, 1235 (1992)

12. O. Joubert, A. Jouanneaux, and M. Ganne, *Mat. Res. Bull.*, 29/2, 175 (1994)

13. A.G. Soldatov, S.N. Barilo, S.V. Shiryawv, V.M. Finskaya, S.N. Ustinovich, W. Reichardt, M. Braden and R. Szymszak, *Physica. B, Condensed Matter*, 285, 1059 (2000)

14. I.D. Brown, Bond Valence Calculator, Institute for Materials Research, McMaster University, Hamilton, Ontario, Canada, L8S 4M1

15. E. Dowty, ATOMS Version 4.1 (1998)

Chapter 5

Unfinished Systems and Future Work

5.1. Introduction

The pursuit of scientific information is a never-ending story. A research project is never truly complete. Components along the way may be solved, but through their study additional quandaries and scientific complexities arise. That is the nature of science.

α-$NaBi_3V_2O_{10}$, $Ca_{0.29}Bi_{0.71}VO_{3.855}$ and $K_{10}Bi_4V_4O_{21}$ were discussed in Chapters 2 – 4. The intent of this chapter is to address seven additional systems within the alkali bismuth vanadate family and discuss suggestions for future investigations.

5.2. Lithium 1-1-1

Single crystals were obtained from a 1:1:1 stoichiometric mixture of Li:V:Bi from Li_2CO_3 (J.T. Baker), Bi_2O_3 (Cerac) and V_2O_5 (Alpha Aesar). The reagents were ground for fifteen minutes in an agate mortar and placed in an aluminaina crucible. The sample was heated in a Lindberg furnace at 800°C for fifteen hours. A subsequent cooling at a rate of 1.0°C/min was initiated. Highly reflective orange-brown crystals were obtained.

Powder X-ray diffraction was used to monitor the content of the products. The patterns were recorded from a Siemens D5000 powder diffractometer with a Kevex detector, CuKα radiation (λ = 1.5418 Å) and vertical Soller slits (Figure 5.1).

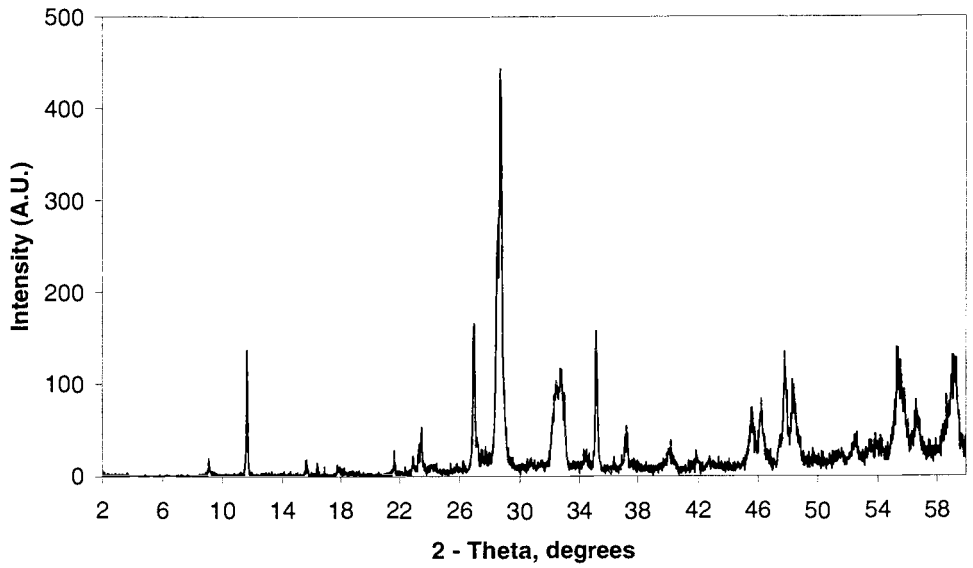

Figure 5.1. Powder X-ray Diffraction Pattern for Lithium 1-1-1

No peaks could be identified as arising from known compounds. Single crystals were prepared for single crystal X-ray diffraction studies. Arc-like spreading observable in the rotational photographs indicated the crystals to be of a nonideal nature. Single crystal X-ray diffraction studies were not pursued further. Another method of crystal growth should be attempted for this material.

All additional synthesis attempts yielded nonideal single crystals. Polycrystalline samples prepared with a 1:1:1 ratio of Li:Bi:V were found to

decompose over time. After nine months, powder X-ray diffraction patterns indicated the presence of both $Bi_4V_2O_{11}$ and $LiVO_4$.

Further investigation of this system should be explored. There are currently no structurally characterized lithium bismuth vanadates in the literature.

5.3. Sodium 3 – 1 – 2

Single crystals were first obtained from a 3:2:3 stoichiometric mixture of Na:Bi:V from $NaNO_3$ (Spectrum), Bi_2O_3 (Alpha Aesar) andV_2O_5 (Johnson Matthey). The reagents were ground for twenty minutes in an agate mortar and heated in a Lindberg furnace, at 800°C for 15 hours. The sample was cooled at a rate of 5°C/min. All crystals were yellow but two different shapes were apparent under a microscope. Some crystals were shaped like very fat needles while others had a more equal three-dimensional appearance.

A similar powder X-ray diffraction pattern and two-phase crystals were obtained from a 2:1:2 stoichiometric ratio of Na:Bi:V from $NaNO_3$ (Spectrum), Bi_2O_3 (Alfa Aesar) and V_2O_5 (Johnson Matthey). Wavelength dispersive electron microprobe analysis(1) with a beam current of 48.5 nA, an accelerating voltage of 15 kV and a 5 μm beam diameter, of both samples indicated the presence of two phases $NaBi_3V_2O_{10}$ (2) and $Na_3BiV_2O_8$.

Single phase, polycrystalline $Na_3BiV_2O_8$ was prepared from a 3:1:2 stoichiometric ratio of Na:Bi:V from Na_2CO_3 (Aldrich), Bi_2O_3 (Alfa Aesar) and V_2O_5 (Johnson Matthey). The reagents were ground in an agate mortar for twenty

minutes and calcinated, in an alumina crucible, in a Lindberg furnace for 72 hours. The sample was slow cooled at a rate of 0.03°C/min. The resulting powder X-ray diffraction pattern is shown in Figure 5.2.

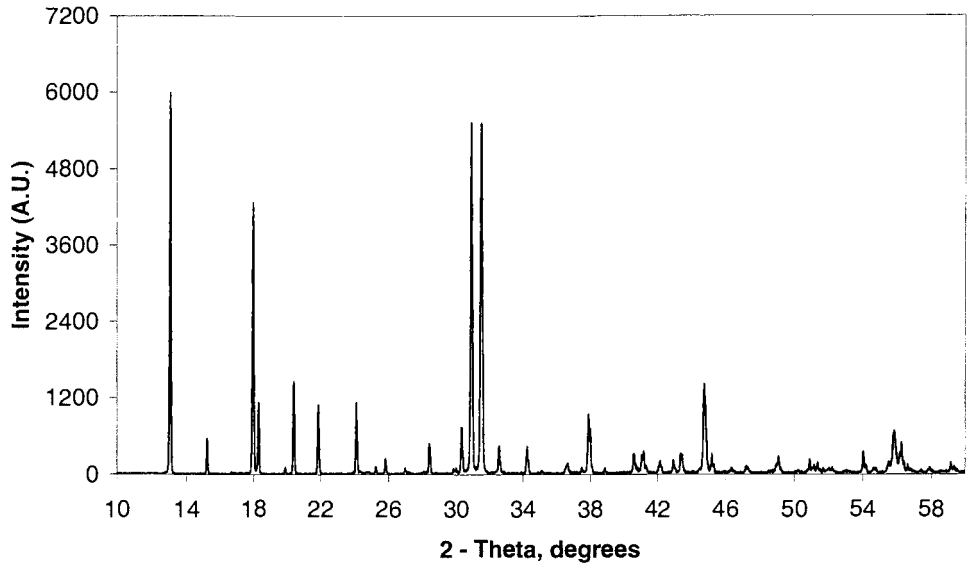

Figure 5.2. Powder X-ray Diffraction Pattern for $Na_3BiV_2O_8$

Powder X-ray diffraction patterns were recorded from a Siemens D5000 powder diffractometer with a Kevex detector, CuKα radiation (λ = 1.5418 Å) and vertical Soller slits. No peaks from known phases were identified.

Two creamy-yellow crystals were used for single crystal X-ray diffraction. Neither data set has been solved. Identification of the space group has proven to be problematic. Lattice parameters determined by single crystal diffraction are depicted in Table 5.1. Single crystal X-ray diffraction data were collected at room temperature on a Rigaku AFC6R diffractometer with monochromatic MoKα radiation (λ = 0.71069 Å). No decay was noted during data collection.

Table 5.1. Selected Single Crystal X-ray Diffraction Data for $Na_3BiV_2O_8$

Property	Collection 1	Collection 2
Crystallite Size (mm)	0.30, 0.10, 0.10	0.20, 0.08, 0.08
Laue Group	Orthorhombic	Orthorhombic
a (Å)	5.664(7)	5.67(2)
b (Å)	7.124(5)	7.11(2)
c (Å)	19.55(2)	19.51(2)

The powder pattern was successfully indexed using the CELREF (3) program and the lattice parameters calculated from single crystal X-ray diffraction data. Lattice parameters were refined to values of 5.679(2), 7.130(2), 19.550(4) for a, b and c respectively. Table 5.2 depicts the indexing results for several hkl reflections.

Table 5.2. Pattern Indexing for $Na_3BiV_2O_8$

h	k	l	2 - Theta
0	1	1	13.075
0	1	2	15.208
1	0	2	17.986
0	0	4	18.284
1	1	1	20.367
1	1	2	21.855
1	0	4	24.087
0	2	0	25.179
0	1	5	25.823

The formula $Na_3BiV_2O_8$ was again confirmed by Wavelength dispersive electron microprobe analysis with a beam current of 50.0 nA, an accelerating voltage of 15 kV and a 5 μm beam diameter (1).

The compound $Na_3BiV_2O_8$ can be produced in single phase and in crystals large enough for single crystal X-ray diffraction. Two data sets of single crystal X-ray diffraction show space group ambiguity. Additional single crystal X-ray diffraction should be collected. Additional high angle scans should be performed to confirm the lattice setting, and axis multiplying should be attempted to search for a supercell.

5.4. Sodium 2 – 1 – 1

Single crystals were obtained from a 2:1:1 stoichiometric mixture of Na:Bi:V from $NaNO_3$ (Spectrum), Bi_2O_3 (Cerac) and V_2O_5 (Johnson Matthey). The reactants were ground for fifteen minutes and heated in an alumina crucible, in a Lindberg furnace. A two-step calcination cycle was used, with an intermediate grind for ten minutes. The calcination cycle is depicted in Table 5.3.

Table 5.3. Calcination Cycles for Single Crystal Growth

Cycle	Plateau Temperature (°C)	Holding Time (Hours)	Cooling Rate (°C/min)
Cycle 1	500	20	5
Cycle 2	700	24	0.5

Powder X-ray diffraction was used to monitor the reaction products. Patterns were recorded from a Siemens D5000 powder diffractometer with a Kevex detector, CuKα radiation (λ = 1.5418 Å) and vertical Soller slits. No peaks due to known compounds were observed. The powder pattern is depicted in Figure 5.3. Single crystal X-ray diffraction data were not collected for these pale yellow crystals due to instrument down time.

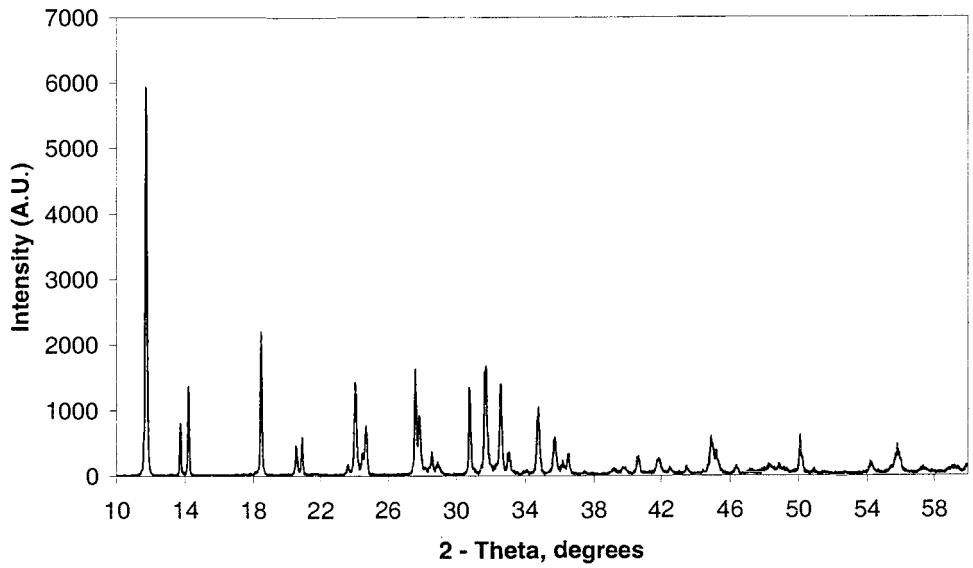

Figure 5.3. Powder X-ray Diffraction Pattern for Sodium 2 – 1 – 1

5.5. Sodium 3 – 1 – 2 , A Second Phase

Single crystals were prepared from a 3:1:2 stoichiometric ratio of Na:Bi:V from Na_2CO_3 (Aldrich), Bi_2O_3 (Cerac) and V_2O_5 (Johnson Matthey). The reagents were ground together for fifteen minutes before heating in a Lindberg furnace. The sample was divided into three containers, two alumina crucibles and one alumina

boat. All containers were covered during the calcination process. The five-step calcination cycle is described in Table 5.4.

Table 5.4. Calcination Cycles for Single Crystal Growth

Cycle	Plateau Temperature (°C)	Holding Time (Hours)	Cooling Rate (°C/min)
Cycle 1	400	18	5
Cycle 2	550	18	5
Cycle 3	550	18	5
Cycle 4	650	24	5
Cycle 5	750	35	5

Container placement within the furnace had an impact on the products obtained. Noticeable differences between samples were detected during intermediate grinds. Crucible A and crucible C differed greatly from one another. The boat, container C, contained gradient regions with one side mimicking A and the other, B. Container placement in the furnace is illustrated in Figure 5.4 and the observable sample differences are displayed in Table 5.5.

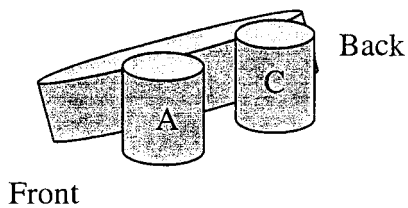

Figure 5.4. Container Arrangement Within the Lindberg Furnace

Table 5.5. Sample Characteristics Throughout the Calcination Process

Calcination Cycle	Crucible A	Boat B	Crucible C
Cycle 1	fluffy powder, color and consistency of baking chocolate	fluffy powder, red-brown on one end, chocolate brown on other	fluffy powder, dark brick red
Cycle 2	no observation made	no observation made	no observation made
Cycle 3	green-brown material, behaves like moist sand	gradient between moist sand and fine powder	fine, yellow-green powder
Cycle 4	pale yellow powder	pale yellow powder	pale yellow powder
Cycle 5	pale green, needle-like crystals	gradient pale green to yellow	Yellow coating, like dry mud

Powder X-ray diffraction data was unobtainable due to instrument down time. Single crystal X-ray diffraction data, for a green crystal from crucible A, were collected at room temperature on a Rigaku AFC6R diffractometer with monochromatic MoKα radiation ($\lambda = 0.71069$ Å). No decay was noted during date collection. Lattice parameters are displayed in Table 5.6.

Table 5.6. Single Crystal X-ray Diffraction Lattice Parameters

a (Å)	c (Å)	α (degrees)	γ (degrees)	Volume (Å^3)
5.637(2)	7.115(3)	90	120	195.67(14)

Initial attempts to solve the structure indicate a possible wagon wheel character, like that observed for the $K_{10}Bi_4V_4O_{21}$ (4) system. High R refinement

statistics and a large number of ghost peaks suggest that the space group is incorrect. Further analysis of these data are underway.

5.6. Potassium 8 – 5 – 5

Single crystals of $K_8Bi_5V_5O_{24}$ were first obtained as a contaminant phase in an attempted synthesis of $K_{10}Bi_4V_4O_{21}$. Wavelength dispersive electron microprobe analysis(1) with a beam current of 50.0 nA, an accelerating voltage of 15 kV and a 5 μm beam diameter performed on a polycrystalline multi-phase sample provided the formula $K_8Bi_5V_5O_{24}$.

Single crystals were obtained from an 8:5:5 stoichiometric ratio of K:Bi:V from KNO_3 (Mallinckrodt), Bi_2O_3 (Cerac) and V_2O_5 (Johnson Matthey). The reagents were dried overnight at 200°C and the intimate mixture was ground for fifteen minutes. The sample was heated, inside an alumina crucible, in a Lindberg furnace for a four-step calcination cycle. The calcination cycle is described in Table 5.7.

Table 5.7. Calcination Cycles for Single Crystal Growth

Cycle	Plateau Temperature (°C)	Holding Time (Hours)	Cooling Rate (°C/min)
Cycle 1	400	18	5
Cycle 2	550	18	5
Cycle 3	650	18	5
Cycle 4	850	36	0.1

Powder X-ray diffraction data were obtained from a Siemens D5000 powder diffractometer with a Kevex detector, CuKα radiation (λ = 1.5418 Å) and vertical Soller slits. The pattern is illustrated in Figure 5.5. No peaks were located from known phases.

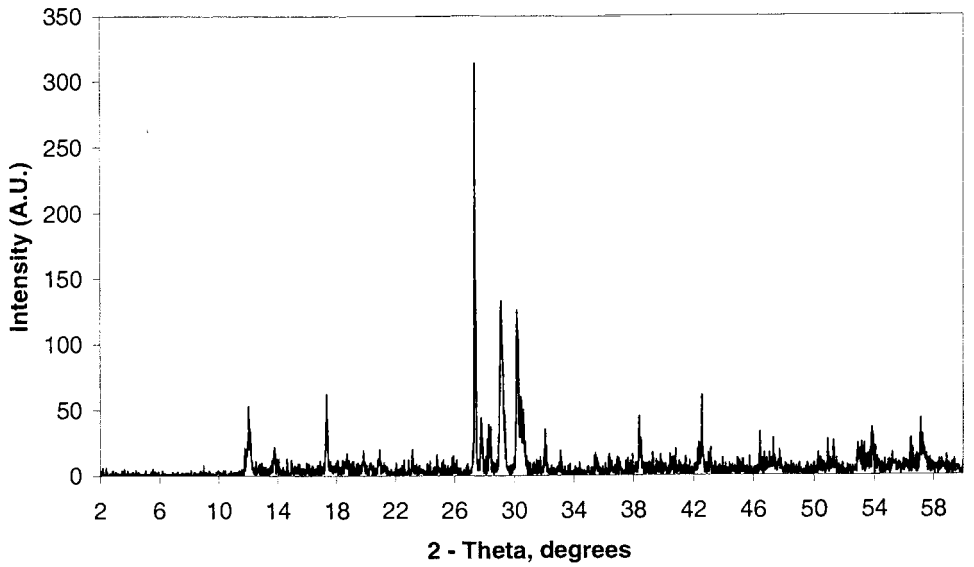

Figure 5.5. Powder X-ray Diffraction Pattern for $K_8Bi_5V_5O_{24}$

A pale yellow, highly static, crystal 0.05 by 0.03 by 0.03 mm was mounted on the tip of a glass fiber with epoxy. Single crystal X-ray diffraction data were collected at room temperature on a Rigaku AFC6R diffractometer with monochromatic MoKα radiation (λ = 0.71069 Å). No decay was noted during date collection. Lattice parameters are displayed in Table 5.8.

Table 5.8. Single Crystal X-ray Diffraction Lattice Parameters

a (Å)	c (Å)	α (degrees)	γ (degrees)	Volume (Å^3)
11.754(6)	7.603(7)	90	120	909.59(1.15)

Three major problems hindered the structure solution for this material. The first problem was in peak breadth. All of the observed single crystal X-ray diffraction peaks had a breadth of two or more 2 – theta degrees. The second problem, reasonably explained by abnormally large peak breadth, was the difficulty of determining space group. R_{int} values for the merging of all Laue classes were ambiguous. This, in conjunction with contradicting systematic absences in both the hexagonal and trigonal Laue classes made space group identification impossible. The third indicator that the structural solution attempts are incorrect lies in the fact that the lattice parameters suggested by single crystal X-ray diffraction are unable to index the powder X-ray diffraction pattern.

An additional synthesis of this material would be quite useful. To avoid possible strain caused by crystal extraction, a crystal should attempt to be collected from the side of the crucible.

5.7. Rubidium 3 – 3 – 2

Single crystals were obtained from a 3:3:2 stoichiometric ratio of Rb:Bi:V from Rb_2CO_3 (Alfa Aesar), Bi_2O_3 (Cerac), and V_2O_5 (Johnson Matthey). The reagents were ground for twenty minutes in an agate mortar before heating to

800°C, for fifteen hours, in a Lindberg muffle furnace. The sample was calcinated in an alumina crucible and slow cooled at a rate of 0.5°C/min.

The powder X-ray diffraction pattern (Figure 5.6) indicated a new material. The pattern was recorded from a Siemens D5000 powder diffractometer with a Kevex detector, CuKα radiation (λ = 1.5418 Å) and vertical Soller slits.

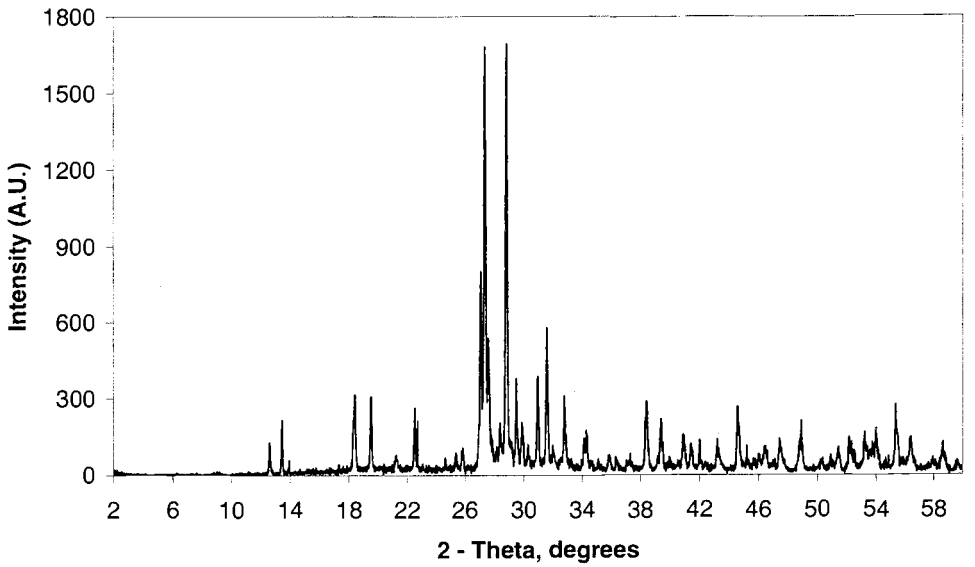

Figure 5.6. Powder X-ray Diffraction Pattern for Rubidium 3 – 3 – 2

A satisfactory single crystal was not found. A new synthetic approach may be necessary to achieve single crystals for use in single crystal X-ray diffraction experiments. A structural solution for this system would provide the first reference for a rubidium bismuth vanadate.

5.8. Rubidium 2 – 1 – 1

Cream-colored single crystals were obtained from a 2:1:1 stoichiometric mix of Rb:Bi:V from Rb_2CO_3 (Alfa Aesar), Bi_2O_3 (Cerac), and V_2O_5 (Johnson Matthey). The reagents were ground for fifteen minutes in an agate mortar before being heated in a Lindberg furnace. A three-step calcination cycle was used and is displayed in Table 5.9.

Table. 5.9. Calcination Cycles for Single Crystal Growth

Cycle	Plateau Temperature (°C)	Holding Time (Hours)	Cooling Rate (°C/min)
Cycle 1	375	24	5
Cycle 2	600	48	5
Cycle 3	800	48	5

Powder X-ray diffraction data, recorded from a Siemens D5000 powder diffractometer with a Kevex detector, CuKα radiation (λ = 1.5418 Å) and vertical Soller slits indicated the presence of a new phase. No peaks could be assigned to known compounds. The powder X-ray diffraction pattern is shown in Figure 5.7.

The material is very environment sensitive. It became clay-like upon grinding and particulates would clump together inside the storage vial. A crystal suitable for X-ray diffraction was not obtained.

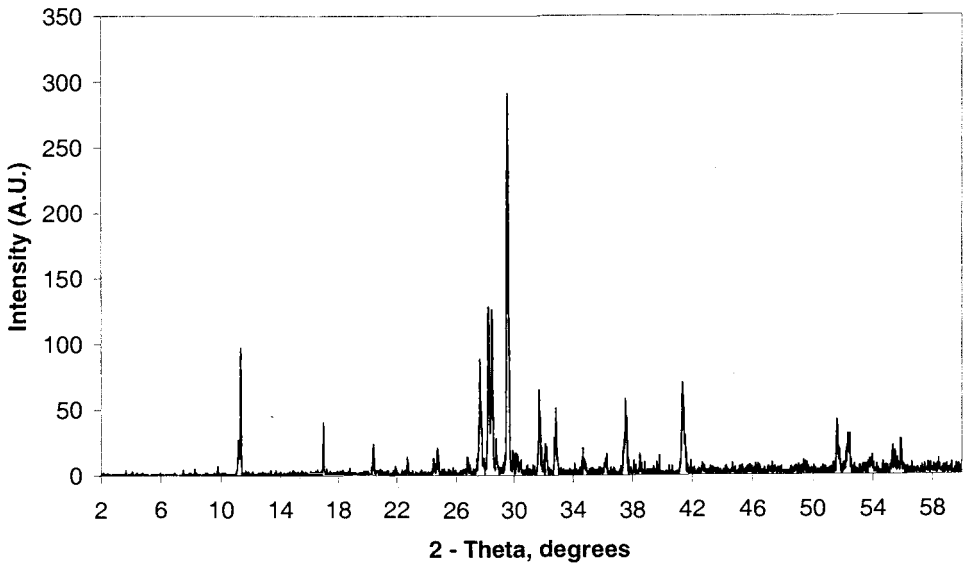

Figure 5.7. Powder X-ray Diffraction Pattern for Rubidium 2 – 1 – 1

Future work with this compound should be completed with the use of a glove box. Synthesis can be in air but grinding, single crystal abstraction and single crystal preparation should all take place in the glove box. Further investigation of this material would be of interest because there are no structurally characterized rubidium vanadates in the literature.

5.9. Conclusions

Any results obtained from exploratory synthesis directs additional exploratory studies. Many bismuth vanadates are known for having good ionic conductivity properties (5-7). Nonlinear optical capabilities should be examined for all systems crystallizing in noncentrosymmetric space groups (8).

Many isostructural families exist with the exchange of vanadium for either phosphorus or arsenic (9). Compounds containing sodium and potassium cations have been observed in $KNa(VO_3)_2$ (10) as well as $NaK_2Bi_2(VO_4)_3$ (11).

Synthesis attempts for phosphate and arsenate variants should be started. Adding a second alkali cation to the alkali metal containing both bismuth vanadate search should be considered. Possible new materials may exist if bismuth can be substituted for lead in the compounds $NaPb_4(VO_4)_3$ and $KPb_4(VO_4)_3$ (12).

Exploratory synthesis never ends. Instead, new beginnings are established with every new material discovered.

5.10. References

1. Electron Microprobe Lab at Oregon State University
2. Chapter 2
3. J. Laugier and B. Bochu, www.inpg.fr/LMGP
4. Chapter 4
5. F. Abraham, M.F. Debreuille-Gresse, G. Mairesse, and G. Nowogrocki, *Solid State Ionics*, 28/30, 529 (1988)
6. T. Takahashi and H. Iwahara, *Mat. Res. Bull.*, 13, 1447, (1978)
7. A. Watanabe, *Solid State Ionics*, 96, 75 (1997)
8. R.W. Wolfe, R.E. Newnham and M.I. Kay, *Solid State Comm.*, 7, 1797 (1969)
9. I. Radosavljevic, J.A.K. Howard and A.W. Sleight, *Int. J. Inorg. Matter.*, submitted.

10. Y. Shan and S.D. Huang, *Acta Cryst.*, C55, 1048 (1999)

11. M.F. Debreuille-Gresse and F. Abraham, *J. Solid State Chem.*, 71, 466 (1987)

12. M. Azrour and L. El Ammari, *J. Solid State Chem.*, 141, 373 (1998)

BIBLIOGRAPHY

Abraham, F. and Ketatni, M. *Eur. J. Solid State Inorg. Chem.*, 32, 429, (1995)

Abraham, F.; Debreuille-Gresse, M.F.; Mairesse, G. and Nowogrocki, G. *Solid State Ionics*, 28/30, 529 (1988)

Ahmed, O.A.S.; Tairi, A.; Chagraoui, A.; Khairoun, S.; Champarnaud-Mesjard, J.-C. and Frit, B. *Ann. Chim. Sci. Mat.*, 25, 201 (2000)

Aizu, K. *J. Phys. Soc. Japan*, 27/2, 287 (1969)

Aizu, K. *J. Phys. Soc. Japan*, 28/3, 706 (1970)

Akimov, S.V.; Mnushkina, I.E. and Dudnik, E.F. *Sov. Phys. Tech. Phys.*, 27, 4 (1983)

Altomare, A.; Cascarano, G.; Giacov, C. and Gualardi, A. *J. Appl. Cryst.*, 26, 343 (1993)

Arroyo y de Dompablo, M.E.; Garcia-Alvarado, F. and Moran, E. *Solid State Ionics*, 91, 273 (1996)

Aurivillius, B. *Ark. Kemi., 1*, 54, 469 (1949)

Azrour, M. and El Ammari, L. *J. Solid State Chem.*, 141, 373 (1998)

Balducci et al., U.S. Patent, No. 4,230,500

Benmoussa, A.; Borel, M.M.; Leclaire, A. and Raveau, B. *J. Solid State Chem.*, 84, 299 (1990)

Bierlein, J.D. and Sleight, A.W. *Solid State Commun.*, 16, 69 (1975)

Blasse, G. and Bril, A. *J. Chem. Phys.*, 47, 1920 (1967)

Blasse, G.; Sytsma, J. and Brixner, L.H. *Chem. Phys. Lett.*, 155, 64 (1989)

Blessing, R.H. *Acta Crystallogr.*, Sect. A, 51, 33, (1995)

Brown, I.D. Bond Valence Calculator, Institute for Materials Research, McMaster University, Hamilton, Ontario, Canada, L8S 4M1

Brown, J.D. *J. Solid State Chem.*, 11, 214 (1974)

Cava, R.J.; Batlogg, B.; Krajewski, J.J.; Farrow, R.; Rupp, L.W.; White, A.E.; Short, K.; Peck, W.F. and Komentani, T. *Nature (London)*, 332, 814 (1988)

De Maayer, P. and Bollen, R. *J. Electrochem. Soc.*, 130, 437 (1983)

Debreuille-Gresse, M.F. and Abraham, F. *J. Solid State Chem.*, 71, 466 (1987)

Dowty, E. ATOMS Version 4.1 (1998)

Enjalbert, R.; Sorokina, R.; Castro, S. and Galy, J. *Acta chemica Scandinavica*, 49, 813 (1995)

Evans, J.S.O.; Huang, J. and Sleight, A.W. *J. Solid State Chem.*, 157, 255 (2001)

Farrugia, L.J. *J. Appl. Cryst.*, 32, 837 (1999)

Galvan, D.H.; Fuentes, S.; Alvalosborja, M.; Cotaaraiza, L.; Early, E.A.; Maple, M.B. and Cruzreyles, J. *J. Phys. Condens. Matter*, 5, A217 (1993)

Garcia-Montalvo, V.; Cea-Olivares, R.; Williams, D.J. and Espinosa-Perez, G. *Inorg. Chem.*, 35, 3948 (1996)

Grant in Aid: Scotland

Grasseli, R.K. and Burrington, J.F. *Adv. Catal.*, 30, 133 (1981)

Haeuseler, H and Jung, M. *Mat. Res. Bull.*, 21, 1291 (1986)

Hoffart, L.; Heider, U.; Jorissen, L.; Huggins, R.A. and Witschel, W. *Solid State Ionics*, 72, 195 (1994)

Holsa, J.; Leskela, M. and Niinisto, L. *J. Solid State Chem*, 37, 267 (1981)

Huang, J. and Sleight, A.W. *J. Solid State Chem.*, 100, 170 (1992)

Huang, J. and Sleight, A.W. *J. Solid State Chem.*, 104, 52 (1993)

Huang, J. and Sleight, A.W. *J. Solid State Chem.*, 96, 154 (1992)

Huang, J. and Sleight, A.W. *J. Solid State.Chem.*, 97, 228 (1992)

Huang, J. and Sleight, A.W. *Physica C*, 169, 169 (1990)

Huang, J.; Gu, Q. and Sleight, A.W. *J. Solid State Chem.*, 110, 226 (1994)

Jacquier, B.; Boulon, G.; Sallavuard, G. and Gaume, F. *J. Solid State Chem.*, 4, 374 (1972)

Jones, N.L.; Parise, J.B.; Flippen, R.B. and Sleight, A.W. *J. Solid State Chem.*, 78, 319 (1989)

Joubert, O.; Jouanneaux, A. and Ganne, M. *Mat. Res. Bull.*, 29/2, 175 (1994)

Joubert, O.; Jouanneaux, A.; Ganne, M. and Tournoux, M. *Mat. Res. Bull.*, 27, 1235 (1992)

Kellendonk, F. and Blasse, G. *Phys. Status Solidi B*, 108, 541 (1981)

Kim, H.K.; Kim, M.S.; Park, S.M. and Sleight, A.W. *J. Crystal Growth*, 219, 61 (2000)

Kodialam, S.; Korthius, V.C.; Hoffmann, R.-D. and Sleight, A.W. *Mat. Res. Bull.*, 27, 1379 (1992)

Kraus, W. and Nolze, G. PowderCell for Windows Version 2.3, Federal Institute for Materials Research and Testing, Berlin, Germany (1999)

Kumada, N.; Kinomura, N. and Sleight, A.W. *Mat. Res. Bull.*, 35, 2397 (2000)

Kumada, N.; Kinomura, N. and Sleight, A.W. *Solid State Ionics*, 122, 183 (1999)

Kumada, N.; Kinomura, N.; Kodialam, S. and Sleight, A.W. *Mat. Res. Bull.*, 29/5, 497 (1994)

Kumada, N.; Takahashi, N.; Kinomura, N. and Sleight, A.W. *J. Solid State Chem.*, 126, 121 (1996)

Kumada, N.; Takahashi, N.; Kinomura, N. and Sleight, A.W. *J. Solid State Chem.*, 139, 321 (1998)

Kumada, N.; Takahashi, N.; Kinomura, N. and Sleight, A.W. *Mat. Res. Bull.*, 32/8, 1003 (1997)

Kumada, N.; Takahashi, N.; Kinomura, N. and Sleight, A.W. *Royal Soc. Chem.*, 239, 212 (1999)

Larson, A.C. and von Dreele, R.B. *Los Alamos Lab. Rep.*, LA-UR-86-748 (1987)

Laugier, J. and Bochu, B. www.inpg.fr/LMGP

Lee, C.K.; Coats, A.M. and West, A.R. *Powder Diffr.*, 12/4, 245 (1997)

Lu, T. and Steele, B.C.H. *Solid State Ionics*, 21, 339 (1986)

Mairesse, G. Fast Ion Transport in Solids, Edited by Scrosati, B.; Kluver Amsterdam, The Netherlands (1993)

Marsh, R.E. *Acta Cryst.*, B51, 897 (1995)

Mary, T.A.; Mackay, R.; Nguyen, P. and Sleight, A.W. *Eur. J. Solid State Inorg. Chem.*, 33, 285 (1996)

Mattheiss, L.F.; Gyorgy, E.M. and Johnson, D.W. *Phys. Rev. B*, 37, 3745 (1988)

Mentre, O.; Dhaussy, A.C. and Abraham, F. *J. Mater. Chem.*, 9, 1023 (1999)

Mo, L.Y.; Guillen, F.; Fouassier, C. and Hagenmuller, P. *J. Electrochem. Soc.*, 132, 717 (1985)

Nadir, S.; Swinnea, J.S. and Steinfink, H. *J. Solid State Chem.*, 148,295 (1999)

Neilson, R. Oregon State University Microprobe Lab

Ng, Y.S.; Rodley, G.A. and Robinson, W.T. *Mat. Res. Bull.*, 15, 303 (1976)

Pannetier, J.; Tranqui, D. and Sleight, A.W. *Mat. Res. Bull.*, 28, 989 (1993)

Pelle, F.; Jacquier, B.; Denis, J.P. and Blanzat, B. *J. Lunim.*, 17, 61 (1978)

Porob, D.G. and Guru Row, T.N. *Chem. Mater.*, 12, 3658 (2000)

Poznyak, S.K.; Sviridov, V.V. and Kulak, A.I. *Elektrokhimiya*, 20/7, 996 (1984)

Radaev, S.F.; Muradyan, L.A. and Simonov, V.I. *Acta Cryst.*, B47, 1 (1991)

Radosavljevic, I.; Evans, J.S.O. and Sleight, A.W. *J. Alloys and Compds.*, 284, 99, (1999)

Radosavljevic, I.; Evans, J.S.O. and Sleight, A.W. *J. Solid State Chem.*, 136, 63 (1998)

Radosavljevic, I.; Howard, J.A.K. and Sleight, A.W. *Int. J. Inorg. Mat.*, submitted

Radosavljevic, I.; Howard, J.A.K.; Sleight, A.W. and Evans, J.S.O. *J. Mater. Chem.*, 10, 2091 (2000)

Radosavljevic, I; Evans, J.S.O. and Sleight, A.W. *J. Solid State Chem.*, 141, 149 (1998)

Roth, R.S. and Waring, J.L. *Amer. Miner.*, 48, 1348 (1963)

Shan, Y. and Huang, S.D. *Acta Cryst.*, C55, 1048 (1999)

Shannon, R.D. *Acta Cryst.*, A32, 751 (1976)

Shannon, R.D.; Bierlein, J.D.; Gillson, J.L.; Jones, G.A. and Sleight, A.W. *J. Phys. Chem. Solids*, 41, 117 (1980)

Sheldrick, G.M. SHELX97-Programs for Crystal Structure Analysis, University of Goettingen, Germany (Release 97-2)

Sinclair, D.C.; Marinou, E. and Skakle, J.M.S. *J. Mater. Chem.*, 9, 2617 (1999)

Sinclair, D.C.; Watson, C.J.; Howie, R.A.; Skakle, J.M.S.; Coats, A.M.; Kirk, C.A.; Lachowski, E.E. and Marr, J. *J. Mater. Chem.*, 8/2, 281 (1998)

Sleight, A.W. and Huang, J. U.S.A. Patent No. 5202,891 (1993)

Sleight, A.W. and Linn, W.J. *Ann. New York Acad. Sci.*, 272, 23 (1976)

Sleight, A.W. *Science*, 242, 1519 (1988)

Sleight, A.W.; Aykan, K. and Rogers, D.B. *J. Solid State Chem.*, 13, 231 (1975)

Sleight, A.W.; Chen, H.-Y. and Ferretti, A. *Mat. Res. Bull.*, 14, 1571, (1979)

Sleight, A.W.; Gillson, J.L. and Bierstedt, P.E. *Solid State Commun.*, 17, 27 (1975)

Soldatov, A.G.; Barilo, S.N.; Shiryawv, S.V.; Finskaya, V.M.; Ustinovich, S.N.; Reichardt, W.; Braden, M. and Szymszak, R. *Physica. B, Condensed Matter*, 285, 1059 (2000)

Sorokina, S.L. and Sleight, A.W. *Mat. Res. Bull.*, 33/7, 1077 (1998)

Subbarao, E.C. *J. Chem. Phys.*, 34/2, 695 (1961)

Subramanian, M.A. and Sleight, A.W. *Mat. Res. Bull.*, 21, 727 (1986)

Subramanian, M.A.; Gopalakrishnan, J. and Sleight, A.W. *Mat. Res. Bull.*, 23, 837 (1988)

Takahashi, T. and Iwahara, H. *Mat. Res. Bull.*, 13, 1447 (1978)

Teller, R.G. *Acta Cryst.*, C48, 2101 (1992)

TEXSAN, Single Crystal Structure Analysis Software, Version 5.0, Molecular Structure Corporation, The Woodlands, TX, 1989

Thompson, P.; Cox, D.E. and Hastings, J.B. *J. Appl. Cryst.*, 20, 79 (1987)

Timmermans, C.W.M. and Blasse, G. *J. Lunim.*, 24/25, 75 (1981)

Timmermans, C.W.M. and Blasse, G. *Phys. Status Solidi B*, 106, 647 (1981)

Timmermans, C.W.M.; Boen Ho, O. and Blasse, G. *Solid State Commun.*, 42, 505 (1982)

Timmermans, C.W.M.; Cholakh, S.O. and Blasse, G. *J. Solid State Chem.*, 46, 222 (1983)

Timmermans, C.W.M.; Cholakh, S.O.; Van Der Woude, R.L. and Blasse, G. *Phys. Status Solidi B*, 115, 267 (1983)

Tsunoda, T.; Hayakawa, T.; Kameyama, T. and Takehira, K. *J. Chem. Soc. Farad. Trans.*, 91, 1117 (1995)

Uma, S.; Bliesner, R.J. and Sleight, A.W. "Gross Oxygen Deficiency and Oxide Ion Conductivity in the Scheelite Structure", presented June 13-17, 2001 NORM American Chemical Society Meeting

Van Der Steen, A.C. *Phys. Status Solidi B*, 100, 603 (1980)

Vinke, I.C.; Diepgrond, J.; Boukamp, B.A.; de Vries, K.J. and Burggraaf, A.J. *Solid State Ionics*, 57, 83 (1992)

Walker, N. and Stuart, D. *Acta Cryst.* A39, 158 (1983)

Watanabe, A. *Solid State Ionics*, 96, 75 (2997)

West, A.R. Basic Solid State Chemistry, 2nd Edition, John Wiley & Sons, 1996.

Wolfe, R.J.; Newnham, R.E. and Kay, M.I. *Solid State Comm.*, 7, 1797 (1969)

Wolfert, A. and Blasse, G. *Mat. Res. Bull.*, 19, 67 (1984)